NASA TECHNICAL NOTE

NASA TN D-8052

NASA TN D-8052

SUMMARY OF FLIGHT TESTS TO DETERMINE THE SPIN AND CONTROLLABILITY CHARACTERISTICS OF A REMOTELY PILOTED, LARGE-SCALE (3/8) FIGHTER AIRPLANE MODEL

Euclid C. Holleman

Flight Research Center
Edwards, Calif. 93523

NATIONAL AERONAUTICS AND SPACE ADMINISTRATION • WASHINGTON, D. C. • JANUARY 1976

1. Report No.	2. Government Accession No.	3. Recipient's Catalog No.
NASA TN D-8052		

4. Title and Subtitle	5. Report Date
SUMMARY OF FLIGHT TESTS TO DETERMINE THE SPIN AND CONTROLLABILITY CHARACTERISTICS OF A REMOTELY PILOTED, LARGE-SCALE (3/8) FIGHTER AIRPLANE MODEL	January 1970
	6. Performing Organization Code
7. Author(s)	8. Performing Organization Report No.
Euclid C. Holleman	H-889
	10. Work Unit No.
9. Performing Organization Name and Address	505-11-24
NASA Flight Research Center P. O. Box 273 Edwards, California 93523	11. Contract or Grant No.
	13. Type of Report and Period Covered
12. Sponsoring Agency Name and Address	Technical Note
National Aeronautics and Space Administration Washington, D. C. 20546	14. Sponsoring Agency Code

15. Supplementary Notes

16. Abstract

An unpowered, large, dynamically scaled airplane model was test flown by a remote pilot to investigate the stability and controllability of the configuration at high angles of attack. The configuration proved to be departure/spin resistant; however, spins were obtained by using techniques developed on a flight support simulator. Spin modes at high and medium-high angles of attack were identified, and recovery techniques were investigated. The results are compared with other scale model results.

A flight support simulation of the airplane model mechanized with low-speed wind-tunnel data over an angle of attack range of ±90° and an angle of sideslip range of ±40° provided insight into the effects of altitude, stability, aerodynamic damping, and the operation of the augmented flight control system on spins.

Aerodynamic derivatives determined from flight maneuvers were used to correlate model controllability with two proposed departure/spin design criteria.

The remotely piloted systems and operational procedures are described.

17. Key Words (Suggested by Author(s))	18. Distribution Statement
Spin High angle of attack controllability Remotely piloted model	Unclassified - Unlimited Category: 08

19. Security Classif. (of this report)	20. Security Classif. (of this page)	21. No. of Pages	22. Price*
Unclassified	Unclassified	125	$5.25

*For sale by the National Technical Information Service, Springfield, Virginia 22161

CONTENTS

SUMMARY OF FLIGHT TESTS TO DETERMINE THE SPIN AND CONTROLLABILITY CHARACTERISTICS OF A REMOTELY PILOTED, LARGE-SCALE (3/8) FIGHTER AIRPLANE MODEL

Euclid C. Holleman
Flight Research Center

SUMMARY

A 3/8-scale model of an air superiority fighter airplane was flown to investigate the stability and controllability of the configuration at high angle of attack. Although the airplane model was unpowered, altitudes from 15 250 meters to 4600 meters were covered and angles of attack as large as 80° and -70° were reached during erect and inverted spins. The remotely piloted technique of control was used. The pilot controlled the airplane model from a ground-based simulator-like isolated cockpit with complete displays and controls and through simulated fighter control systems (two basic control systems mechanized for research and two control systems mechanized to represent full-scale airplane control systems) programed on a ground computer. A six-degree-of-freedom flight support simulator was used to provide a better understanding of the spin and controllability characteristics of the configuration.

The airplane configuration proved to be departure/spin resistant. By using the control augmentation system, which provided increased control authority, the model could be spun by several techniques developed on the simulator. High and medium-high angle of attack erect spins were made. Correlation of the data with smaller scale model results was good. The standard recovery technique of using roll control with and yaw control against the spin provided satisfactory recovery from the erect spins. The airplane model was recovered with recovery control at all altitudes and more readily at low altitude. Inverted spins were also made and were easily recovered from by neutralizing the control deflections.

Two proposed spin controllability criteria predicted good departure/spin characteristics for the configuration, based on aerodynamic stability and control derivatives determined from flight data. High and low Reynolds number wind-tunnel data generally predicted satisfactory stability except for a narrow range of angle of attack at about maximum lift for the low Reynolds number data where the values of the usual aerodynamic derivative were not well defined.

INTRODUCTION

For tactical advantage the pilots of high-performance airplanes use the entire maneuvering capability of the airplanes. To do this, maximum angle of attack is often commanded. Unless the airplane has good controllability at the extreme angles of attack, the tactical advantage sought, and perhaps even control of the airplane, may be lost. Inordinate losses of airplanes from attempts to use extreme angles of attack have prompted studies of the requirements for high angle of attack stability and control and of designs that provide good controllability.

The NASA Flight Research Center flight tested a large-scale (3/8) model (fig. 1) of a current air superiority fighter airplane to high angles of attack in an attempt to better understand the handling of a particular configuration at high angle of attack and to produce data for correlation with other model test data. Stability and control derivatives were determined to maximum trim angle of attack, and attempts were made to depart and spin the model. The tests were performed between 15 250 meters and 4600 meters, altitudes at which the full-scale airplane will be flown.

The large-scale model was selected to provide intermediate-scale data for correlation with full-scale airplane test data and small-scale spin tunnel and drop model test results. For many years spin and drop model tests have been made with models prior to the actual full-scale stall/spin tests and have provided valuable information on model spin characteristics and procedures for recovery from out-of-control flight (ref. 1). However, the piloting techniques used were not as realistic as would be desired for extrapolation to full-scale flight techniques.

In the NASA Flight Research Center tests, the model was piloted (remotely) and maneuvered much as the airplane would be during actual flight. The ground-based pilot was not subjected to the high accelerations and rates of normal piloted flight. Although these motions would provide cues for the pilot in the airplane, they could also interfere with the accomplishment of some piloting tasks. Perhaps more important, the ground pilot was not subjected to the risks associated with stall/spin tests and so could concentrate fully on the piloting task. The primary objectives of these tests were to investigate controllability at high angle of attack, to determine spin modes, and to develop spin entry and recovery techniques. An additional objective was to evaluate the remotely piloted test method, described in detail in appendix A, for possible use in other flight investigations.

Preliminary results from this high angle of attack controllability program were reported in reference 2, and in-flight experience with the "fly by wireless" control system used during the program is discussed in reference 3. The aerodynamic derivative data for the large-scale model are given in reference 4. Controllability of the model at high angle of attack and the results of attempts to depart and spin the model are summarized herein and compared with results from other model tests. The data presented are scaled to those for the full-scale airplane.

SYMBOLS AND ABBREVIATIONS

a_x, a_y, a_z	longitudinal, lateral, and vertical acceleration along the body X-, Y-, and Z-axes, respectively, g
Δa_z	incremental change in vertical acceleration, g
b	wing span, m
CAS	control augmentation system
CD	computer direct
C_D	drag coefficient
C_L	lift coefficient
C_l	rolling-moment coefficient
C_{l_β}	roll due to sideslip derivative, 1/deg
C_{l_δ}	roll due to control deflection derivative, 1/deg
C_{n_β}	yaw due to sideslip derivative, 1/deg
$C_{n_{\beta,dyn}}$	dynamic directional stability derivative, 1/deg
C_{n_δ}	yaw due to control deflection derivative, 1/deg
$C_{n_{\delta_r}}$	rudder effectiveness derivative, 1/deg
F_{δ_a}	pilot's lateral stick force, N
F_{δ_e}	pilot's longitudinal stick force, N
g	acceleration due to gravity, m/sec^2
h	altitude, km

I	moment of inertia, kg-m^2
I_X, I_Y, I_Z	moment of inertia about the body X-, Y-, and Z-axes, respectively, kg-m^2
I_{XZ}	product of inertia, kg-m^2
$K_{a_y}, K_{a_z}, K_p, K_q, K_{r_s}$	control system gain for a_y, a_z, p, q, r_s, respectively, deg/g and deg/deg/sec
LCSP	lateral control spin parameter, $C_{n_\beta} - C_{l_\beta} C_{n_\delta} / C_{l_\delta}$, per deg
l	distance from airplane model center of gravity to angle of attack and angle of sideslip vanes; in table 2, linear dimension, m
MCS	mechanical control system
m	mass, kg
p, q, r	body axis roll, pitch, and yaw rate, respectively, deg/sec
$\bar{q}$	dynamic pressure, N/m^2
r_s	stability axis yaw rate, deg/sec
s	Laplace transform variable, 1/sec
t	time, sec
V	velocity (body X-direction), m/sec
V_R	velocity along the wind axis, m/sec
α	angle of attack at center of gravity, deg
α'	stall inhibiter scheduled command, deg
α_i	vane-indicated angle of attack, deg
β	angle of sideslip at center of gravity, deg
β_i	vane-indicated angle of sideslip, deg

$\Delta\delta_e$	nose-down stall inhibiter command, deg
δ_a	aileron deflection, deg
δ_d	differential stabilator deflection, deg
δ_e	collective stabilator deflection, deg
δ_{pb}	pitch boost servo output, deg
δ'_{pb}	lagged pitch boost servo output, deg
δ_r	rudder deflection, deg
θ	pitch angle, deg
ρ	air density, kg/m^3
φ	bank angle, deg
ψ	heading angle, deg
Ω	time per spin turn, sec/turn

Subscripts:

a	roll-to-rudder interconnect; in table 2, airplane
CAS	commanded by control augmentation system
c	commanded
L	left
MCS	commanded by mechanical control system
m	model
max	maximum
p	pilot
R	right
trim	control stick or rudder pedal trim

Dots over a symbol represent derivatives with respect to time.

MODEL DESCRIPTION

Model

The model (figs. 1 and 2) flown in these tests was a 3/8-scale model of a single place, advanced air superiority fighter airplane with 45° swept leading edge wings, two engines, and twin vertical tails. (Pertinent full-scale airplane dimensions are given in table 1.) The model was built primarily of fiber glass with metal load-carrying members in each section. It was designed to be as stiff as the full-scale airplane and to withstand normal loads five times 1*g* flight. The model was unpowered. The inlets were drooped 11° to correspond to the low-speed configuration of the airplane and were blocked by a flat plate normal to the duct which was positioned just inside the inlet lip. There was no flow through the ducts, nor was there any thrust or simulation of thrust. Engine angular momentum effects were not accounted for.

TABLE 1.—AIRPLANE DIMENSIONS

Fuselage length, m	19.05
Wing —	
Area, m^2	56.48
Span, m	13.05
Aspect ratio	3.0
Mean aerodynamic chord, m	4.86
Leading-edge sweep, deg	45
Taper ratio	0.25
Dihedral, deg	-1.0
Incidence, deg	0
Ailerons:	
Span (both), m	3.30
Deflection, deg	±20
Horizontal tail —	
Planform (exposed), m^2	11.15
Span, m	8.64
Aspect ratio	2.046
Taper ratio	0.34
Leading-edge sweep, deg	50.0
Mean aerodynamic chord (exposed), m	2.52
Dihedral, deg	0
Length, m	6.12
Deflection, deg:	
Symmetrical	15, -27.5
Differential	±11
Vertical tails —	
Area (both), m^2	11.63
Span (exposed), m	3.15
Aspect ratio	1.70
Taper ratio	0.27
Leading-edge sweep, deg	36.57
Mean aerodynamic chord, m	2.06
Length, m	5.39
Rudders:	
Area, m^2	1.85
Span, m	1.44
Mean aerodynamic chord, m	0.64
Maximum deflection, deg	±30

Control for the pilot was provided by conventional aerodynamic surfaces. Roll control was provided by aileron deflection of 40° maximum and by differential horizontal stabilator deflection of 22° maximum. The roll control authority varied with the amount of longitudinal control commanded and with the control system being used. A portion of each vertical stabilizer was deflected for rudder control. Rudder control was also commanded through an interconnect between the lateral stick position and the rudder. In this report the deflections of each of the two rudders are averaged, as are the deflections of each side of the horizontal stabilator in pitch. The total aileron deflections are given, and the left and right horizontal stabilator differential deflections are summed.

The full-scale airplane control surface limit deflections were duplicated accurately by the model control system. Control stick forces in pitch and roll were the same as those on the airplane; however, the rudder pedal forces were selected as desired by the pilot. The scaling of control surface rate limits and actuator dynamic characteristics was either accounted for on the ground-based computer or in the model actuator characteristics. Actual full-scale mechanical control system (MCS) characteristics and control augmentation system (CAS) characteristics were scaled and programed on the ground-based computer for the model flight tests. The term "mechanical control system" refers to the full-scale airplane open-loop controls which have traditionally been mechanical. The term "control augmentation system" refers to the full-scale airplane mechanical control system plus augmentation loops that make up the operational control system.

The model, which was launched from a B-52 airplane, had no landing gear and was recovered by parachute with midair retrieval by helicopter. A drogue parachute was used to decelerate the model and to stream the main parachute; it also served as a spin recovery parachute. The drogue parachute was scaled to represent the full-scale spin recovery parachute of 10 meters diameter with a riser length of 32 meters.

During the program the configuration was changed to a "production" configuration. As shown by the dashed lines in figure 3, trailing edges of the wingtip were rounded and the horizontal stabilator chord was reduced by about one-sixth from the fuselage to about one-third of the movable surface span.

Model Scaling

The model was scaled geometrically to be as large as practical and was to be flown at flight levels similar to those of the full-scale airplane. The motivation was to provide a model large enough that it could be controlled "normally" by a pilot and to obtain data at near full-scale Reynolds number conditions for correlation with other model test results. As noted previously, a primary program objective was to evaluate controllability at high angles of attack. Therefore the model was scaled dynamically according to the relationships shown in table 2. It was concluded in reference 5 that tests of a model designed and tested in accordance with these dynamic similarity relationships should give results that may be interpreted to predict full-scale results if Reynolds number and Mach number effects are nonexistent. Also, basic model angles should be the same as full-scale angles, and

TABLE 2.–DYNAMIC RELATIONSHIPS

Mass	$\frac{m_m}{m_a} = \frac{\rho_m}{\rho_a}\left(\frac{l_m}{l_a}\right)^3$
Moments of inertia	$\frac{I_m}{I_a} = \frac{\rho_m}{\rho_a}\left(\frac{l_m}{l_a}\right)^5$
Time	$\frac{t_m}{t_a} = \left(\frac{l_m}{l_a}\right)^{1/2}$
Linear velocities	$\frac{\dot{l}_m}{\dot{l}_a} = \left(\frac{l_m}{l_a}\right)^{1/2}$
Linear accelerations	$\frac{\ddot{l}_m}{\ddot{l}_a} = 1$
Angles	$\frac{\theta_m}{\theta_a} = 1$
Angular velocities	$\frac{\dot{\theta}_m}{\dot{\theta}_a} = \left(\frac{l_a}{l_m}\right)^{1/2}$
Angular accelerations	$\frac{\ddot{\theta}_m}{\ddot{\theta}_a} = \frac{l_a}{l_m}$

angular velocities (time-dependent quantities) should be predictable by the relationships shown.

Originally, the model was geometrically scaled to the full-scale airplane and the inertias (table 3) were specified so that the model would be scaled to typical full-scale design values. However, when the model was completed and the instrumentation and controls were installed, the mass and inertias (determined experimentally) were larger than the desired values. Therefore, an average value of density ratio correction (for mass and inertia) was applied to the model data. The data presented in table 3 are for the full-scale airplane and have been corrected by the density ratio to the altitude shown.

Instrumentation

The model instrumentation system (ref. 2) consisted of regulated power supplies, sensors, signal conditioning, a pulse code modulation (PCM) system, and an L-band telemetering transmitter. The sensed quantities were transmitted to the ground station for display to the pilot, for inputs to the flight control system computer, and for recording. Quantities recorded included angles of pitch, roll,

TABLE 3.–TEST CONDITIONS AND INERTIA CHARACTERISTICS

Scale, percent	Configuration	Center-of-gravity position, percent mean aerodynamic chord	Simulated altitude, m	Reynolds number	Weight, N	I_X, kg-m^2	I_Y, kg-m^2	I_Z, kg-m^2	I_{XZ}, kg-m^2	$\frac{I_X - I_Y}{mb^2}$	$\frac{I_Y - I_Z}{mb^2}$	$\frac{I_Z - I_X}{mb^2}$
37.5	Basic	26.0	12 040	4.3×10^6	128 554	30 845	213 541	250 148	1 302	-826×10^{-4}	-164×10^{-4}	990×10^{-4}
			9 144	5.3								
		30.3	15 240	3.6			203 101	239 708	281	-778		942
			15 758	4.1								
			9 449	5.3								
	Production		13 106	3.6	127 575	30 587		239 302		-779		943
			10 211	5.4								
			9 906	6.4								
			14 326	3.6								
			11 643	5.9								
			17 069	2.2								
			12 802	3.9								
			9 906	5.2								
			15 301	4.6								
			10 759	5.7								
13.0	Basic	24.03	10 600	3.6	141 444	33 880	209 766	232 103		-718	-91	809
3.3	Basic	26.9	7 620	0.7	152 151	35 366	210 936	234 172		-666	-88	754
100.0 (design)	Basic	26.0	------	---	142 343	31 590	204 700	230 489	-651	-690	-108	800

heading, sideslip, and attack; pitching, rolling, and yawing angular rates; longitudinal, lateral, and normal acceleration (center of gravity); airspeed; and altitude. The model control surface positions—each aileron position, each rudder position, and each horizontal stabilator position—were also recorded. The pilot's lateral and longitudinal stick position and force and rudder position and force as well as the commanded pitch, roll, and yaw trim were recorded. Twelve operational quantities, including battery voltages and hydraulic pressures, twelve discrete command signals, and twelve control system mode switch positions were recorded.

The resolution of the full-scale range of the recording indicates the accuracy of the model response variables. In each instance the measured quantity could be resolved to less than 1 percent of the full-scale recording range. Eight of the quantities (attitudes, rates, and accelerations) were recorded with full and expanded scales in the range of primary interest.

Each model quantity was transmitted at a rate of 200 samples per second. These sensed quantities were prefiltered in the telemetry system by a 40-hertz first-order lag filter before they were sampled.

Postflight digital data processing routines applied a digital filter with a notch at 19 hertz and a third-order low-pass filter at 20 hertz to reduce the structural noise sensed primarily above 15° angle of attack in the acceleration and rate data. Additional digital data processing routines applied calibrations to the raw data, corrected angle of attack and angle of sideslip for local flow deflection, angular rates, and linear accelerations, and converted total and static pressure to the conventional air data functions. The angle of attack and sideslip vanes were 5.4 meters ahead of the center of gravity and were mounted on a "dogleg" boom (fig. 2).

Attitudes were measured by a four-gimbal, two-gyro platform system. The pitch, roll, and yaw angles were measured relative to the stable platform but were converted to and are presented as attitudes relative to an earth reference system as seen by the pilot.

Control System Modes

Only a brief description of the control system mechanization is included here. A more complete description is given in reference 3. Two research-related control modes were available for evaluation as well as the two basic full-scale airplane control modes. The pilot's control system mode panel switching (fig. 4) provided individual control of the pitch, roll, and yaw channels which could be switched to computer direct, rate damper, mechanical control system, and control augmentation system. A gain control was provided for each channel. The computer direct mode provided the pilot with direct proportional control of pitch, roll, and heading. A nonlinear gearing (for details, see ref. 3) in the pitch control provided an optimum slope near zero stick deflection and still gave the pilot the capability of commanding full stabilator deflection (δ_e = 15° or -27.5°). The rate damper modes provided a rate feedback for the pitch, roll, and yaw channels. Each rate gyro signal was low-passed at 6 hertz and notch-filtered to eliminate the dominant structural resonance near 20 hertz. Pitch, roll, and yaw damper authority was limited to ±10°, ±10°,

and ±15° in the pitch, roll, and yaw axes, respectively. Maximum damper gains were 0.4 deg/sec in pitch, 0.8 deg/sec in roll, and 4 deg/sec in yaw.

Mechanical control system.—The MCS mode was a simulation of the unaugmented flight control system of the full-scale airplane in which the pilot was assisted in pitch and roll control by hydraulic power boost servos (fig. 5). These boost servos were simulated on the ground computer for the scale-model MCS mode. The pitch boost servo output, δ_{pb}, was combined with the roll MCS command to form the commands to the left and right stabilator power actuators. These power actuators were duplicated on the model by the hydraulic actuators and were not simulated in the ground computer. Similar functions were performed by the aileron and rudder actuators.

The longitudinal stick position controlled the collective stabilator positions, and the lateral stick position controlled the ailerons and differential position of the stabilators. The rudders were controlled by the rudder pedals and the lateral stick-to-rudder interconnect. Lateral control authority was scheduled as a function of the lagged pitch boost servo output, δ'_{pb}, and resulted in the authority being restricted at rearward and forward longitudinal stick positions (fig. 6). The differential deflection of the stabilators was also restricted as a function of δ'_{pb} and had an authority of about one-fourth that of the total aileron deflection. The interconnect was also scheduled as a function of δ'_{pb} (fig. 7) and resulted in rudder commands proportional to lateral stick deflection. The interconnect feature of the MCS was also used with the computer direct and rate damper system (previously discussed) mechanized for research purposes.

Control augmentation system.—A block diagram of the model CAS mode is also shown in figure 5. A complete description of the CAS is given in reference 3. The CAS utilized pitch, roll, and yaw rates and normal and lateral accelerations as feedback variables. Each of these five signals was notch-filtered to suppress the approximately 20-hertz resonance. The three rate gyro signals used the same notch filters as those for the rate damper mode.

The pitch CAS command was composed of a modified form of the blended normal acceleration and pitch rate response parameter (ref. 6). The commanded normal acceleration signal was derived by passing the longitudinal stick force through a dual-gradient gearing schedule and a first-order shaping filter.

The pitch CAS command was passed through a proportional plus integral feedforward network and limited by the schedule shown in figure 8 to form the pitch CAS command, which summed with the roll CAS command. The combined pitch and roll CAS commands positioned the series servos. The outputs of the servos were then summed with the pitch boost servo output and the MCS differential stabilator signal to form the left and right stabilator uplink commands for the remotely piloted operation.

The roll CAS command to the differential stabilator was formed by comparing roll rate to commanded roll rate from the lateral stick force. The commanded roll

rate signal was derived by passing lateral stick force through a dual-gradient gearing schedule. The resulting command was limited by the roll CAS angle of attack schedule shown in figure 9 to form $\delta_{d_{CAS}}$ and summed with the pitch CAS command.

In the yaw CAS mode, rudder pedal gearing was effectively doubled over that of the MCS mode. Lateral acceleration and washed out stability axis yaw rate were fed to the rudders. The stability axis yaw rate signal was computed as $r_s = r - \alpha p$.

To account for different accelerometer locations in the full-scale airplane and the scale model, pitch rate and yaw rate were differentiated and summed in proportion to displacement with a_z and a_y, respectively, to simulate lever arm effects.

The full-scale airplane CAS contained an automatic downmode feature which switched from the CAS to the MCS for departure/spin prevention. Downmoding occurred when the yaw rate exceeded ±42 deg/sec. (For the model the downmode value of scaled yaw rate was ±70 deg/sec.) The downmoding restricted control authority to that of the MCS, which commanded about 55 percent of the δ_d authority of the CAS, and deactivated the feedback controls. Full control authority or feedback augmentation, or both, could augment the departure rather than oppose it.

Stall inhibiter.—A model of a proposed stall inhibiter for the full-scale airplane (fig. 10) was included in the mechanization of the CAS. The stall inhibiter responded proportionally to angles of attack from 13° to 23° and to a pitch rate signal that was washed out to prevent response to steady low-frequency pitch rates but would respond to rapid, high-frequency pitch rates. The inhibiter signal effectively increased the longitudinal stick force required to pitch the model up to a higher angle of attack or to maintain the same angle of attack over the normal stick force gradient by commanding nose-down stabilator deflection.

OPERATIONAL PROCEDURES

Preflight Preparation

All manned air-launched flights at the NASA Flight Research Center are planned in detail on a fixed-base flight procedural simulator in order to obtain as much flight data as possible during each flight. The pilot practices the flight plan before each flight to become thoroughly familiar with the flight. This procedure was used in preparing for the large-scale airplane model flights. The simulator was mechanized and updated between each flight to reflect control system changes and the best estimate of model aerodynamics based on data from previous flights. Several hours of practice on the flight simulator made it possible for the pilot to compress a high workload flight plan of about 40 individual maneuvers into a 5- to 7-minute flight. Even with this preparation, the remote pilot of the model was more hurried during actual flight than during simulated flight. (Previous full-scale flight program pilots were also usually more hurried during actual flight than during simulated flight.) Therefore, the simulation time scale was changed to provide practice for the pilot

at a more rapid pace than in actual flight. After considering several time factors faster than real time, a factor of 1.4 was accepted as providing satisfactory training. This was also found to be an effective time factor during other programs.

On the day of the flight, the pilot practiced the flight plan with the predicted winds for the test altitudes, and the turns for control of flight range were finalized. During the practice and the actual flights, the pilot was assisted in following the flight plan by a flight engineer who switched control modes and called out maneuvers to be performed. A flight director monitored model range position and gave heading information to the pilot to keep the model in its assigned area.

Flight Techniques

The model was launched from a B-52 carrier airplane at about 14 000 meters altitude and a Mach number of 0.65 for the unpowered glide flight. Three seconds after launch the model control actuators were unlocked and the pilot assumed control. The desired test conditions were set up and the test maneuvers performed according to the flight plan (table 4). Progress of the flight was monitored by radar and

TABLE 4.—FLIGHT REQUEST

Purpose:	1. CAS checks 2. Stability and control (α = 7°, 32°) 3. Determine departure and spin characteristics in CAS
Launch:	East boundary of bombing range, magnetic heading 254°, 13 710 m, 175 knots indicated airspeed. Surface settings: δ_e = -0.75°, δ_a = 0°, δ_r = 0°. Cockpit control settings: δ_e = -1.5°, δ_a = 0°, δ_r = 0°. Mode panel: computer direct. Airspeed as per attached schedule.
Recovery:	Parachute deployment 4572 m. Midair retrieval system (MARS) pickup over bombing range.
B-52 track:	NASA drone track 2

Item	Altitude, m	Control mode	α, deg	Event
1	13 710	CD	-3	Launch
2	13 560	CD	4	Trim α = 7°
3	14 020	CD	7	Select MCS
4	14 020	MCS	7	Pitch frequency sweep
5	13 860	MCS	7	Pitch CAS on, pulse series
6	13 710	CAS	7	All CAS on, control step input
7	13 410	CAS	20	Trim full back stick
8	12 800	CAS	32	All SAS (low gain), pulse series
9	11 890	Dampers	--	All CAS; initiate departure maneuver
10	9 140	CAS	70 to 90	Initiate recovery
11	7 620	CAS	25	Initiate departure maneuver; recovery with drogue chute
12	4 510	CAS	70 to 90	Drogue chute electrics on
13	------	MCS	--	30 sec to MARS; hydraulics on
14	------	MCS	--	Missed engagement; hydraulics off

television, and the flight director advised the pilot of the headings required to keep the model within the test area. After the flight was completed, or at about 4600 meters altitude, the model recovery sequence was initiated by either the pilot, the flight engineer, or automatically. Midair snatch by helicopter recovered the model.

Data from conventional maneuvers such as control steps and doublets were recorded for stability and control derivative analysis. Pullups to extreme attitudes with large coordinated and uncoordinated control inputs and windup turns were made during deliberate attempts to stall, depart, and spin the model. The model proved to be spin resistant; however, special control sequences during specific maneuvers were developed to force the model to spin, and various techniques, including the use of the drogue parachute, were used to recover from the spin.

One technique for entering a spin required the pilot to roll over to inverted flight, pull through to a near vertical descending flightpath (split-S type of maneuver), and at the desired airspeed apply back stick to achieve a high angle of attack and normal acceleration. At high angle of attack, roll control and opposite rudder were commanded and the control stick was eased forward, taking advantage of the control system design which allowed more roll control near neutral stick position. The control's yawing moments forced the model into the spin. This and other techniques were finalized on the six-degree-of-freedom simulator. A simulation mechanization that used only wind-tunnel derivatives provided a control task for the pilot that was representative of that for the model airplane.

RESULTS AND DISCUSSION

The flight envelope coverage for a particular flight usually progressed from the higher velocities to the lower velocities and from the higher to the lower altitudes because the model was unpowered. Stability and control data were recorded over the entire velocity range. Departure tendencies were checked first at low velocities. The first several flights were made with the center of gravity at 26-percent mean aerodynamic chord. With this center-of-gravity location, the model could be trimmed to an angle of attack of about 32°.

Eight flights were made with the center of gravity at 30.3-percent mean aerodynamic chord, the approximate rearward limit for the full-scale airplane. With the center of gravity at this location, the airplane could be trimmed to about 40° angle of attack erect, beyond maximum lift, and to about -20° angle of attack inverted.

The envelope shown in figure 11 includes pullups and turns to high angles of attack, in attempts to make the model depart, and the angles of attack reached during erect and inverted spins. During the erect spins, pitch attitudes were about -10° and angles of attack were measured to be approximately 80°, resulting in a flightpath angle of near vertical descending flight. These maneuvers are discussed in more detail in a later section. Negative angles of attack of -70° were reached during inverted spins. Stability and control data were recorded and analyzed over an angle of attack range of 50° to -20°. The stability and control derivative results are summarized in reference 4.

Among the distinguishing features of this model program are the relatively complete instrumentation possible with the large-scale model, the complete simulation of the airplane control system, and the use of the pilot to control the flight much as he would have if he had been on board the full-scale airplane. Some pilot observations on the effectiveness of the remotely piloted technique are summarized in appendix B.

All data presented are scaled to the full-scale airplane.

Lift and Drag

Measurements of normal and longitudinal acceleration and airplane attitudes were made during stabilized flight, and the data were reduced to lift and drag coefficients for comparison with results from low-speed wind-tunnel tests with a 1/10-scale model at a Reynolds number of approximately 0.8×10^6 (fig. 12). Reasonable agreement is indicated through the midlift range. The lift generated in flight near maximum lift appears to be less (no more than 5 percent) than that predicted by the wind-tunnel data. It was more difficult to record stabilized flight at the high angles of attack than it was at the low angles of attack.

The drag coefficient was calculated from stabilized flight data, and the results are compared with the low-speed wind-tunnel data in figure 13. Good agreement is indicated, although the flight data show slightly less drag throughout the angle of attack range covered. It should be noted that the large-scale model tests were made with the model inlets blocked; thus neither engine thrust nor flow through the duct is accounted for.

Longitudinal Stability

The apparent longitudinal stability of the airplane was determined from stabilized flight data for two center-of-gravity locations, 26-percent and 30.3-percent mean aerodynamic chord (figs. 14 and 15). Two levels of longitudinal stability are shown in the data for the 26-percent location (fig. 14). Approximately 0.5° of longitudinal control produces approximately 1° of angle of attack change at low angle of attack, whereas in the higher angle of attack range approximately 1.4° of longitudinal control results in a 1° change in angle of attack. The airplane has more apparent longitudinal stability at the higher angles of attack, certainly a desirable design feature. Comparison of the flight data with low Reynolds number (0.8×10^6) wind-tunnel data obtained from two stabilizer settings, 0° and -25°, on the 10-percent scale model shows generally good agreement.

Data for the center-of-gravity location of 30.3 percent (fig. 15) show the expected decrease in longitudinal stability as compared to the data for the 26-percent location. However, there is a trend toward a further change in stability at the extreme positive angles of attack, indicating a decrease in longitudinal stability from $\alpha = 30°$ to $\alpha = 40°$. Also, the stability near zero angle of attack is less than that for the 26-percent location. At negative angles of attack, a small region of instability was indicated; however, at angles of attack less than -14°, the airplane model

apparently became stable, so that the maximum achievable steady-state angle of attack was approximately -20°.

The longitudinal stability data for the 30.3-percent center-of-gravity location are compared with unpublished full-scale flight data in figure 15. Although the agreement is not exact in the midrange of angle of attack, the trend is closely predicted by the large-scale model which has blocked inlets and no thrust. Inlet angle alone could alter the exact trim. The measurement of angle of attack is discussed in a later section.

Two flights were made with the center of gravity at 38.5-percent mean aerodynamic chord. The model controllability was not good, so apparent longitudinal stability data could not be obtained. Some stability and control derivatives for an angle of attack range of 40° to 50° were obtained by using digital analysis methods and are presented in reference 4.

Pullups and Turns

The first several maneuvers to investigate departure were made with a center-of-gravity location of 26-percent mean aerodynamic chord with the MCS. The first maneuver (fig. 16) was started with a 2g pullup to about 30° angle of attack and a right roll to a bank angle of about 100°. As the roll developed, the airplane pitched down through -90° and was recovered by completing the roll to an upright attitude. Although the maneuver was rapid, no deliberate control disturbances were made. The aileron-to-rudder interconnect provided the commanded rudder control. The second maneuver was made with computer direct controls. A pullup with an overshoot to about 38° angle of attack and 2.3g was made with rapid control commands. The airplane motions were oscillatory, although only small aggravating roll control was commanded. Recovery was simple and straightforward by relaxing back pressure on the control stick. A third maneuver was made to an angle of attack of 30°, again with the computer direct controls (no augmentation). Some roll control was commanded and, through the aileron-to-rudder interconnect, some rudder control. The heading and angle of attack show no evidence of departure, and recovery was prompt when commanded.

Figure 17 shows data from three rapid pullups with overshoots in angle of attack to about 37°. The MCS was used for all three maneuvers. With no augmentation the maneuvers were oscillatory, but recovery was immediate when commanded. The first and third pullups were accompanied with aileron and aileron-to-rudder interconnect commanded rudder disturbances, yet there is no evidence of departure. The second maneuver was a longitudinal control pullup to 2.3g. From these tests, controllability seemed to be good at high angle of attack. Additional damping would have been appreciated by the pilot. The actual flight maneuvers were similar to motions predicted by simulation.

Experience With Simple Rate Damper System

As might be expected, the airplane was predicted to be less controllable at very high angle of attack. Although a simulated mechanization of the actual model control

system was used during most of the program, a mechanization of simple rate feedback damper augmentation was used during the recording of data for stability and control derivative determination. The δ_d roll control was used for roll damper control inasmuch as its roll effectiveness was satisfactory at high angle of attack; however, its yawing moments due to control deflection were greater than desired. It was recognized that the roll-control-to-rudder interconnect was necessary, so it was also mechanized. However, at high angle of attack the rudders were ineffective and the needed coordinating yawing moment from the rudder was not provided for the roll control. Several divergences occurred while the pilot was attempting to stabilize the airplane model for stability and control maneuvers. Some, but not all, of the divergences appeared to be either induced or reinforced by roll control; however, the pilot did not attempt "tight" control once the stability and control sequence (frequency sweep, for instance) was initiated. In some instances the stability and control sequence may have prompted the divergence. Recovery from the divergences was simple and straightforward by reducing angle of attack to more stable and controllable conditions.

Figure 18 illustrates one of these divergences. An attempt was made to stabilize and hold the wings level at an angle of attack of approximately 30°. At that angle of attack, C_{n_β} and C_{l_β} were negative but $C_{n_{\beta,dyn}}$ was positive, which indicates positive dynamic lateral-directional stability. Figure 18 shows that a left yaw and roll produced right sideslip that was countered by right roll control and rudder (although ineffective) from the damper system. The roll control produced sideslip, which produced more roll requiring more roll control, which produced more sideslip. Recovery was made by pitching over to a lower angle of attack. Shown in the differential stabilator time history (fig. 18(c)) is a frequency sweep used to obtain data for analysis for stability and control derivatives.

Poststall Gyrations

Data format.—The time histories of poststall gyrations and spins in figures 19 to 31 include angles of attack and sideslip; pitch, bank, and heading attitudes; pitching, rolling, and yawing angular rates; and longitudinal, lateral, and vertical accelerations at the center of gravity. The time histories also include commanded stick and pedal positions, surface deflections, pressure altitude, forward velocity derived from a standard pitot head measurement, and dynamic pressure. At the extreme angle of attack the airspeed pitot head was unable to sense the velocity accurately. Because velocity was used to correct the indicated angles of attack and sideslip for body angular rates, an alternate method of obtaining velocity was required.

Angle corrections.—During simulation of spins it was noted that when a developed high angle of attack spin occurred, the airplane model descended at a constant dynamic pressure and that minimum dynamic pressure was approximately 1200 N/m^2. Velocity was calculated from the minimum dynamic pressure for the altitude derived from the airplane model static pressure source. The velocity was then used to correct the indicated angles of attack and sideslip for pitch rate and yaw rate, respectively. The angle of attack was corrected for location by using the equation $\alpha = (0.93\alpha_i + ql/V)$ for angles of attack less than 32°. For angles of attack greater

than 32°, no upwash correction (0.93) was made, inasmuch as the model wing was completely stalled. Therefore, the angle of attack was corrected only for location. The angle of sideslip was corrected by using the equation $\beta = (0.96\beta_i - rl/V) \cos \alpha$.

As previously stated, the attitude angles presented are referenced to the earth reference as seen by the pilot in the airplane. Steep nose-down attitudes were necessary to achieve the desired airspeed; therefore, bank, heading, and pitch attitude were updated when $\theta = -90°$ as it would occur with a flight attitude indicator. For example, for a split-S type of maneuver with a rollover to inverted flight and a pullthrough to vertical descending flight, the heading and bank angle were switched 180° as the airplane model pitched through -90°.

Spin attempts.—Both flight and simulation of flight had shown the configuration to be departure resistant, so techniques were considered to force the model to depart with the center of gravity at 26-percent mean aerodynamic chord. Time histories of the first attempt to force a departure are shown in figure 19. A pullup to maximum angle of attack was made with the CAS. Full left rudder was held while left roll and then full right roll were commanded. As back stick was released, the airplane pitched down to approximately 20° angle of attack, and pitch attitude reached -90°. With full right roll, left yaw, and near neutral pitch control, the airplane yaw rate reached 30 deg/sec. The airplane recovered to a steep nose-down attitude with angle of attack averaging 30° and entered a high-speed spiral. The motion became more oscillatory as five turns were completed before recovery controls were commanded. Full roll and yaw control produced recovery in one turn. Approximately 200 meters of altitude were lost during a 5-second turn. The maneuver was performed near maximum lift with a -60° pitch angle. The control system downmoded to the MCS as it should have as yaw rate barely reached the downmode limit; however, after recovery the pilot selected the CAS again.

A second attempt to spin resulted in the maneuver presented in figure 20. After full back stick was commanded, full right rudder was applied, followed by full left roll command. The CAS remained engaged throughout the maneuver, the airplane maintained an angle of attack of approximately 30°, and yaw rate increased to approximately 20 deg/sec. As longitudinal back stick was released, the model recovered to an angle of attack of approximately 23°. Yaw rate increased to approximately 36 deg/sec, and the airplane completed a two-cycle spiral before the recovery altitude was reached and the drogue parachute was automatically deployed. Recovery was immediate, in less than one turn. The yaw rate did not reach the value (42 deg/sec) at which the CAS would automatically downmode to the MCS.

Erect Spins

High g entry; basic configuration.—After attempts to spin with the center of gravity at 26-percent mean aerodynamic chord resulted in poststall gyrations, the center of gravity was moved to 30.3-percent mean aerodynamic chord, the approximate rearward limit for the full-scale airplane. At this center-of-gravity location, the high *g* entry technique resulted in departures and spins much of the time. The airplane was rolled inverted, pulled through to vertical descending flight ($\theta = -90°$), and, at the desired airspeed, pulled rapidly to high angle of attack and normal

acceleration while full rudder and opposite full roll control were commanded and then full back stick was relaxed to neutral longitudinal control. Examples of erect spins accomplished by using this technique are shown in figures 21 to 26.

As used in this report, a spin is identified by the stabilized maximum angle of attack or the frequency or time per revolution of the spin, or both. The basic spin mode is defined by these same characteristic measurements, but the airplane model in a basic spin mode is stabilized in a spin with the controls neutral. There are no control moments contributing to nor subtracting from the spin momentum.

The spin entry maneuver was a relatively violent maneuver (fig. 21), even for a remotely piloted vehicle. From inverted flight the nose was allowed to drop to near vertical descending flight where a rapid pullup from 0g to 4g in about 0.4 second produced an overshoot in angle of attack of approximately 63°. The spin entry was extremely oscillatory with the rapid control changes commanded; however, the motions damped to a high angle of attack spin with a near vertical descent flightpath angle. The spin stabilized at an angle of attack of approximately 80° and a yaw rate of approximately 120 deg/sec, producing a turn in about 3 seconds. The rate of descent was indicated to be about 120 meters per turn.

The magnitude of the inertia coupling that produced the large angle of attack is indicated in figure 21(b). Roll and yaw rates are usually of the same sign during spin maneuvers and make up a multiplier for the inertia differences which produces the pitchup moment. In this maneuver a multiplier of about 2.5 was produced which drove the angle of attack to 80° and produced the spin at high angle of attack.

Figure 21(c) shows histories of the pilot's control motions and the actual airplane surface motion. The maneuver was started with the CAS operating. The initial buildup in yaw rate was sufficient to downmode the control system to the MCS (no feedback loops). This also resulted in more restricted control authority, as previously discussed. Feedback loops are normally designed to oppose unwanted airplane motions, yet roll control opposing spin motion usually augments the spin with a roll control that produces a yawing moment opposite the sign of the rolling moment it produces. With controls neutral, the spin shows some tendency to recover to a lower yaw rate, and with roll control in the direction of the spin, the recovery yawing acceleration produced a recovery in four turns.

Figure 21(d) shows longitudinal acceleration, velocity, altitude, and dynamic pressure during the spin maneuver. Minimum dynamic pressure was assumed and velocity was computed for the high angle of attack conditions during the spin.

Repeated spin; basic configuration.—The spin maneuver of figure 21 was repeated by another pilot and was accomplished as planned. The same entry technique was used to enter the spin (fig. 22). The forward movement of the longitudinal control was somewhat more deliberate and the oscillatory motions were not as large in amplitude nor did they persist as long, although the maneuver was made at about the same altitude. The maximum yaw rate was approximately 120 deg/sec, and the angle of attack reached approximately 80° to 81°, about the same as during the previous spin. The basic spin was the same, and the time per turn was similar, approximately 3 seconds.

The control technique used for recovery was full roll control with the spin, with the aileron-to-rudder interconnect providing approximately 3° of rudder. This technique produced a slightly faster recovery during this spin maneuver, although it is doubtful that the difference is significant. The rate of descent during the spin (fig. 22(d)) was nearly the same as that for the first spin. The only significant difference was the lower amplitude oscillation in pitch, roll, and yaw excited by the control inputs. The time base of the longitudinal control pullup and release of the second maneuver was approximately 8 seconds, compared to 4 seconds for the first spin. A decrease in yaw rate was indicated when the controls were neutralized during the fully developed part of the spin, and full roll control with the spin produced recovery in about three turns.

Lower altitude entry; basic configuration.—The high g entry technique was used to enter a spin with the basic configuration at an altitude of 9500 meters (fig. 23). This was the second spin during the flight and was entered at a lower airspeed than the first spin. Control manipulation was similar; however, the buildup in yaw rate was slower. The yaw acceleration generated was only about half that of the spin shown in figure 21 and only one-quarter of that in figure 22. The airplane model did reach the high angle of attack (approximately 80°) and 120 deg/sec yaw rate previously obtained. The pilot started to abort this attempt, removing the roll control briefly, but then decided to continue the maneuver. A high yawing acceleration (approximately 5 deg/sec^2) was generated. Maximum angle of attack was approximately 80°. Pro-spin controls were held until the recovery parachute was commanded. The airplane model had recovered to an angle of attack of approximately 40° by the time the parachute was effective. Neutralizing the controls in combination with the disturbance caused by deploying the parachute resulted in recovery from the spin in about three turns. The altitude lost per turn was only about 70 percent of that for the high-altitude spins. With the piloting technique used for this maneuver, the only effect of altitude appeared to be a definite indication of greater yaw deceleration with neutral controls than at the higher altitude. The simulator predicted that the airplane would be somewhat more resistant to spin and would recover more rapidly at lower altitudes.

1g entry; production configuration.—As shown in figure 24, full back stick placed the airplane at about 42° angle of attack at about 1g, and full right roll control and left rudder were commanded. As back stick was relaxed, the airplane tended to recover in angle of attack, but then pitched down and rolled left as yaw rate increased. At the 1g condition, the forward velocity was lower than in the high g entries, and yawing acceleration generated by the yawing moment forcing the spin was one-half of that generated during the high g entries, or less. Note that the airplane motions were not in equilibrium, inasmuch as there was an immediate drop in yaw rate as soon as the controls were removed. Maximum yaw rate was approximately 95 deg/sec, which produced an average angle of attack of approximately 75°. Minimum time per turn was about 3.7 seconds, about 25 percent greater than expected from the previously determined steady-state spin characteristics.

The first application of recovery control showed a potential for rapid recovery, giving a yawing acceleration of approximately 6 deg/sec^2 using full roll control and finally full rudder control. However, the pilot allowed the stick to command 6° of δ_e (airplane nose down), which severely restricted the differential stabilator

deflection that could be commanded (fig. 24(c)). Only a 0.9 deg/sec^2 recovery yawing acceleration was obtained, and the recovery was slow. The spin persisted for six or seven turns before recovery to low angle of attack was achieved. The poor recovery technique of moving the stick too far forward, which limited the roll control that could be commanded during the spin, resulted in low recovery yawing moments. The initial altitude of the spin was approximately 13 000 meters, and the rate of descent was approximately 140 meters per turn.

High g entry; production configuration.—A high g entry spin was attempted at an altitude of about 10 000 meters (fig. 25). The entry maneuver was particularly violent, inasmuch as it was attempted soon after recovery from a previous spin. After a pushover to $-2.8g$ and a pullup to $5g$, full cross roll and yaw controls were commanded, and the stick was moved forward. This resulted in a spin with a maximum yaw rate of 78 deg/sec with an angle of attack of 65° to 75°. The minimum time per turn was 4.2 seconds. Recovery controls were commanded at this point, and the recovery yawing acceleration was about 4.5 deg/sec^2, about 50 percent higher than the acceleration that forced the spin. Recovery was rapid, requiring less than two turns. The recovery illustrates the importance of commanding full roll control with the spin as a recovery device. Longitudinal stick position was nearly neutral, which allowed the full differential stabilator deflection of 12° to produce the required recovery yawing moment. The altitude lost per turn was consistent with that lost in some of the other maneuvers, about 150 meters per turn.

MCS controls; production configuration.—Although normal "flying" on the simulator early in the program showed that the airplane could not be spun with MCS controls, a method was developed later that produced spins on the simulator. The technique required that the airplane be slowed to steady flight, rolled 90°, and the nose allowed to fall through to near vertical nose-down flight. At vertical nose-down flight, simultaneous rudder and opposite roll control were commanded with fixed longitudinal control. This approach was used to obtain the spin shown in figure 26. Holding left rudder and right roll control produced an initial yaw rate of about 30 deg/sec and an angle of attack of 32°. An adjustment to slightly forward of neutral longitudinal stick position resulted in greater roll and yaw control, an increase in yaw rate to about 100 deg/sec, and a flat spin at an angle of attack of about 80°. The yaw rate appeared to be nearly stabilized at 100 deg/sec and the minimum time per turn was about 3.5 seconds when the controls were neutralized and the airplane model was allowed to stabilize in the spin. The yaw rate stabilized at about 60 deg/sec, and the time per turn was about 5 seconds. The airplane model was stable in this spin mode of approximately 61° angle of attack for seven turns before recovery controls were commanded, which showed a definite basic spin mode at that angle of attack and time per turn. These results are in good agreement with results from experimental tests on a 13-percent-scale model by C. E. Libby and E. L. Anglin of the NASA Langley Research Center. The altitude lost per turn for the spin was about 110 meters.

Both the entry and the recovery are interesting from the standpoint of control usage. Note that 14° of rudder, 32° of δ_a, and 10° of δ_d resulted in a yawing acceleration of 4 deg/sec^2; 17° of rudder, 38° of δ_a, and 11° of δ_d produced a yawing acceleration of about 6.3 deg/sec^2. For recovery from the spin, 40° of δ_a, 11° of δ_d,

and 2° of rudder resulted in a recovery acceleration of 6.3 deg/sec^2, indicating, as expected, that the rudder control was ineffective at the high angles of attack.

Inverted Spins

In an attempt to make inverted spins (fig. 27), the airplane model was rolled inverted and trimmed to full forward stick, which resulted in about -1g at an angle of attack of approximately -22°. At this condition full right rudder and left roll were commanded through the CAS. Only about 7° of aileron and almost no differential stabilator deflection were obtained. These controls and the rudder produced a yaw rate of about 43 deg/sec, resulting in an angle of attack of approximately -58°. The time per turn was about 6 seconds. By using the technique that provided additional yawing moment to force the erect spins, the longitudinal stick was moved rearward to provide additional differential stabilator deflection, and the roll control was reversed to right roll, since the derivatives for the airplane at large negative angles of attack were unknown. The rudder remained at full right deflection with full right rudder pedal command. With these control deflections, the yaw rate decreased to about 32 deg/sec and the angle of attack increased to -42°, indicating that the yawing moment due to right roll control may be negative. Commanding left roll and forward stick did not recover the yaw rate and angle of attack reached at the beginning of the maneuver. It appears that the roll control was relatively ineffective and that the yaw resulted primarily from the rudder deflection. Full forward control aided somewhat in forcing the angle of attack to the large negative angle of attack. The airplane model recovered in less than one turn when the controls, primarily the rudder, were neutralized.

A second maneuver was performed using essentially the same technique with similar results (fig. 27, $t \approx 80$ sec). A yaw rate of about 41 deg/sec produced an angle of attack of approximately -54°. Pitch and roll control reversal reduced the yaw rate to about 34 deg/sec and the angle of attack to approximately -38°. The yawing moment of the roll control appears to be opposite the yawing moment of the rudder control but of a relatively low magnitude compared to that of the rudder control. When the controls were suddenly neutralized, recovery was rapid, in less than one turn. The yawing acceleration in nondimensional coefficient form would be approximately 0.05, about the magnitude of estimated $C_{n_{\delta_r}}$ $\delta_{r_{max}}$ at low angle of attack.

For forward stick position the roll-control-to-rudder interconnect was designed to command positive rudder for positive roll control based on positive yawing moment due to roll control. However, the data in figure 27 as well as the stability derivatives calculated from the flight data indicate that the yawing moment due to roll control may be negative at an angle of attack less than -20°. If the yawing moment due to roll control were positive, the recovery controls would be left roll control as well as left rudder for recovery from a right inverted spin. It appears, however, that the use of the roll control to recover from inverted spins may be academic, inasmuch as the rudder control is the dominant recovery control and the roll controls were relatively ineffective.

These maneuvers (fig. 27) illustrate that a good recovery can be achieved with the correct recovery technique. Neutralizing the rudder deflection produced

immediate recovery; however, the mechanization of the roll-control-to-rudder interconnect, made it possible to command rudder by either roll control or rudder pedal. The mechanization commanded positive rudder for positive roll with forward stick positions and negative rudder for positive roll with rearward stick positions (fig. 7). Therefore, it is important that the pilot neutralize the longitudinal stick to insure that the rudder commanded will be of the proper sign for recovery. It should be noted that these maneuvers were rudder-initiated and would be of consequence only if attempted at low altitude, since about 240 meters were lost per turn.

The inverted spin maneuvers were repeated (fig. 28) by another pilot. The CAS was used and the system downmoded to the MCS as expected. The airplane model was stabilized and rolled to an inverted attitude. With full nose-down longitudinal control, full left roll and right rudder were commanded. Thirty degrees of rudder and 7° of aileron resulted. The airplane right yaw rate increased to approximately 60 deg/sec, which resulted in an angle of attack of -72°. The time to complete a turn was about 5.4 seconds. Several momentary attempts were made to recover, but controls were not held long enough to be completely effective. The angle of attack and yaw rate did decrease with each recovery attempt. Finally, a longitudinal pullthrough (nose up to the pilot when inverted) reduced the angle of attack, and yaw rate immediately decreased. The recovery yawing acceleration was high, higher than the maximum control moment available to the pilot. The spin was relatively flat with a low value of dynamic pressure and a rate of descent of about 270 meters per turn.

Recovery from the maneuver was followed by an entry into another similar maneuver. Although a similar control technique was used, the airplane did not stabilize at as high a rate of yaw or angle of attack. The time per turn was slightly longer, but the maneuvers were similar, and the airplane recovered almost immediately with recovery control. Full rudder was commanded by the pilot initially but was relaxed during the maneuver. The rudder command remained until the roll command was relaxed when the rudder was removed by the interconnect (fig. 28(c)). Yaw rate decreased with the removal of the rudder, but the yaw rate decrease was more dramatic with the "pullup" by longitudinal control. It appears that the lower altitude and higher dynamic pressure did not permit the airplane yaw rate and angle of attack to reach as high a value during the second spin maneuver as during the first.

The previous spins were entered at about -1g with the control stick trimmed to the maximum forward position. The maneuver in figure 29 shows a rapid "pullup" to -2.0g with full roll control and with the roll-control-to-rudder interconnect commanded rudder. Thirty degrees of rudder and 7° of aileron resulted. About 27 deg/sec of yaw rate and -42° of angle of attack were reached. The time per turn was approximately 8 seconds, and the rate of descent was approximately 250 meters per turn. This maneuver appeared to be more of a spiral at high velocity and dynamic pressure than the other maneuvers. Recovery required less than one turn.

These time histories show that the inverted maneuvers were obtained by several techniques, and that the rudder was the primary initiating and recovery control. The maneuver at the highest altitude (approximately 17 000 meters) was similar to a spin, whereas the maneuver at the lower altitude (approximately 10 000 meters) appeared to be more nearly a spiral.

Effectiveness of the Stall Inhibiter

The in-flight check of inhibiter effectiveness included an attempt to spin by using the high g entry technique (fig. 30) with the model center of gravity at 30.3-percent mean aerodynamic chord. The technique involved a quick pullup with maximum back stick to an angle of attack of 54° and 4g normal acceleration with simultaneous application of full left rudder control and right roll control. The resulting motion was a complete roll to the left with a pitchover to nearly a nose-down vertical attitude. The technique required the pilot to relax back stick force while holding right roll control. The pilot appeared to hold back stick longer than on some previous flights, which resulted in less roll and yaw control to force the airplane to rotate. The effects of the angle of attack and pitch rate on longitudinal control position are shown in figure 30(b). At t = 48 seconds the yaw rate reached the CAS trip level and the stabilator angle commanded reverted to the pilot commanded angle when the inhibiter switched out as the CAS downmoded to the MCS. The yaw rate then reached only about 36 deg/sec and angle of attack was only 38° to 42°. The airplane was in a diving spiral, as evidenced by the large pitch angle, high airspeed, and high dynamic pressure (fig. 30(d)). Neutralizing the controls resulted in immediate recovery.

A second attempt (fig. 31) was made to spin the airplane with the inhibiter active using a technique developed on the simulator that allowed a spin to be entered during slow, gradual maneuvering. The airplane was rolled to -90° bank angle and the airplane nose was allowed to drop to -90° pitch angle where full rudder and opposite roll control were commanded. The longitudinal control was held nearly constant. A yaw rate of approximately 40 deg/sec was forced, and an angle of attack of approximately 40° resulted. The pushover command of the inhibiter is shown in figures 31(a) and 31(c) during the increase in angle of attack. Neutralizing the roll and yaw controls resulted in recovery in less than one turn. The data indicate a spiral rather than a spin, large pitch angle, high normal acceleration, and high dynamic pressure. The inhibiter was designed to be active only when control was in the CAS mode, since the airplane was more resistant to departure/spin in the MCS mode. From these flights it appears that the inhibiter performed as designed, preventing spins even during attempts to force the model to depart and spin.

Predicted Airplane Basic Spin Characteristics

Fifteen spin attempts were recorded at simulated altitudes from 15 500 meters to 9150 meters. Six resulted in erect spins, five in inverted spins, two in poststall gyrations, and two in inhibiter-prevented spins. For most of the tests the airplane model center of gravity was at 30.3 percent and the weight and inertia characteristics were generally similar (table 3). The airplane model was resistant to departures and spins; however, one of the erect spins resulted in a stabilized spin mode with the controls neutral (fig. 26). Another spin (fig. 21) appeared to be stabilized during the short time the controls were neutral. These two maneuvers indicate a basic spin mode at a medium-high angle of attack (approximately 61°) that required 5 seconds to turn, and a possible basic spin mode at a high angle of attack (approximately 80°) that required 3 seconds to turn (fig. 32). Time histories of the maneuvers are presented in figures 21 and 26. The flightpath angle of each maneuver was

approximately -90°. The angles of attack were high, and the pitch angles were relatively small. The airplane model descended nearly vertically. Additional spin characteristics obtained during the program are included in figure 32 for the two airplane model configurations, basic and production. Since the controls were used to augment the yaw rate obtained, the rate and subsequently the angle of attack achieved depended on the amount and duration of the control deflections. The mid-range data were purely the result of the piloting technique. The maneuvers were performed at different altitudes with the two different airplane configurations. However, the complete set of stability and control derivatives obtained during the program showed no significant differences between the derivatives for the two configurations. Therefore, the results presented subsequently will not be distinguished by configuration.

Studies of spins analytically and on piloted simulators show that the stabilized spinning airplane will descend at constant dynamic pressure and constant spin rate (discussed more fully later). Only aerodynamic damping changes during the descent. The basic balance of inertial and aerodynamic moments that stabilized the airplane at the high attitude and at the high rotational rate remains unless disturbed, inasmuch as the aerodynamic damping moments are usually small compared to the inertial moments. Therefore, it appears that the effect of altitude on the stabilized spin characteristics may not be as important as might have been expected from the scaling laws (table 2).

Correlation With Smaller Scale Model Test Results

The 3/8-scale model tests and the Langley Research Center 13-percent-scale model test program were conducted with similar objectives: to evaluate the spin entry, spin, and spin recovery characteristics of a modern swept-wing fighter aircraft design. Tests were also conducted in the NASA Langley Research Center Spin Tunnel to determine the fully developed spin and recovery characteristics of the same design.

The results from both the 3/8-scale and the 13-percent-scale tests indicate that corresponding full-scale aircraft will be spin resistant but that spins can be obtained with some control techniques. The spin and recovery data obtained by all three test techniques indicate that two erect spin modes are possible on the airplane: a mode with an angle of attack of approximately 80° and a spin rate of about 3 seconds per turn; and a mode with an angle of attack of approximately 55° to 65° and a spin rate of about 5 seconds per turn. A comparison of the time histories of figure 26 and figure 33 shows excellent correlation between the 3/8- and 13-percent-scale model data. In figure 26 the 3/8-scale model maneuver was initiated with a pullup to about 32° angle of attack where cross roll and yaw controls were applied. As the yaw rotation started, the control stick was eased forward while full roll control was held to promote the spin. The yaw rate increased to approximately 105 deg/sec and the angle of attack to approximately 80°. The spin rate was about 3 seconds per turn. When the controls were neutralized, the airplane model stabilized in a basic spin mode. The yaw rate decreased to approximately 60 deg/sec and the angle of attack decreased to approximately 60° with a spin rate of about 5 seconds per turn.

The results in figure 33 for the 13-percent-scale model show remarkably good agreement with the 3/8-scale model results. The peak yaw rate was approximately 110 deg/sec with a spin rate of about 3 seconds per turn. The angle of attack was approximately 80°. When the controls were neutralized, the model stabilized in a spin mode with a yaw rate of approximately 60 deg/sec and a spin rate of about 5 seconds per turn. The angle of attack was approximately 60°. In both spins, recovery was rapid by commanding full roll control in the direction of the spin.

Comparisons of the model test results are shown in figure 34. As summarized in table 3, scaled altitudes for the tests ranged from approximately 7600 meters to 15 700 meters. Center-of-gravity positions differed from 24-percent to 30.3-percent mean aerodynamic chord for the data presented. Despite the different test conditions, the predicted variation of spin angle of attack as a function of time per spin turn appears to be well defined, and the agreement of the basic spin mode data is considered to be excellent.

The inverted spin data obtained with the 3/8-scale airplane model were not as well defined as the erect spin data. The airplane model became stable at large negative angles of attack, and consequently a large inertial moment was required to decrease the angle of attack. During inverted flight, full rudder and roll control produced gyrations that resulted in an angle of attack of approximately -45° with a time to turn of about 8 seconds, and an angle of attack of -70° with a time to turn of about 5 seconds. At similar test conditions the Langley Spin Tunnel data predicted airplane inverted spins at an angle of attack of 40° to 50° with a time to turn of 8 seconds and at an angle of attack of 70° to 80° with a time to turn of 4 to 3 seconds. These correlations are considered to be good, inasmuch as it is known that the Spin Tunnel underpredicts spin rate for very flat spins.

Spin Simulation

Although only limited data were obtained during the large-scale model flight program, a complete simulation was mechanized to support the program. The simulation had six degrees of freedom with body axis differential equations representing linear and angular acceleration of the body center of mass. Airplane symmetry about the X-Z body plane and no change in airplane mass were assumed. The airplane model had no thrust. Airplane absolute value of angle of attack was less than 90°, and angle of sideslip was less than 40°. There were no small-angle approximations.

Aerodynamic data for the full-scale airplane were obtained from tests in the Langley Full-Scale wind tunnel and the NASA Ames Research Center's 12-Foot Tunnel. Data tables of force and moment coefficients were generated from the wind-tunnel data in 5° angle of attack and sideslip increments. Dynamic derivatives were programed as functions of angle of attack only at increments of 5°. Only low-speed data were used; Mach effects were not considered.

The first several attempts to spin the airplane model on the simulator were unsuccessful. The simulation predicted that the airplane configuration would be spin resistant. This prediction agreed with the results of the Langley 13-percent-scale model tests.

Persistent spin attempts in some maneuvers which might be considered to be abusive to a full-scale airplane produced two methods of control application which consistently resulted in spins. Although the first few spins on the simulator appeared to the pilot (or engineer observer) to be similar to the spins subsequently achieved in flight, closer scrutiny showed differences between the flight and simulated spins. The original approach to verifying the simulated spin was to use actual flight control surface deflection time histories as inputs to the simulator. The resulting simulated airplane motions were unlike the flight motions because as time increased and actual airplane model motions diverged from predictions, the control motions became inappropriate to the actual flight condition. However, there was a need for a simulated spin capability, inasmuch as it is always impossible to completely document the behavior of an airplane in a spin during flight tests. Attempts to compute flight spins continued by returning to comparisons of piloted simulated spins and flight histories rather than calculated responses to actual flight control motions that had resulted in flight spins. With this approach, the continual updating of the simulation aerodynamics with flight data together with a small change in yaw damping derivative at high angle of attack produced simulated spin histories which had the character of flight-recorded spins. These simulated spins may provide information applicable to airplane configurations that are spin resistant, even though it may not be generally applicable to configurations with the usual departure and spin characteristics.

Figure 35 presents data from a piloted, simulated spin which was made in an attempt to duplicate the spin of figure 22. Airspeed was bled off to approximately 200 meters per second when the airplane was rolled inverted, and a pushover was made to increase speed to approximately 300 meters per second. A quick pull-through to a maximum acceleration of about 4.6g was made and, as the stick was moved forward, full roll and rudder were commanded. Pitch rate peaked at approximately 61 deg/sec, as it did in actual flight. Maximum roll rate was approximately 67 deg/sec, whereas the flight value was 100 deg/sec. The buildup in yaw rate was steady at about 5.6 deg/sec^2, whereas the flight value was about 7.9 deg/sec^2. The maximum yaw rates were about equal at approximately 122 deg/sec. The minimum time per turn was about 3 seconds, the same as the flight value. The average maximum angle of attack was approximately 77° for the simulated flight, whereas the flight value was approximately 80°. The simulated recovery required about 15 percent longer than the flight recovery. The rates of descent were comparable, and simulated minimum dynamic pressure was approximately 1000 N/m^2. This quantity was not measured accurately during the flights at high angles of attack. In general, the simulated spin record is considered to be comparable to flight, thus providing confidence that spins can be simulated with what has become a standard simulation mechanization for flight research.

Effect of altitude.—The capability of simulating the spin of the model airplane provided the means for investigating the effect of altitude on spin characteristics and control. The simulated behavior of the airplane model in a spin from approximately 15 200 meters to 600 meters is shown in figure 36. The high g entry technique was used to spin the model in the high angle of attack mode. The controls were neutralized at $t \approx 83$ seconds, and the model stabilized in the spin and descended in the same spin mode until the maneuver was terminated. The initial time per turn at approximately 12 200 meters altitude was about 2.8 seconds, and

yaw rate was about 122 deg/sec. After 5 minutes of spinning to below 1520 meters, the time per turn was about 2.9 seconds and the yaw rate was about 116 deg/sec. Spin angle of attack was constant at approximately 78°. Dynamic pressure was constant at approximately 1000 N/m^2 for the entire stabilized part of the spin with the controls neutralized, and velocity decreased with altitude. This spin maneuver was piloted, and the spin entry closely simulated the actual model flights shown in figures 21 and 22.

The airplane model with a center-of-gravity location of 30.3-percent mean aerodynamic chord could be forced into a high angle of attack spin at any altitude. The technique had to be more exact at the lower altitudes in order to force the spin. A medium-high angle of attack spin was more likely at low altitude. The increase in damping at low altitude made it more difficult to force the airplane model to a high angle of attack. Recovery from either a high or a medium-high angle of attack spin was rapid with recovery controls at all altitudes. The airplane model recovered more rapidly at low altitude than at high altitude and at times recovered with the controls neutral. The airplane model usually recovered from oscillatory spins without recovery controls at low altitudes.

Effect of longitudinal stability.—Moderate changes in static stability (to more stability, center-of-gravity change of 0.05) did not change the ability of the simulator pilot to spin the airplane model. High angle of attack spins could be readily forced; however, the motions were more oscillatory (lighter damping) and, consequently, the model was more likely to oscillate out of the spin and recover. Attempts to spin were more likely to result in medium-high than high angle of attack spins, and very stable configurations usually spiraled rather than spun.

A recent study (ref. 7) considered the effect of a large change of stability (center-of-gravity change of 0.20) on the calculated spin characteristics of a model. These results indicated that the effect of the stability change was significant but not large. The difference in spin angle of attack was small (82° to 85°). The spin of the more stable case was much more oscillatory (lower damping) than that of the less stable case. The primary effect of stability on the spin was in susceptibility to spin, the mode of spin that could be forced, and the oscillatory nature of the spin maneuver. The basic mode characteristics were similar for the changes considered in this report.

Predicted Stability and Control

Stability criteria.—Although the large-scale airplane model was departure/spin resistant, control techniques were developed that produced spins. The controllability was poor at angles of attack greater than that at which the wing stalled; however, the airplane model could be controlled through the CAS. The roll control through the horizontal stabilator was effective, but a roll-control-to-rudder interconnect was essential for controlling the yaw generated by roll control. At present there are no accepted criteria for good stability and control at extremely high angles of attack. Some have been proposed, but further correlation with flight data is needed. Thus, since the large-scale model stability and control characteristics as well as controllability were determined during this program, comparisons were

made with proposed criteria to provide some insight into the effectiveness of the criteria.

The importance of the dynamic directional stability parameter, $C_{n_{\beta,dyn}}$, for stability at high angle of attack is indicated in several studies (refs. 8 and 9, for example). Comparisons of this parameter derived from four tests of airplane models are presented in figures 37, 38, and 40. Figure 37 gives the values for the 3/8-scale flight tests and shows data up to an angle of attack of 53° for trimmed flight conditions at low speed. The basic data were obtained at altitudes from 6000 meters to 12 000 meters and Reynolds numbers of approximately 4×10^6 for a clean configuration model with inlets drooped 11°. Faired variations of C_{n_β} and C_{l_β} are presented; detailed data are given in reference 4. The derivative C_{n_β} is positive up to approximately 20° angle of attack, and the C_{l_β} derivative remains negative through the angle of attack range covered, with some relatively minor variations. Combining these derivatives by using the abbreviated formulation of

$$C_{n_{\beta,dyn}} = C_{n_\beta} \cos \alpha - \frac{I_Z}{I_X} \sin \alpha C_{l_\beta}$$

(from ref. 8) resulted in a generally increasing parameter with angle of attack. Although a dip is indicated, no reversal in sign for the parameter was indicated, so the airplane was predicted to be stable to the test limit of $\alpha = 53°$. This generally supports the stability observed during the model flights.

The flight data obtained with the large-scale airplane model were the most complete recorded in a NASA Flight Research Center flight test program; however, the data coverage was not continuous so some judgment was required in fairing the results for analysis. At near maximum lift ($\alpha = 35°$ to 40°) the airplane model controllability was less satisfactory than at lower and higher angles of attack. Small control commands or perhaps atmospheric disturbances appeared to cause significant changes in vortex shedding which influenced the flow around the vertical tails, thus changing the level of directional stability. This was evident in the flight data for angles of attack of 35° to 40°. The fairings in figure 37 are based on the "highest confidence" data, but additional acceptable data are represented by the crosshatched region. The calculation of $C_{n_{\beta,dyn}}$ shows the predicted lateral-directional stability of the airplane model, including the most pessimistic prediction, to be good throughout the angle of attack range.

Figure 38 shows similar parameters derived from 10-percent- and 7.5-percent-scale model tests at Reynolds numbers of approximately 0.8×10^6 in the Langley Full-Scale wind tunnel and approximately 4×10^6 in the Ames 12-Foot Tunnel. Some of these results indicated significant effects of horizontal control surface position, inlet cowl position, and simulated power on the lateral-directional stability of the model configuration. An attempt was made to select data applicable to the present

tests for presentation (stabilator position, for example). Both the low and high Reynolds number wind-tunnel test results showed nonlinear rolling moments with angle of sideslip in the region of maximum lift, where the wing would be stalled (for example, see fig. 39). Determination of bounds for the low Reynolds number roll-due-to-sideslip derivatives in the $\alpha = 30°$ to $35°$ region was attempted by taking slopes for positive and negative angles of sideslip. These slopes indicate that C_{l_β} may be zero or positive near zero angle of sideslip over a small range of angle of attack. This would, of course, result in a negative value for $C_{n_{\beta,dyn}}$ and a possible directional divergence. Other than in the range of angle of attack from 30° to 35°, a stable airplane was predicted. The results for the higher Reynolds number were generally more linear in the angle of attack region of wing stall. With the derivatives assumed (fig. 38), stable variations with angle of attack were obtained.

From the data presented, one would probably conclude that the airplane would be predicted to be stable in the lateral-directional mode and that the effects of Reynolds number would not be large over most of the angle of attack range of interest. However, additional test results from the Ames 40- by 80-Foot Wind Tunnel (Reynolds number of 10×10^6) showed large stabilizing effects of simulated thrust and a region of angle of attack near 35° where $C_{n_{\beta,dyn}}$ was negative without thrust (fig. 40). These results were used in the Langley study to correlate the divergence identified during the 13-percent drop model tests with wind-tunnel predictions. The free-flight Reynolds number of the 13-percent drop model tests was about 4×10^6.

From these results it appears that the airplane configuration stability at high angles of attack was very sensitive to flow over the fuselage because the wings were beyond the stall angle of attack. Although flows at comparable Reynolds numbers (low Mach number) are expected to be similar, it appears that inconclusive results may be obtained. Full-scale results for correlation are sorely needed.

Control criteria.—At high angles of attack, control is as important as stability and may be difficult to provide. Two criteria (refs. 9 and 10) have been proposed that consider control requirements as well as stability. These criteria resulted from design and simulation studies. Both utilize the $C_{n_{\beta,dyn}}$ parameter and a lateral control parameter, since it was recognized that spins are usually initiated by a yawing motion. Either directional divergence or yaw due to control, or both, may initiate the divergence that may result in an uncontrollable maneuver. Each of the criteria attempts to identify regions that predict the possibility of a divergence and perhaps a spin.

The criteria parameters were calculated using the flight data for the large-scale airplane model and are presented in figures 41 and 42. The operational control system for the airplane (as for the large-scale airplane model) has a roll-control-to-rudder interconnect, so calculations were made for the basic airplane and for the airplane with the interconnect. As previously indicated, $C_{n_{\beta,dyn}}$ (fig. 37) was shown to be stable to the highest angle of attack for which flight data were obtained.

Reference 9 indicates that a roll control parameter more negative than -0.001 may cause a forced divergence and so should be avoided. The data for the 3/8-scale airplane model (with interconnect) predict no crossing of the divergence boundary, and, indeed, no unintentional divergence was encountered in flight with the CAS. The need for the interconnect is shown, since the control parameter for the basic airplane crosses the criteria boundary at an angle of attack of approximately 35°, which would predict unsatisfactory roll control. Lateral control without the CAS was shown to be unsatisfactory using the six-degree-of-freedom simulation mechanized for the program. Adverse yaw at high angle of attack made roll control unsatisfactory, and divergences were noted during dampers-only flight. The yaw controls could be used to spin the model by several control techniques.

The criterion of reference 10 (fig. 42) utilizes the same parameters; however, regions of spin susceptibility and severity and type of spin were mapped from piloted simulator and analytical studies. Comparing the experimental aerodynamic characteristics for the large-scale airplane model with the criterion of reference 10 shows the prediction of only mild rolling departures and low susceptibility to spin for the basic model and no departures or instability for the model with the roll-control-to-rudder interconnect. Again, flight experience tended to substantiate these predictions.

CONCLUDING REMARKS

An unpowered, large, dynamically scaled airplane model was flight tested by the remotely piloted technique to investigate the stability and controllability of the configuration at high angle of attack. The model was flown through a ground-based computer that was programed to provide simulated control systems that were designed for the full-scale airplane. The following comments may be made regarding the use of the test method:

(1) The remotely piloted flight technique proved to be satisfactory for obtaining flight data quickly and completely over a large flight envelope.

(2) The pilot's capability was satisfactorily utilized, and projections to actual flight situations appear to be possible.

(3) The effects of sophisticated control systems used in current airplanes were satisfactorily provided by the use of a digital computer on the ground. The versatility of the concept was proved by the updating of the control mechanization that was possible between flights.

The airplane configuration proved to be departure and spin resistant with the control augmentation system operating. Techniques were developed on a six-degree-of-freedom flight and research support simulator that permitted the pilot to depart and spin the airplane model both erect and inverted. This simulation provided valuable support for the flight program for pilot indoctrination and practice and research on spin techniques. Stabilized spins revealed an erect spin mode at approximately 61° angle of attack and the possibility of another at approximately

80° angle of attack. The mechanization of a stall inhibiter effectively prevented the airplane model from being forced into a spin.

Spins were recorded at high and low altitudes, and the results were supplemented by simulator studies. Data from simulated flight spins agreed satisfactorily with the airplane model flight data. Altitude had little effect on the ability of the pilot to force the model to spin, although the increased damping at the lower altitudes did make it easier to spin at lower angles of attack than at higher angles of attack. The model recovered more readily from the low-altitude spins than the high-altitude spins. The roll-control-with and rudder-against recovery technique proved to be the most satisfactory method of recovering from the erect spins. The inverted spins were forced by full control deflections and were easily recovered from by neutralizing the controls.

Comparison of the large-scale model spin characteristics with smaller scale model results showed good agreement at the medium-high angle of attack and satisfactory agreement at the high angle of attack.

The airplane model flight-derived dynamic stability and control characteristics for an angle of attack range of 0° to 53° generally supported the prediction that the configuration was departure and spin resistant. For the low Reynolds number wind-tunnel data, there appeared to be a narrow region of angle of attack at about maximum lift where the slope of rolling moment versus sideslip was nonlinear, perhaps zero. This led to uncertainty in defining the usual stability derivative. Large-scale airplane model controllability generally supported the prediction of departure/spin criteria that the configuration would be resistant to departures and spins. However, the need for a roll-control-to-rudder interconnect was indicated. Full-scale airplane test data are required to complete the correlation of the scale model results.

Flight Research Center
National Aeronautics and Space Administration
Edwards, Calif., June 24, 1975

APPENDIX A

REMOTELY PILOTED SYSTEM

The NASA Flight Research Center's remotely piloted system is described in this appendix. A functional block diagram of the system is shown in figure 43. The aircraft response variables were telemetered to a ground station where they were routed to a ground computer, the cockpit instrument panel, and analog strip chart recorders for real-time flight monitoring. The ground cockpit proportional control functions (longitudinal and lateral stick and rudder pedals) were processed by the analog-to-digital converter and were trunked to the ground computer together with the mode panel signals. The ground computer calculated the command variables for the uplink encoder.

The remotely piloted system used two uplink encoders. The computer encoder received command variables from the computer, and the bypass encoder received command variables directly from the ground cockpit. The pilot selected an encoder by means of a pushbutton on the mode control panel. The bypass encoder served as a backup to the computer encoder if the computer malfunctioned. The command signals were transmitted to the airplane where they were decoded and sent to the appropriate servochannel.

The pilot could also select one of two telemetry uplink antennas, one slaved to a radar tracking antenna and the other to a fixed antenna. The uplink antennas and the uplink encoders were the only dualized components of the system. Because the purpose of the system was flight research, it was designed to be single channel.

Pilot's Control Station

The pilot's control station was a part of the ground facility and was composed of the pilot's fixed ground-based cockpit, the flight engineer's station, and two observer posts, all housed in a closed, insulated room within the ground facility. Two communication links were used in the control station. The pilot used UHF radio to talk to the flight controller, to the launch, escort, and recovery aircraft, and to air traffic control agencies. The flight engineer used an intercom to talk to the flight director, range facilities director, and ground facility director, as well as to listen to UHF conversations.

Ground Cockpit

The pilot was given direct control of the airplane model in the operation of the remotely piloted system, which permitted experienced test pilots to extract the maximum research capability from the system. Accordingly, the ground cockpit was configured to give the remote test pilot information about the airplane model similar to that which would be provided in an airplane cockpit. Figure 44 shows the displays, which are typical of a simulation type of cockpit although no particular aircraft

cockpit was simulated. The displays included airspeed, altitude, rate of climb, angle of attack, angle of sideslip, yaw rate, pitch rate, normal acceleration, control positions, and commanded control position. These quantities were presented in conventional round-dial aircraft instrument face format. Aircraft attitude and heading were presented on a three-axis attitude indicator. All the instruments displayed processed telemetered data from the model. The pilot controlled the airplane model with a conventional control stick and rudder pedals. The stick and pedals were part of an artificial feel system. Position limits and force gradients were adjustable. The control feel was provided in each axis by a high-quality, computer-controlled, electric force-feel system which accurately simulated the full-scale airplane force-feel in pitch and roll. Rudder pedal forces were selected as desired by the pilot. Pitch and roll were trimmed with a standard switch on the pilot's stick. Yaw was trimmed with a toggle switch on the left instrument subpanel.

Also shown in figure 44 is the mode control panel with which the pilot selected various control modes and gains. A pulse panel with which the pilot applied control surface steps or doublets under computer control was located on the left console. The mode control panel was used to select from four control modes in three axes (pitch, roll, and yaw) and provided programable gain switches in each axis. The panel also allowed the pilot to select the bypass mode or computer modes and informed him if any downlink variable failed a check which would result in telemetry lockout. The model panel pushbutton switches were rear lighted. They were controlled by the computer and indicated the control mode of the computer.

Discrete commands, such as drogue parachute deploy, autopilot select, hydraulics off, electrical power off, and uplink antenna selector, were made with a set of guarded toggle switches on the instrument panel that was operated by either the pilot or the flight engineer. A set of lights on the instrument panel indicated the status of systems such as the autopilot, recovery, hydraulic, and electrical.

A 23-centimeter, 525-line, black-and-white television monitor was displayed above the instrument panel. It showed the view from a forward-looking television camera in the model cockpit. The television monitor was used as a backup navigation and control display and was the primary visual display if recovery parachute failure made an emergency horizontal landing necessary.

Telemetry Links

The telemetry links were essentially "line of sight" transmission paths. A signal could be blocked by the model wing or by flying the model below the horizon at extreme range. It was estimated that operations would be limited to approximately 55 kilometers at low altitudes and 185 kilometers at high altitudes. Signal strength was monitored during climbout to launch to insure an acceptable signal during the flight.

In addition to a requirement for high reliability, the telemetry link could not introduce unacceptable time delays if the links were to be used in the operation of closed-loop systems. The time delay of the data links was approximately 3.3 microseconds per kilometer, or about 0.5 millisecond for the uplink and downlink for an operational range of 75 kilometers. This delay is small compared to the update rate

of 18.75 milliseconds and proved to be satisfactory for the computation times through the remotely piloted system.

Telemetry downlink. —The NASA Flight Research Center's telemetry flight data acquisition system was used for the telemetry downlink portion of the remotely piloted system. This data acquisition system provided aircraft response variables to the ground station at 200 samples per second. The characteristics of the PCM system were as follows:

144 000 bits per second
9 bits per data word
80 words per PCM frame
200 PCM frames per second
No parity check
L-band transmission
12-foot parabolic receiving antenna slaved to radar tracking antenna

The system had 40-hertz first-order-lag analog prefilters on all channels. Reasonability checks were made in the software to discriminate against bad telemetry data, because there was no parity check on the downlink and the power was relatively low. The downlink provided satisfactory data at ranges as great as 320 kilometers for high-altitude aircraft.

Telemetry uplink. —The telemetry uplink used for the system was developed by the U.S. Navy for the remote control of drone aircraft. The system was capable of several modes of operation, from the control of a single drone to the time-multiplexed control of a fleet of drones; therefore, the update rate of the system when controlling a single aircraft was comfortably high, and acceptable for the remotely piloted program. The characteristics of the system were:

16 bits per data frame (10-bit proportional command signal and 6 discrete signals)
4 data frames per cycle
53.33 cycles per second
Two parity checks per data frame
Synchronization and parity checks on each cycle
UHF band transmission
Frequency shift keying

The telemetry uplink cycle (fig. 45) consisted of four data words (frames) and a sync word transmitted at 53.33 samples per second (18.75 milliseconds cycle time). The transfer of each data word from encoder to receiver output on board the test airplane required 3.75 milliseconds. The four command signals were coded in the 10 most significant bits of the uplink words, and the remaining 6 bits were available for discrete signals to the test vehicle. Since parity checks were performed on each data word, intermittent dropout of the telemetry uplink signal was not expected to cause serious problems.

Ground Computer

The computer (ref. 3) used in the remotely piloted system was a general purpose rack-mounted Varian 620 minicomputer with a 16K memory consisting of 16-bit

words and with 750-nanosecond cycle time. The peripheral equipment included a card reader, line printer, magnetic tape unit, disc unit, teletype, paper tape reader/punch, and peripheral floating point processor. The software was composed of an assembler, a FORTRAN compiler, and a mathematical subroutine support library. During real-time operation, data inputs to the computer (cockpit data and downlink data) and data outputs from the computer (uplink commands) were made by means of interrupt-initiated inputs and outputs.

The peripheral floating point processor received and transmitted data associated with the hardware floating point operation over the input/output bus by means of the priority memory access unit. Although this operation consumed the major portion of the 75-microsecond hardware floating point execution time, it was faster than the computer's software floating point option. It was slower, though, than could be achieved with the integrated floating point hardware. A floating point data word required two memory locations and had an 8-bit exponent and a 22-bit mantissa (six-place accuracy).

The open-loop and closed-loop control law computations were implemented through the computer program which used floating point FORTRAN. Thus the FORTRAN compiler was used to debug and check out programs, and the floating point feature eliminated the need for variable scaling. The obvious advantage of this mode of programing in a research environment was the ease with which programs could be written and modified by a control systems engineer. The remotely piloted computer program also contained the assembly language subroutines which performed the input/output of data, and which passed the data to the FORTRAN main program and received the uplink command signals from the main program.

As an indication of the capability of the computer to perform feedback control law computations, only approximately 0.7 millisecond was required to sum two feedback variables and a pilot command signal (each multiplied by a gain) and to operate on the resulting error signal with a first-order digital filter.

APPENDIX B

SOME IMPRESSIONS OF REMOTE PILOTING

The large-scale airplane model program was the first research program at the NASA Flight Research Center in which a remotely located pilot attempted to fly and test an airplane (model) as an airplane would be flown from the cockpit. As such, pilot impressions were important, both for the accomplishment of the objectives of this program and for evaluating the use of the test method in future programs. Some pilot impressions from the first several flights follow.

The flights were efficient in producing good quality flight data for analysis in a short flight time. The flight envelope of the airplane was rapidly expanded to its limits. On some flights unplanned angles of attack and sideslip were reached that might have resulted in loss of control in an unforgiving airplane. After only four flights, the maximum lift capability had been reached and data had been recorded for analysis over a range from zero lift to maximum lift.

The displays provided the cues necessary for maneuvering and controlling an airplane. The remote pilot did not have the motion cues provided the onboard pilot. It took longer for the pilot to assess and evaluate the situation and decide on the necessary course of action. The pilot reported that he did indeed feel remote from the flight. There were no verifying and comforting sensations as in actual flight. The gross cues from contact flight were compressed onto a 12.5-centimeter, three-axis attitude indicator. All cues were visual and could be sampled only sequentially. This meant more time was required for verifying and confirming a situation before making corrective commands. Only the most superficial cues may be sufficient for flying a simulator, but flying an untried airplane requires definitive and diverse evidence of the situation and the action required. For the remote pilot, cues were sparse and the time required to accumulate evidence on which to base confident control seemed long.

The isolated ground cockpit provided the necessary isolation from distractions. Isolation had been thought to be necessary because of the strong concentration required during remotely piloted flight, and it was. The pilot estimated that the attitude indicator received about 90 percent of his attention during the flights. It was also an important display during spins, but yaw rate and roll rate displays were also included and proved to be important for these flights. Roll and yaw rate meters helped in characterizing the type of spin and in assessing the progress of the entry and recovery phases.

As with most flight research programs, before the actual flight the pilot practiced on a fixed-base simulator, becoming thoroughly familiar with the flight. Even so, the actual flight seemed to be more hurried than the simulated flight. (This was also true during the X-15 program and other tightly scheduled and dynamic flight programs.) Flights were practiced at various simulation times, increased relative to model real time. A rate of 1.4 times real time seemed to provide a pace comparable to that of real-time flight, so preparation for flight at 1.4 times real time appeared to prepare the remote pilot for real-time actual flight.

The piloting task of flying a scaled model was more demanding than flying the airplane. Provisions were made for a flight engineer to aid the pilot during the flight. The pilot reported that the presence of the flight engineer, prompting when necessary, was unobtrusive and helpful in monitoring the progress of the flight.

REFERENCES

1. Neihouse, Anshal I.; Klinar, Walter J.; and Scher, Stanley H.: Status of Spin Research for Recent Airplane Designs. NASA TR R-57, 1960.

2. Holleman, Euclid C., compiler: Initial Results From Flight Testing a Large, Remotely Piloted Airplane Model. NASA TM X-56024, 1974.

3. Edwards, John W.; and Deets, Dwain A.: Development of a Remote Digital Augmentation System and Application to a Remotely Piloted Research Vehicle. NASA TN D-7941, 1975.

4. Iliff, Kenneth W.; Maine, Richard E.; and Shafer, Mary F.: Subsonic Stability and Control Derivatives for an Unpowered, Remotely Piloted 3/8-Scale F-15 Airplane Model Obtained From Flight Test. NASA TN D-8136, 1976.

5. Neihouse, Anshal I.; and Pepoon, Philip W.: Dynamic Similitude Between a Model and a Full-Scale Body for Model Investigation at Full-Scale Mach Number. NACA TN 2062, 1950.

6. Tobie, Harold N.; Malcom, Lawrence G.; and Elliott, Elden M.: A New Longitudinal Handling Qualities Criterion. NAECON/66; Proceedings of the IEEE 18th Annual National Aerospace Electronics Conference, May 1966, pp. 93-99.

7. Bihrle, William, Jr.; and Barnhart, Billy: Effects of Several Factors on Theoretical Predictions of Airplane Spin Characteristics. (Grumman Aerospace Corp.) NASA CR-132521, 1974.

8. Moul, Martin T.; and Paulson, John W.: Dynamic Lateral Behavior of High-Performance Aircraft. NACA RM L58E16, 1958.

9. Titiriga, A., Jr.; and Weyl, C. J., Jr.: Northrop Experience — Spin Characteristics for Fighter Type Aircraft. Stall/Post-Stall/Spin Symposium, 15-17 December 1971, F-1 — F-25. (Available through Air Force Flight Dynamics Laboratory (FGC), Wright-Patterson Air Force Base, Ohio 45433.)

10. Weissman, Robert: Preliminary Criteria for Predicting Departure Characteristics/Spin Susceptibility of Fighter-Type Aircraft. J. Aircraft, vol. 10, no. 4, 1973, pp. 214-219.

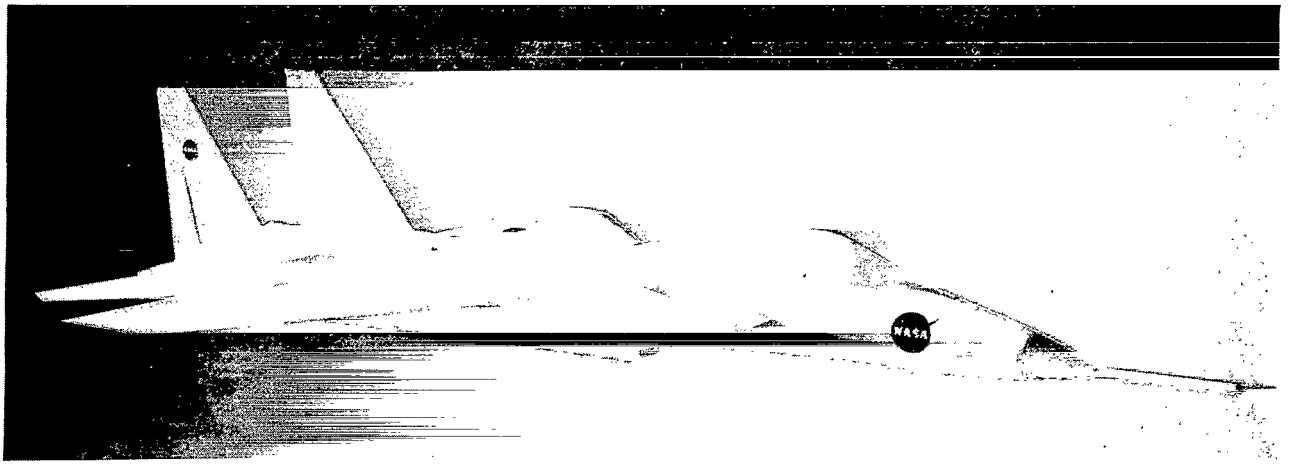

E-25487

Figure 1. Three-eighth-scale airplane model.

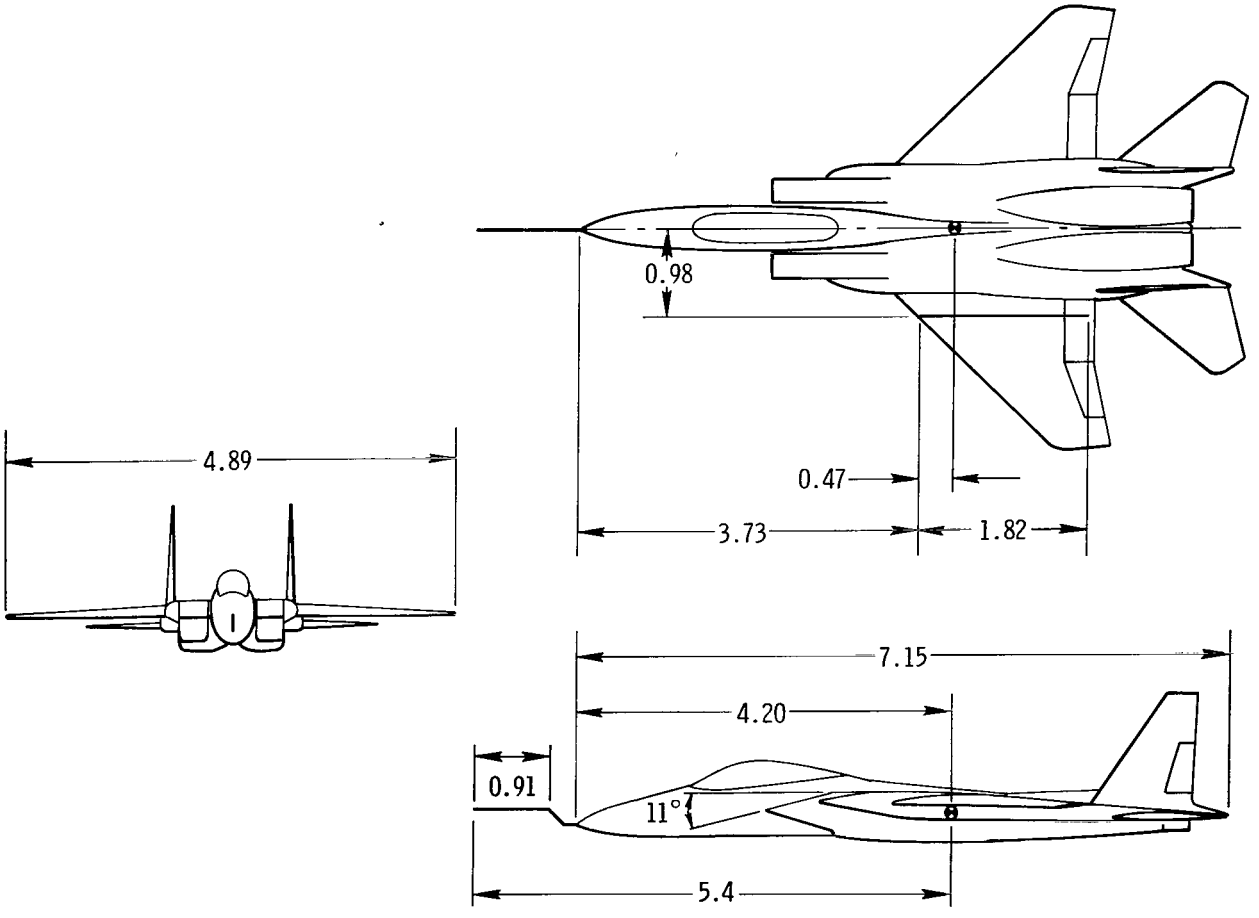

Figure 2. Three-view drawing of the model. Dimensions in meters.

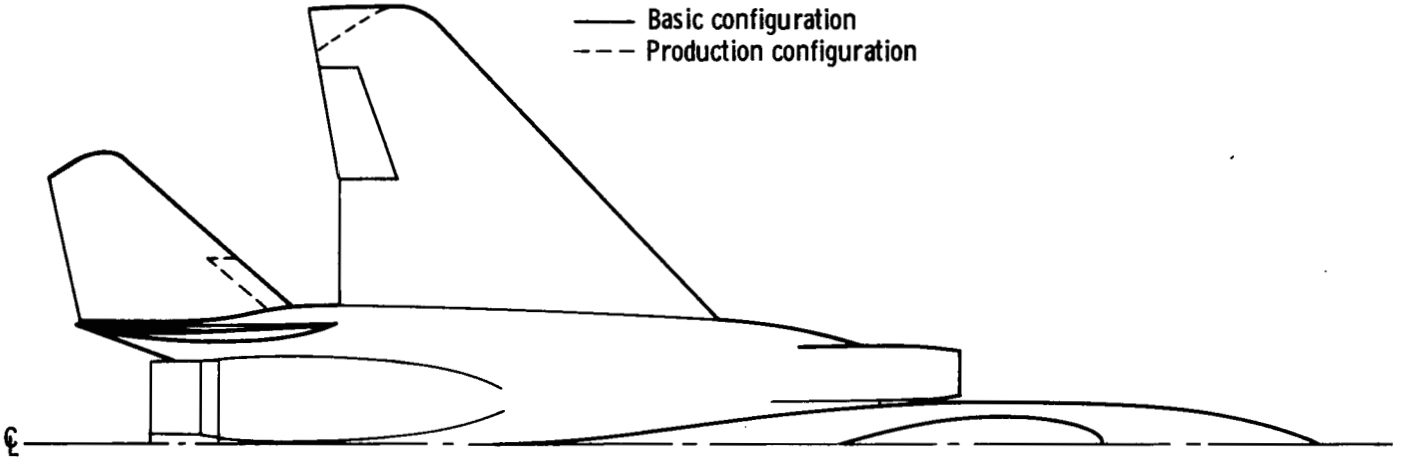

Figure 3. Modification (dashed lines) of the 3/8-scale model to the production configuration.

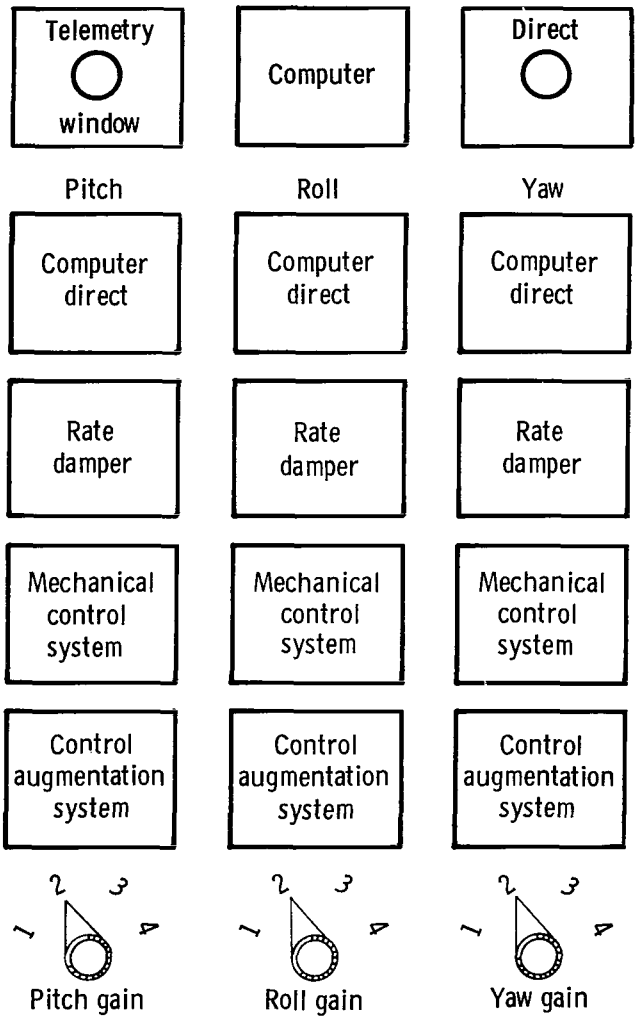

Figure 4. Model control mode panel.

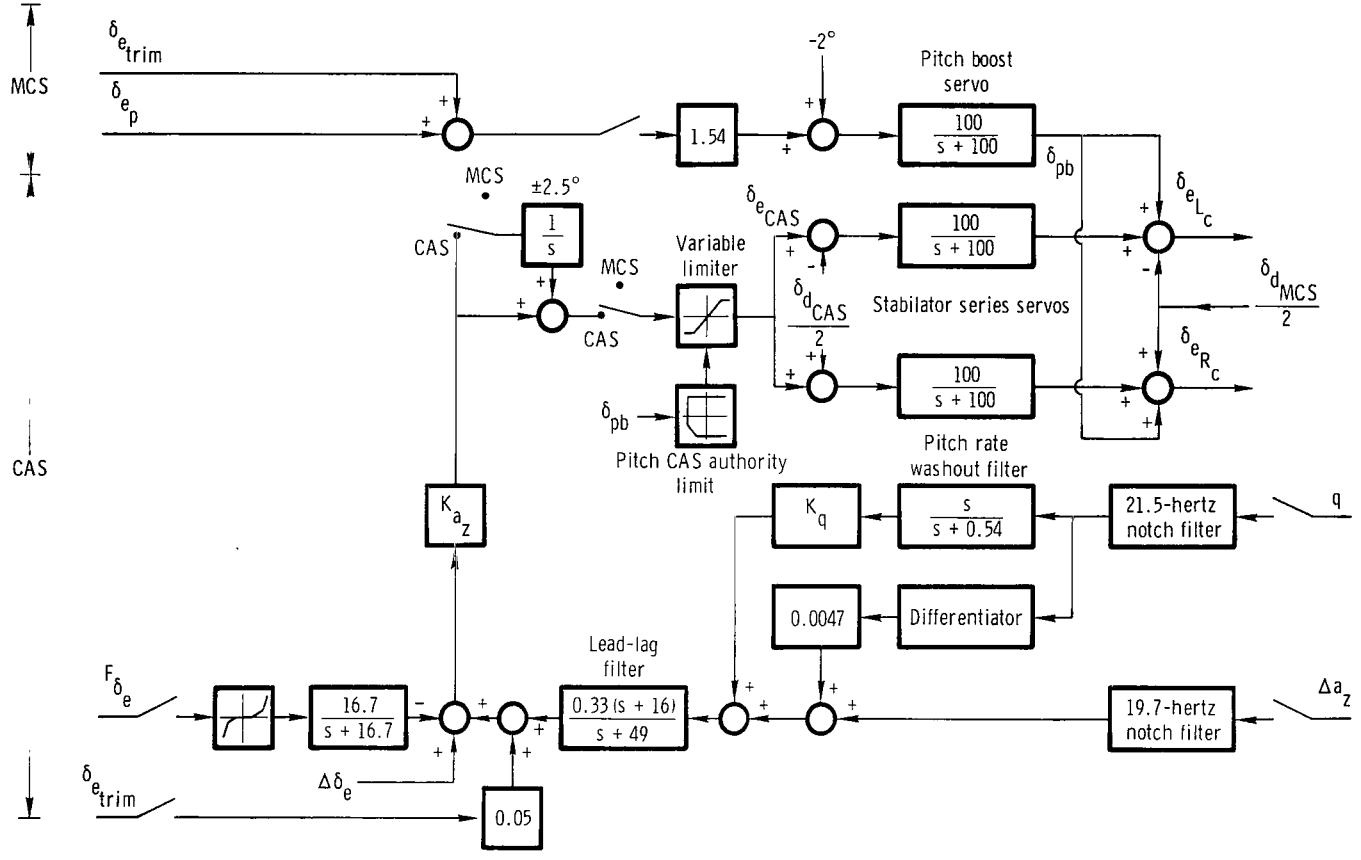

(a) Pitch axis.

Figure 5. Block diagram of the scale-model control system.

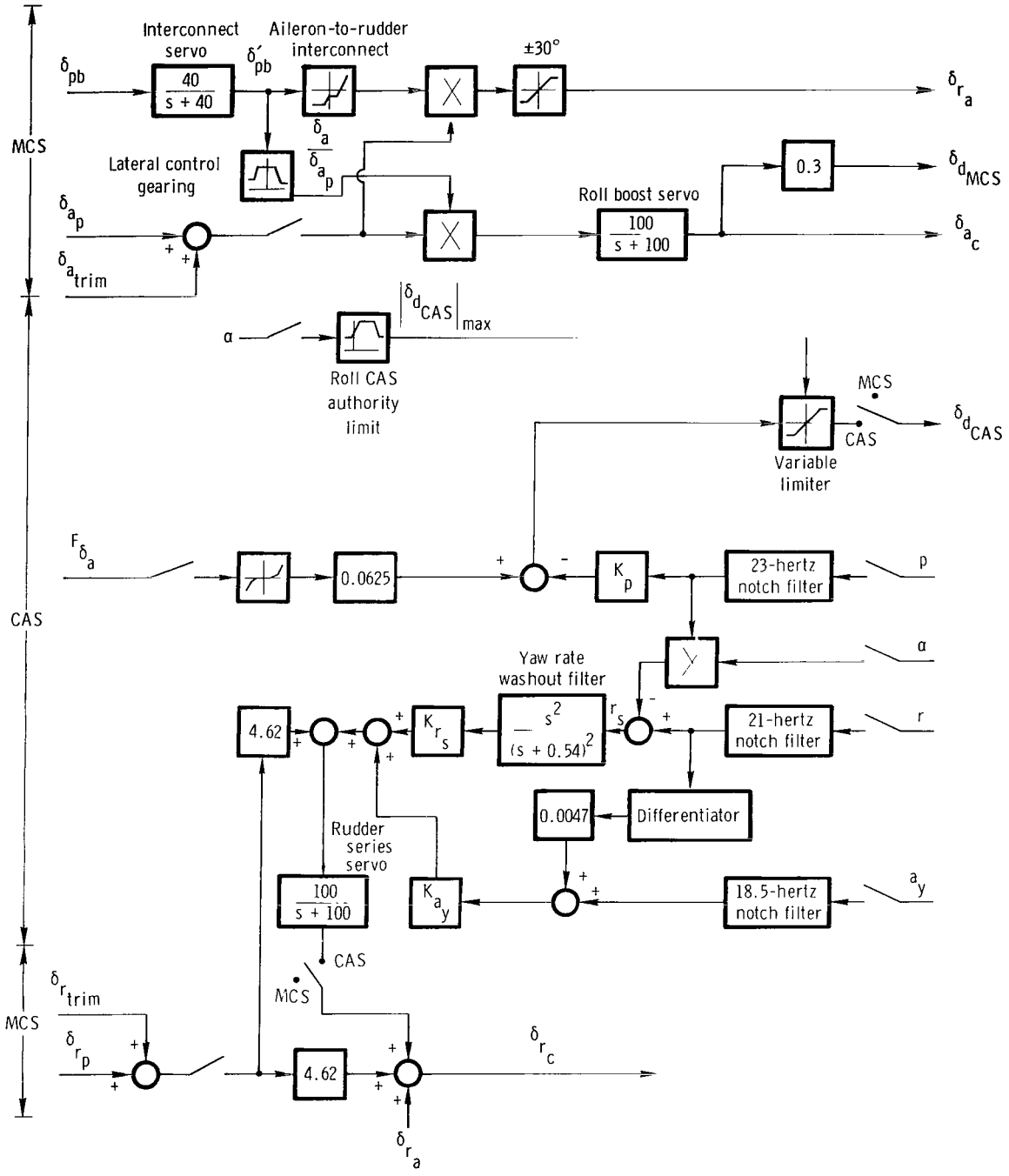

(b) Roll and yaw axes.

Figure 5. Concluded.

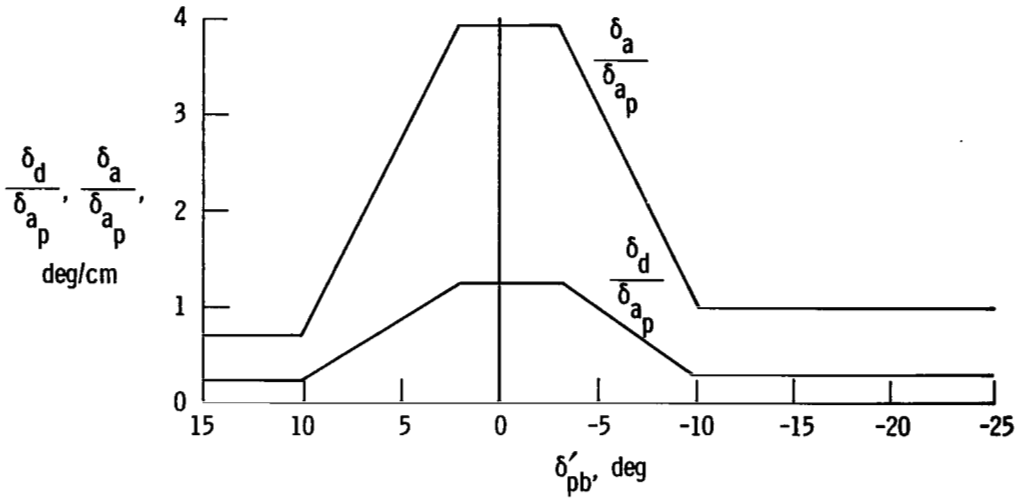

Figure 6. MCS lateral control gearing schedule as a function of lagged pitch boost servo output.

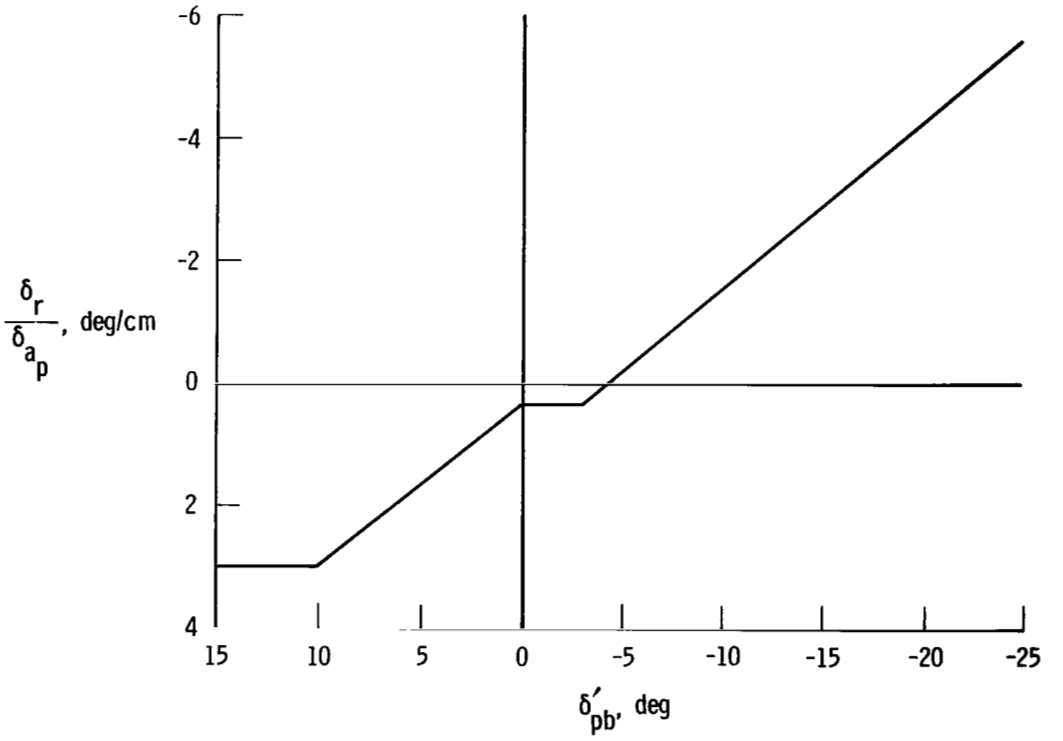

Figure 7. MCS aileron-to-rudder interconnect gearing as a function of lagged pitch boost servo output.

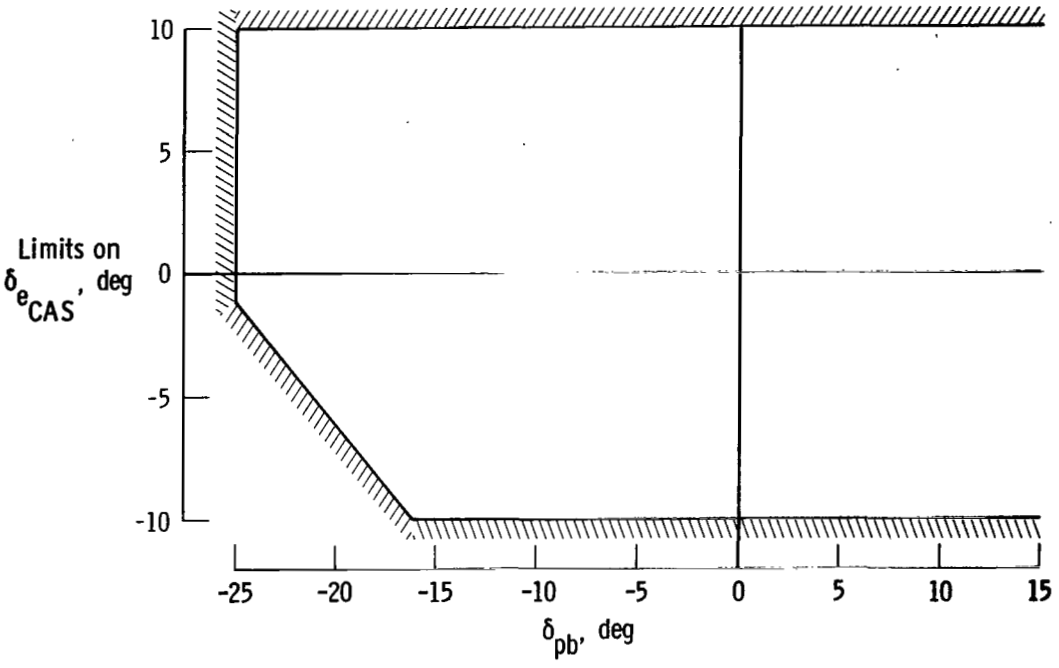

Figure 8. Pitch CAS authority limit as a function of pitch boost servo output.

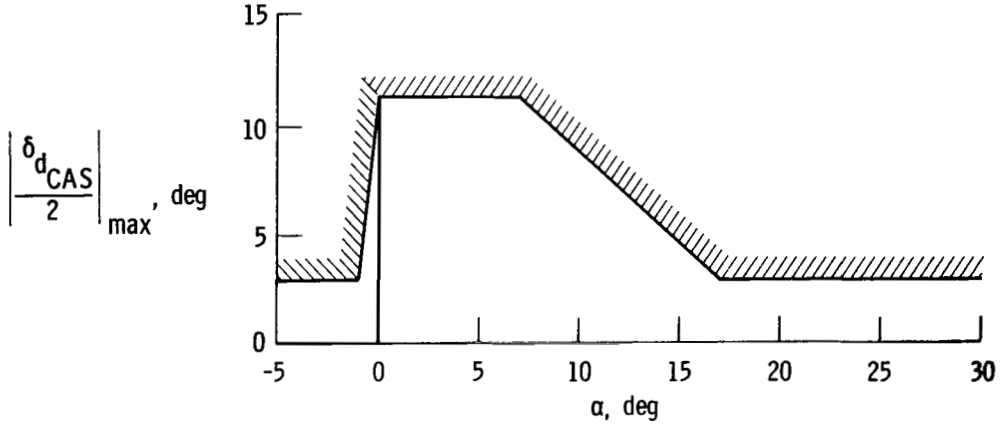

Figure 9. Roll CAS authority limit as a function of angle of attack.

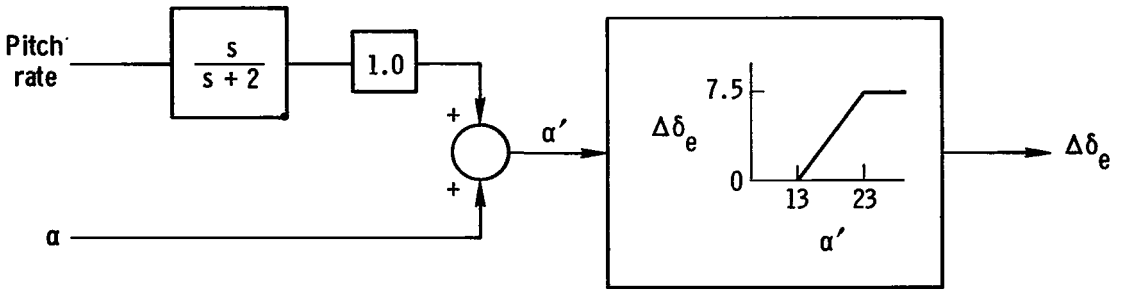

Figure 10. Diagram of stall inhibiter mechanization.

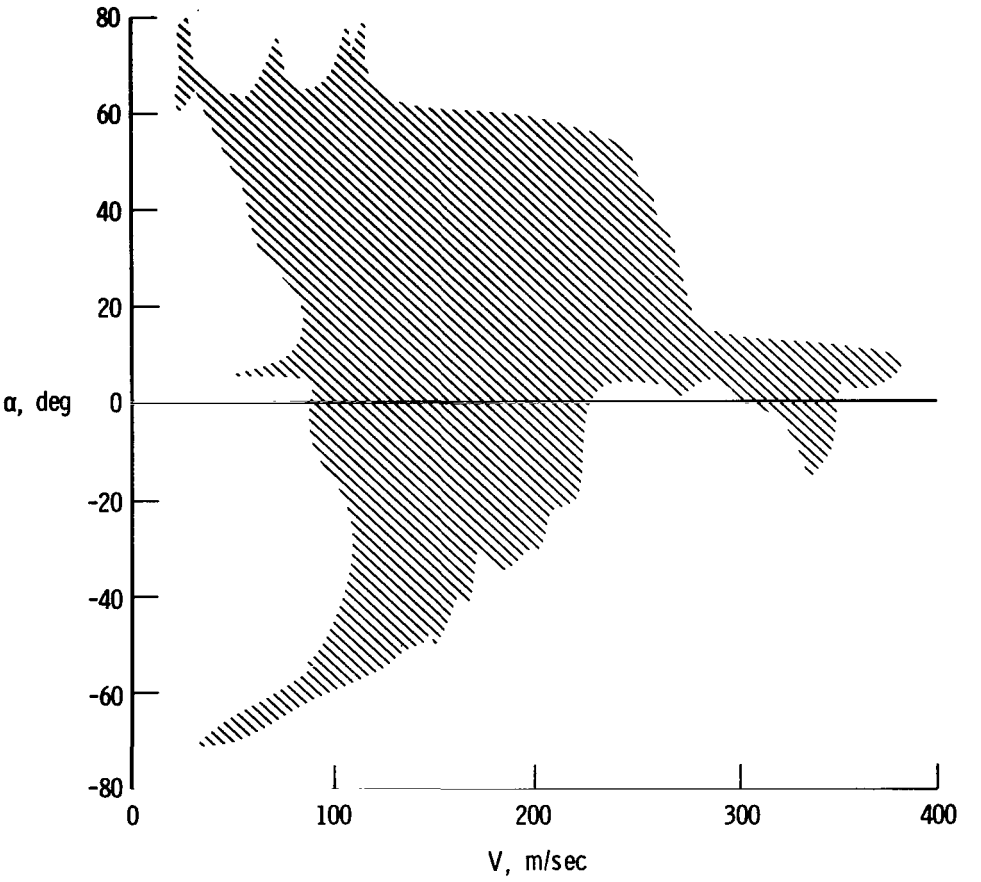

Figure 11. Flight envelope covered. Scaled to the full-scale airplane.

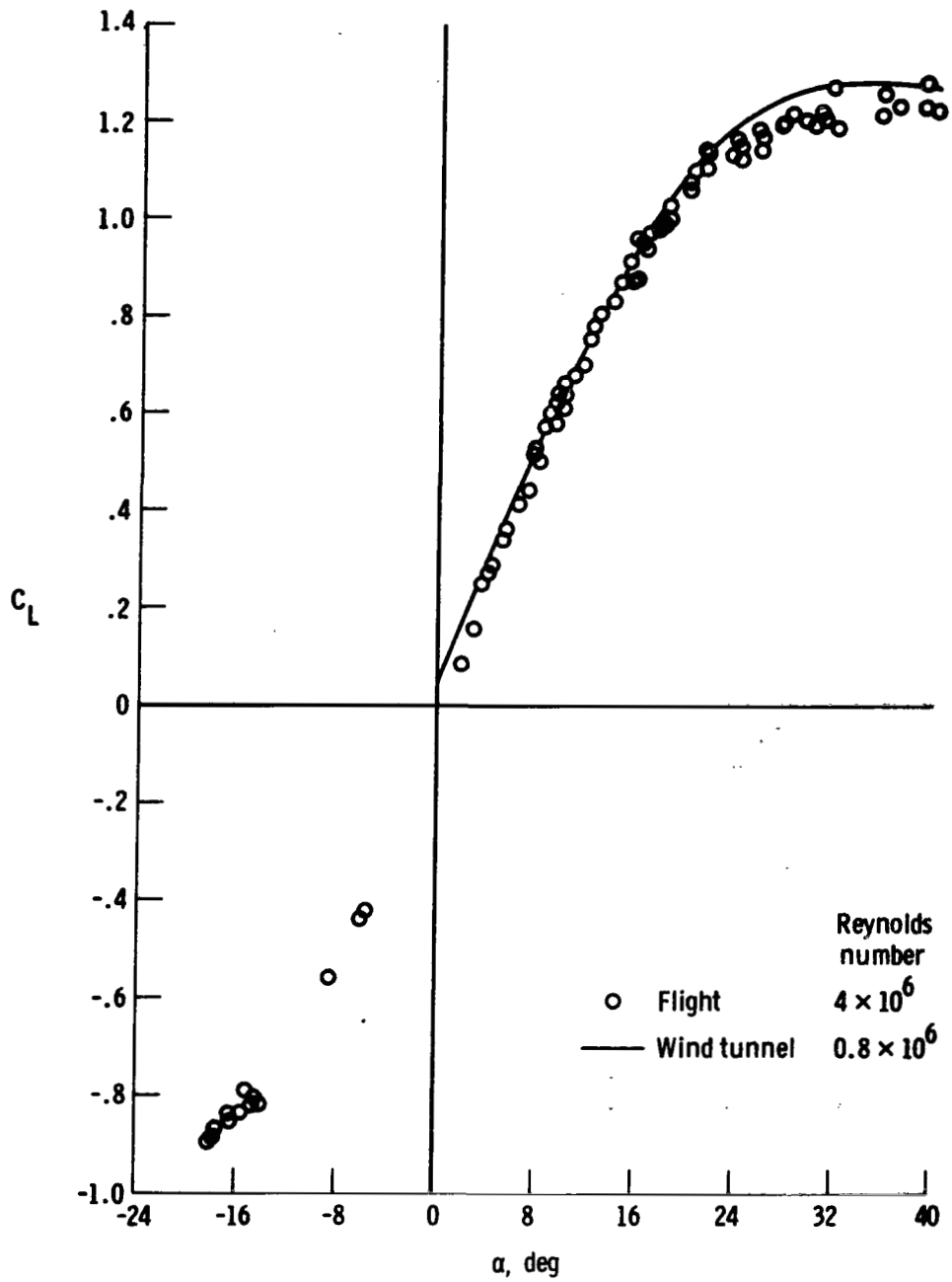

Figure 12. Large-scale model flight lift coefficient variation with angle of attack compared with 10-percent-scale model wind-tunnel data. Inlets drooped 11° and blocked.

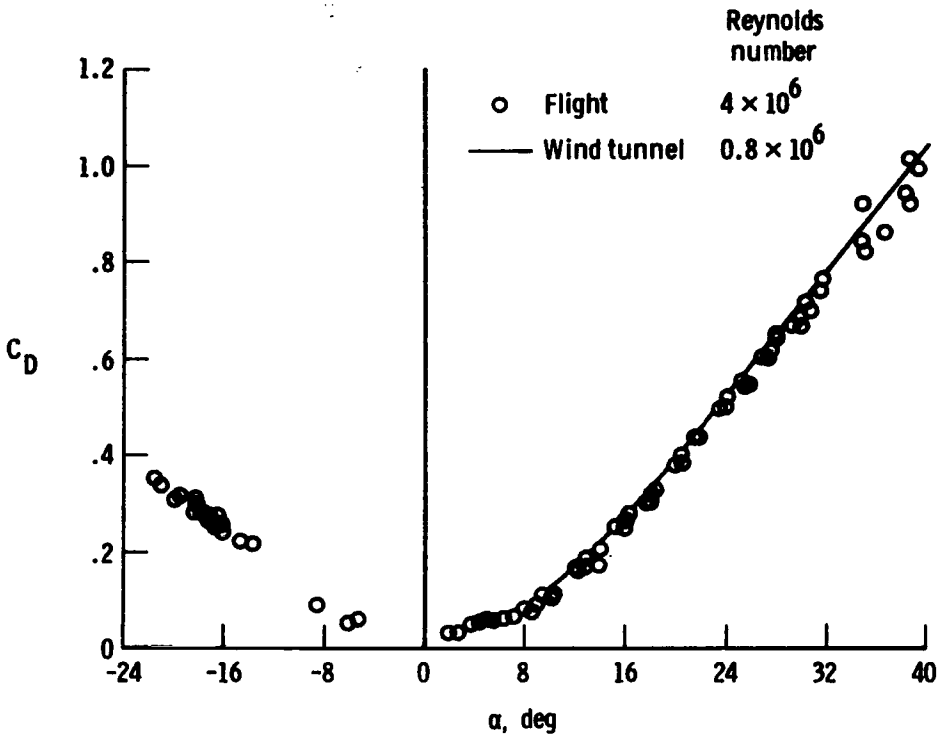

Figure 13. Large-scale model flight drag coefficient variation with angle of attack compared with 10-percent-scale model wind-tunnel data. Inlets drooped 11° and blocked.

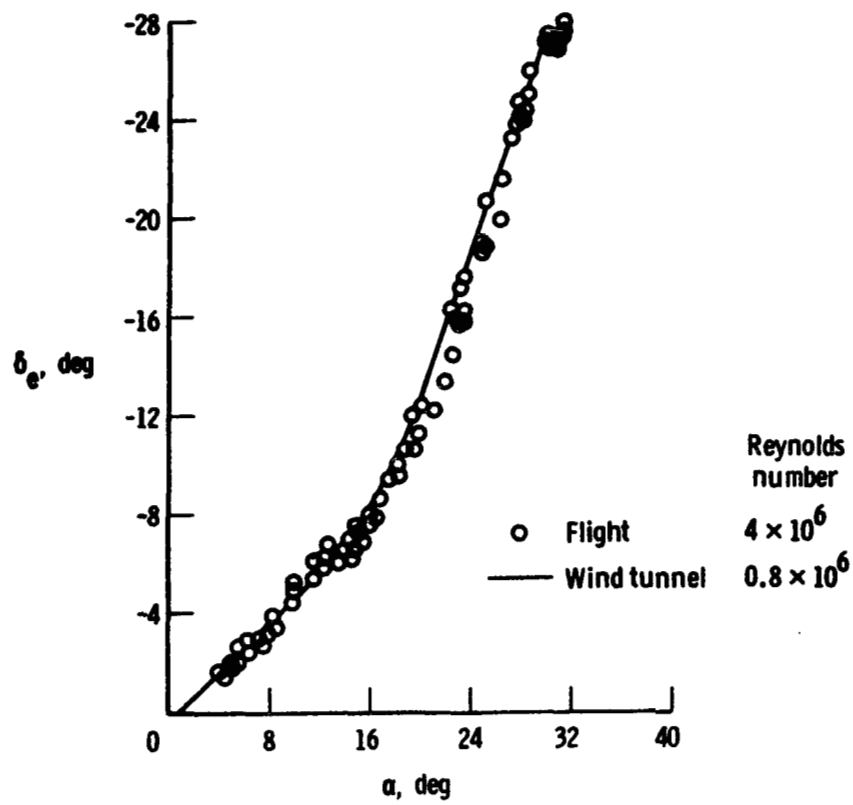

Figure 14. Comparison of collective stabilator deflection required for trim from flight tests of the large-scale model and wind-tunnel tests of the 10-percent-scale model. Center of gravity at 26-percent mean aerodynamic chord.

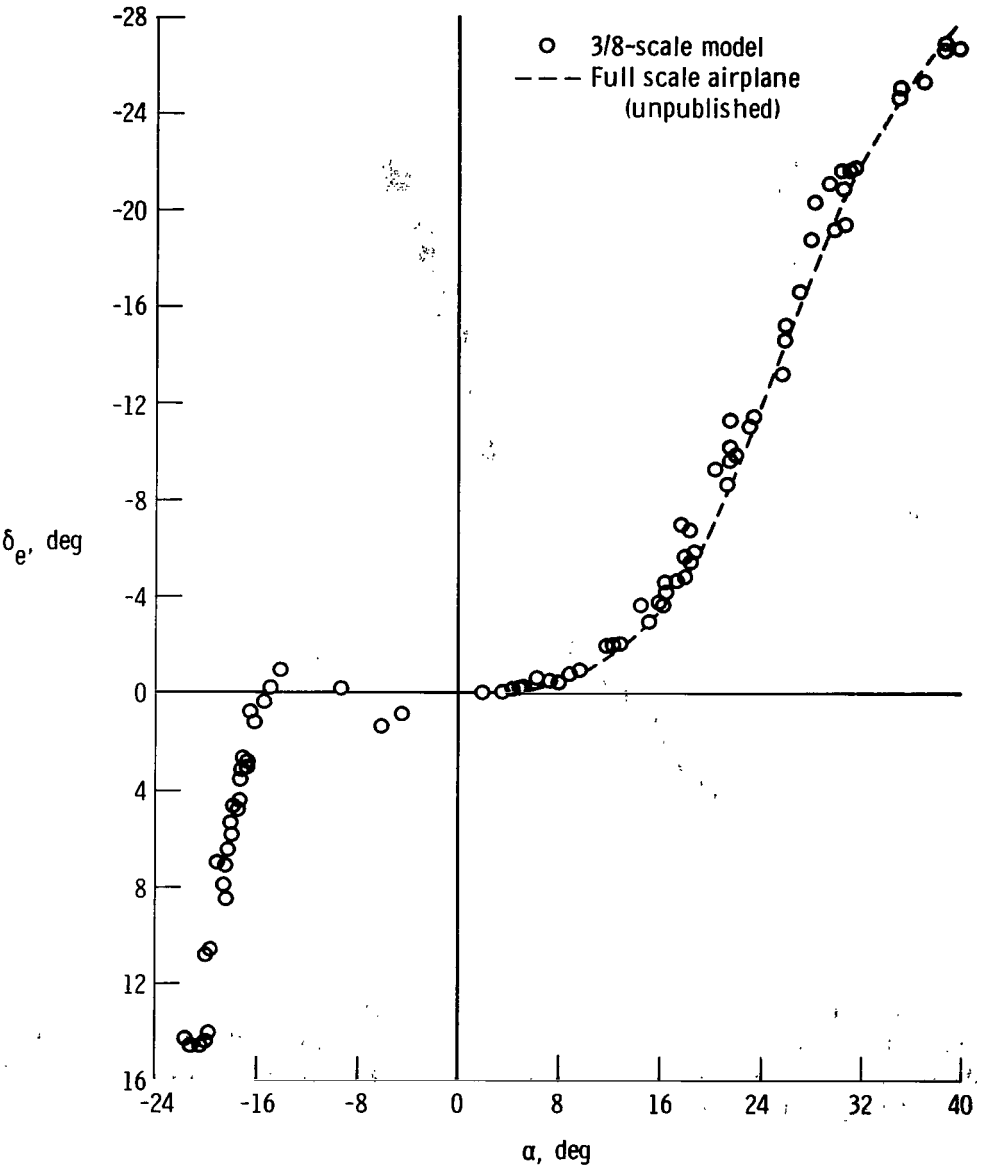

Figure 15. Comparison of large-scale model flight apparent stability with full-scale flight results. Center of gravity at 30.3-percent mean aerodynamic chord.

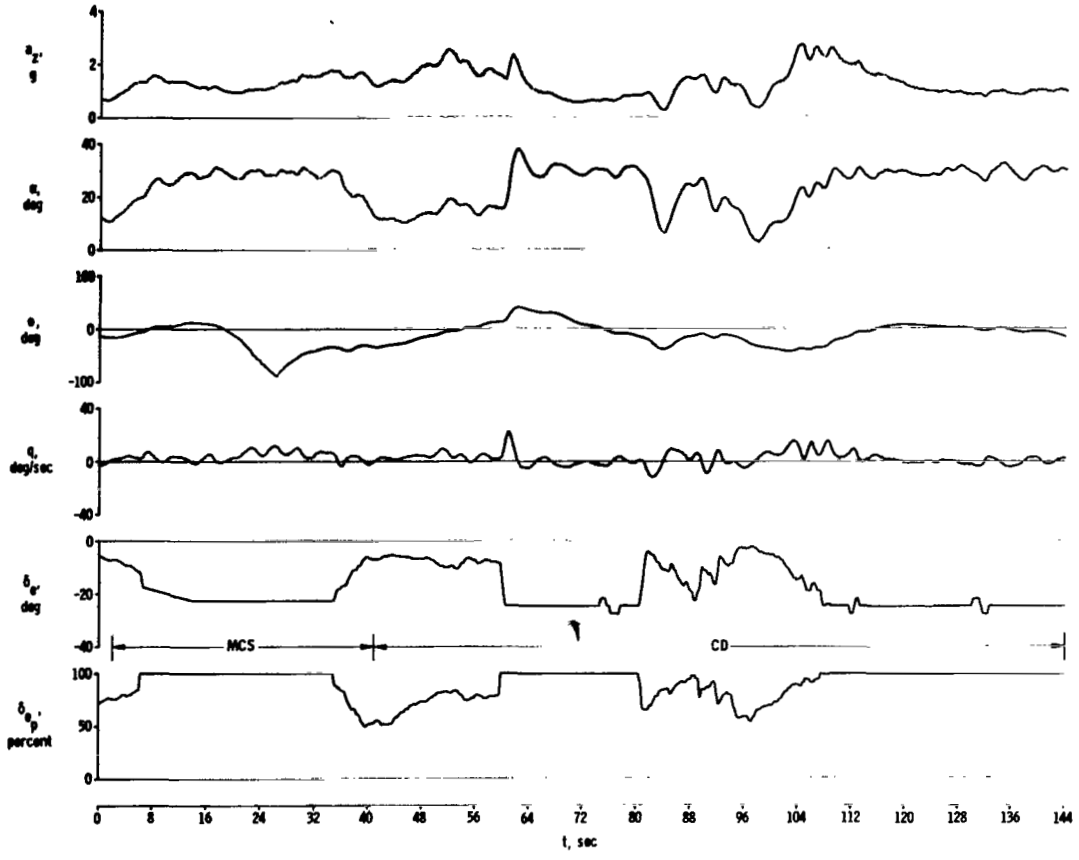

(a) Longitudinal quantities.

Figure 16. Time histories of pullups and turns to high angle of attack to determine controllability.

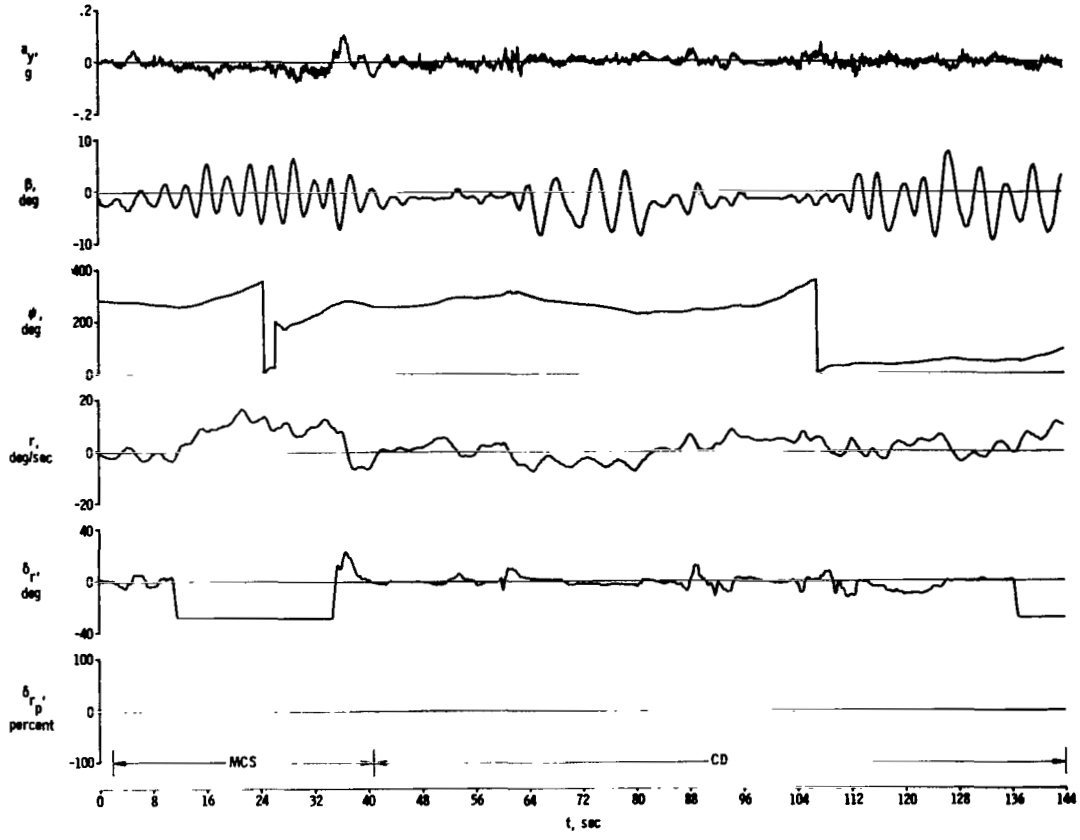

(b) Directional quantities.

Figure 16. Continued.

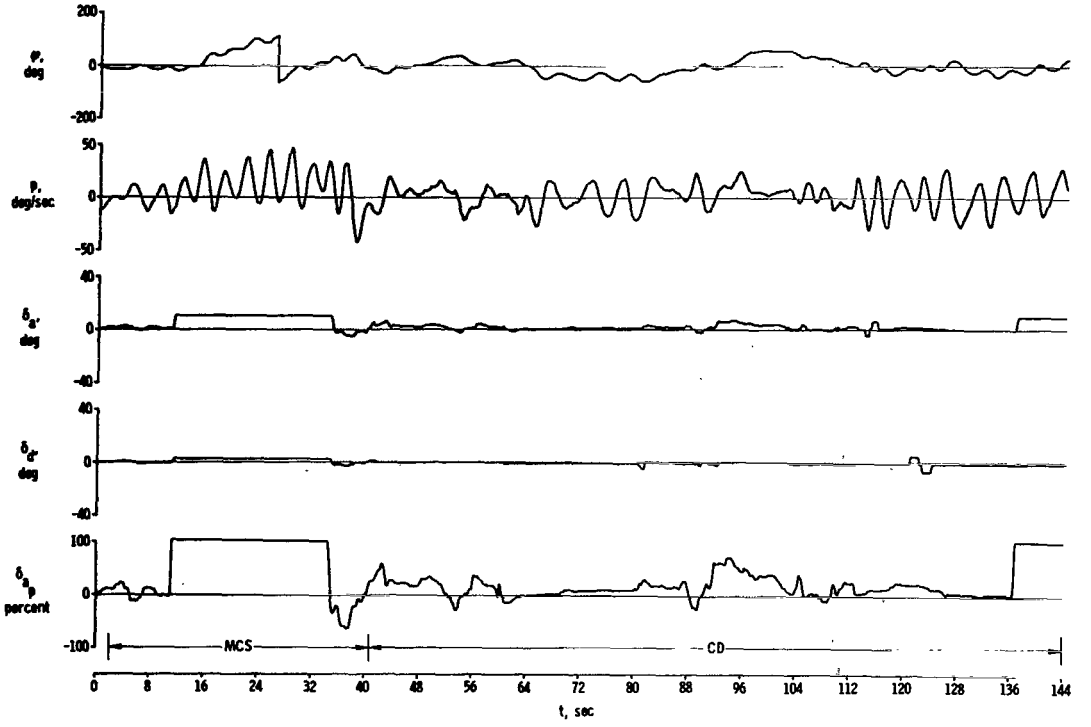

(c) Lateral quantities.

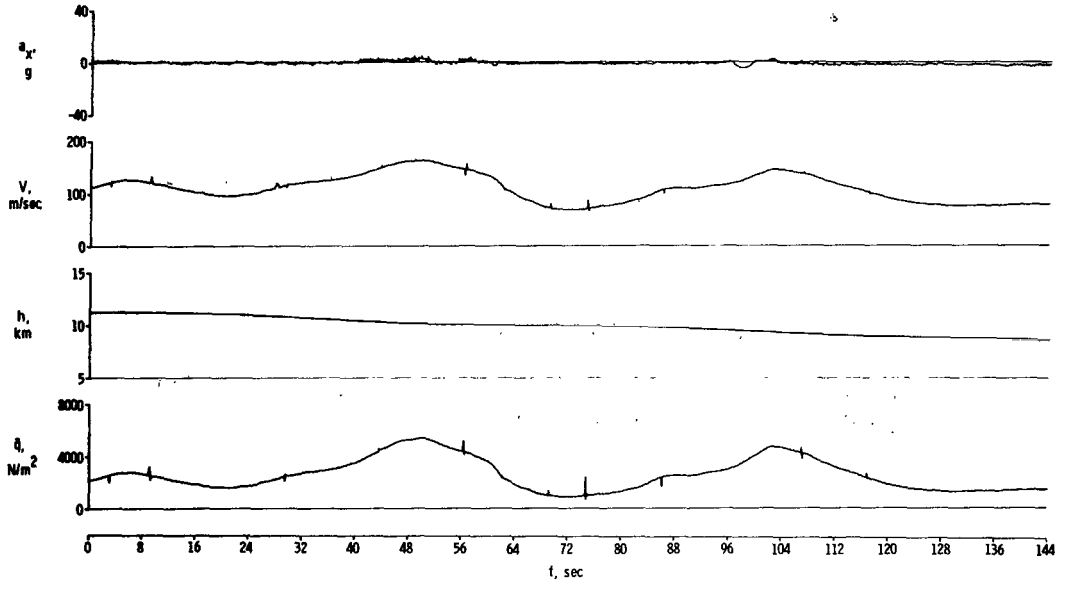

(d) Performance quantities.

Figure 16. Concluded.

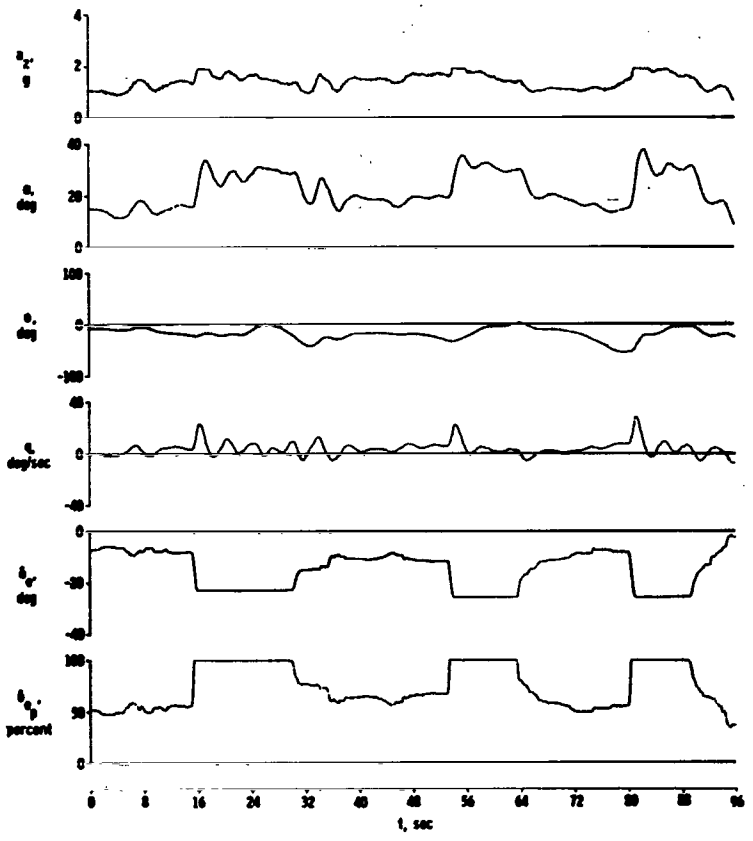

(a) Longitudinal quantities.

Figure 17. Time histories of rapid pullups to high angle of attack with the MCS.

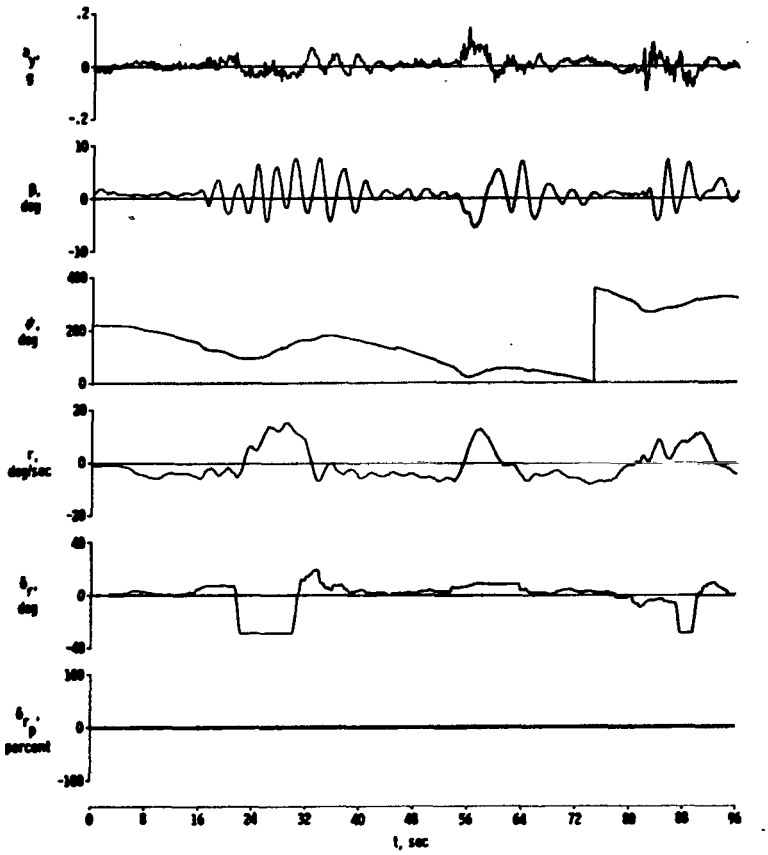

(b) Directional quantities.

Figure 17. Continued.

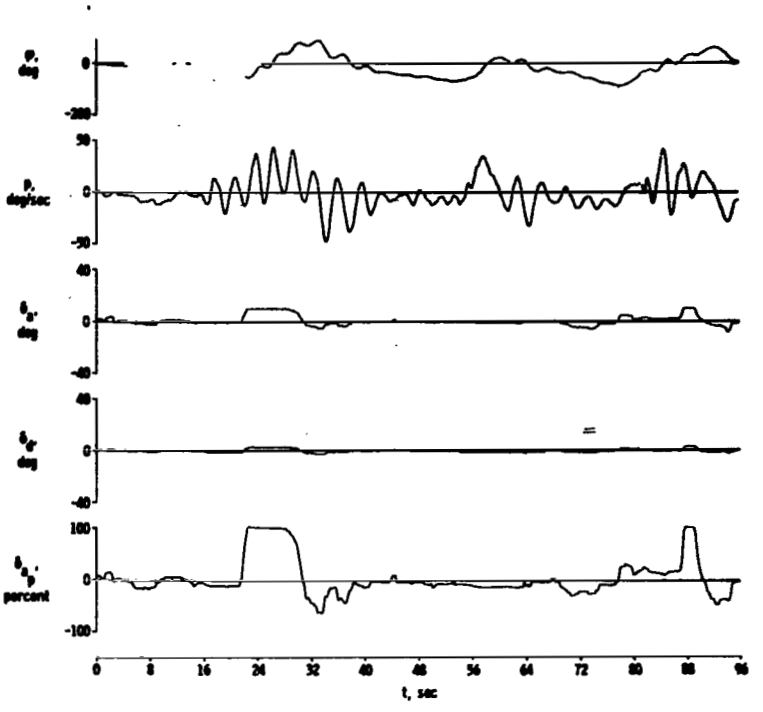

(c) Lateral quantities.

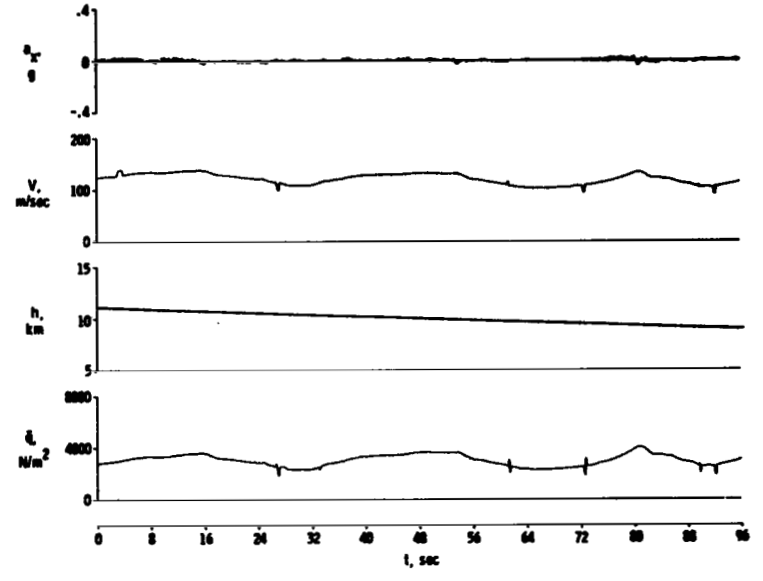

(d) Performance quantities.

Figure 17. Concluded.

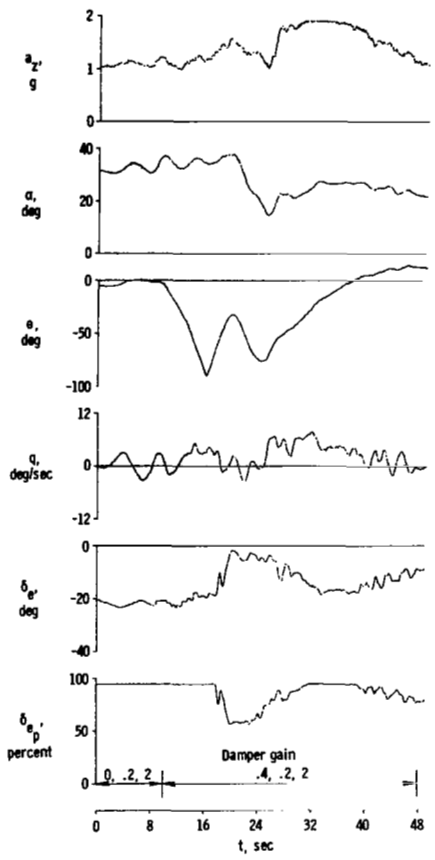

(a) Longitudinal quantities.

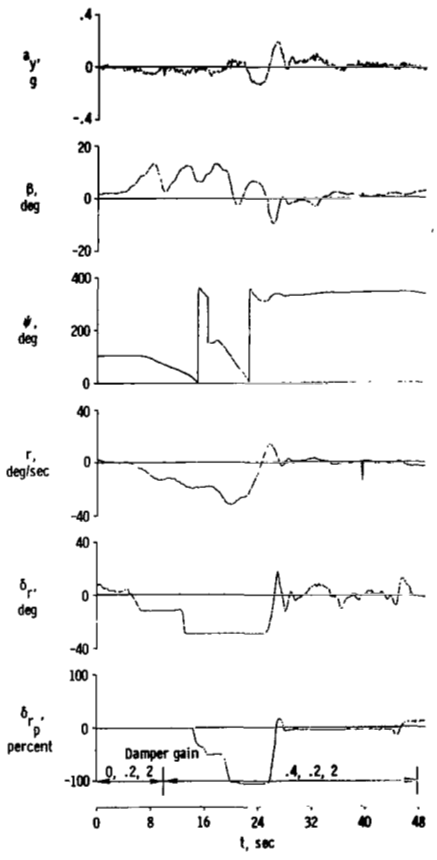

(b) Directional quantities.

Figure 18. Time histories of a directional divergence at approximately 30° angle of attack with the damper control system. Pitch, roll, and yaw gains in deg/deg/sec indicated.

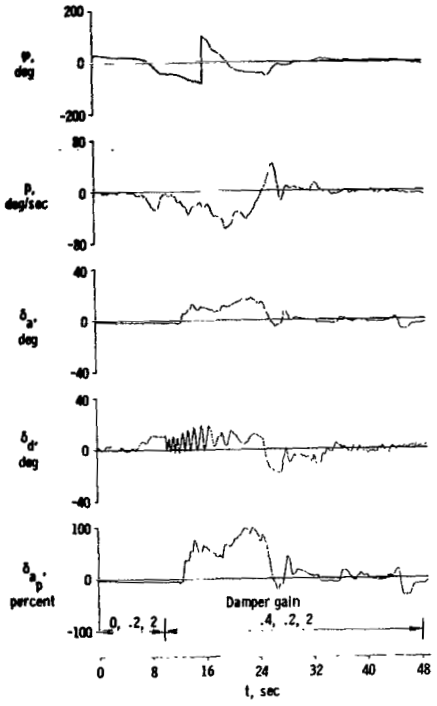

(c) Lateral quantities.

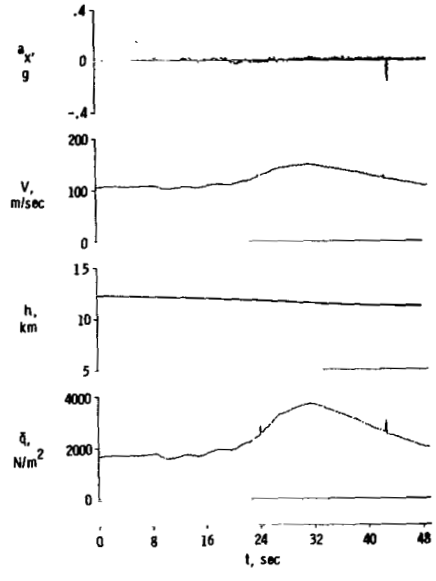

(d) Performance quantities.

Figure 18. Concluded.

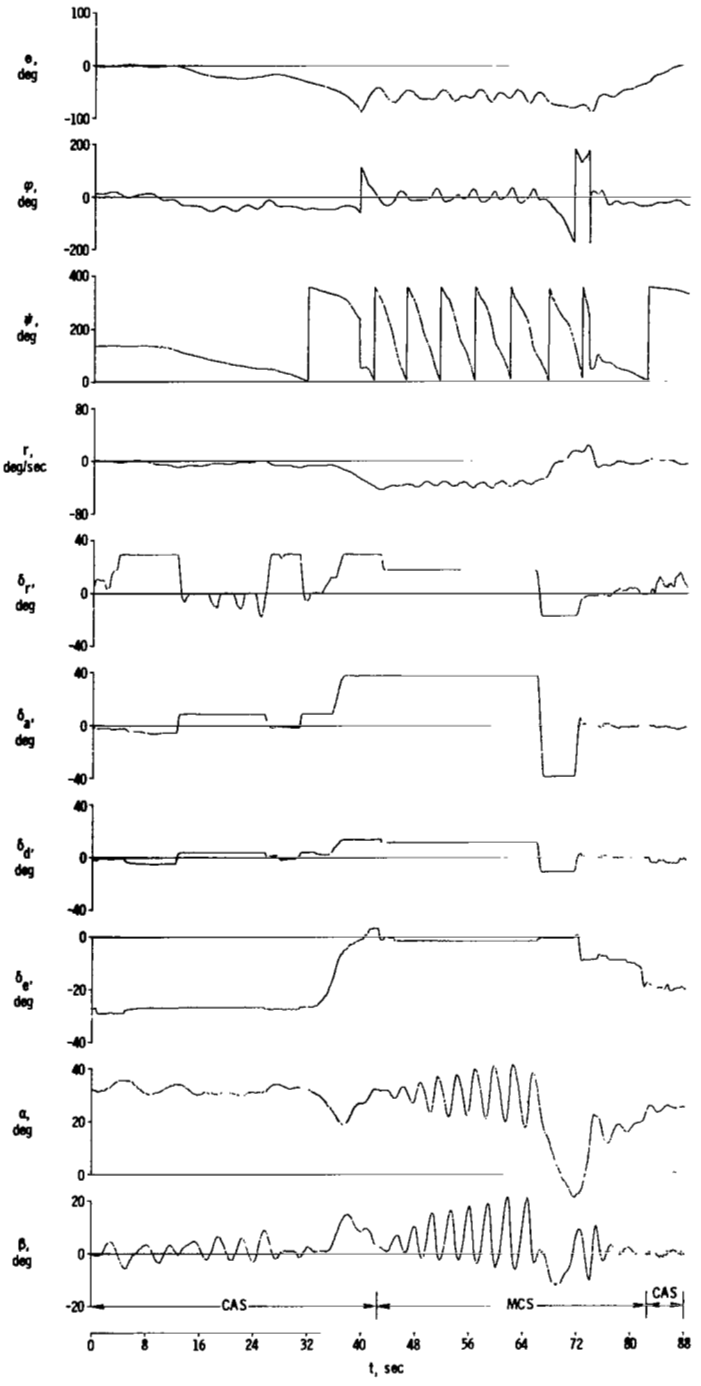

(a) Attitudes and related quantities.

Figure 19. Time histories of the first attempt to spin the large-scale model. Center of gravity at 26-percent mean aerodynamic chord.

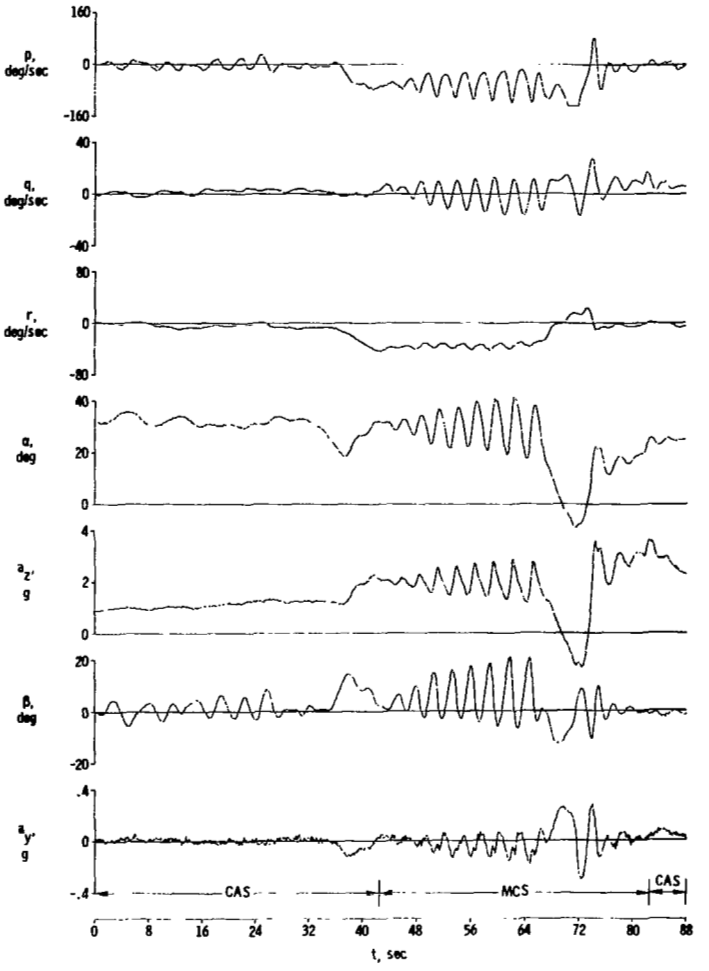

(b) Angular rates and related quantities.

Figure 19. Continued.

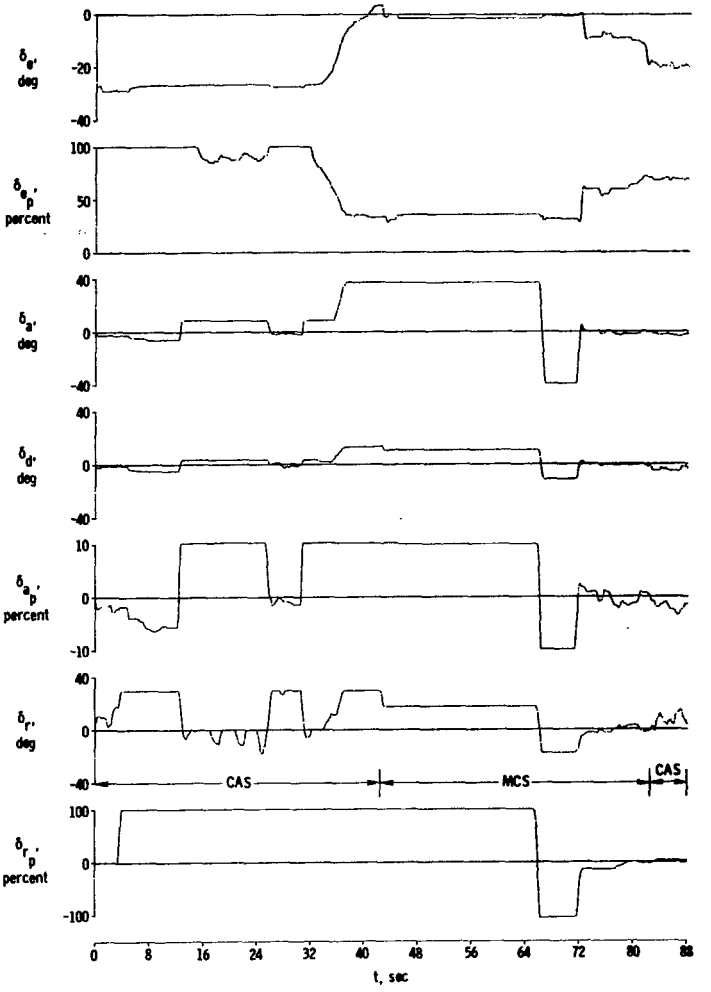

(c) Controls.

Figure 19. Continued.

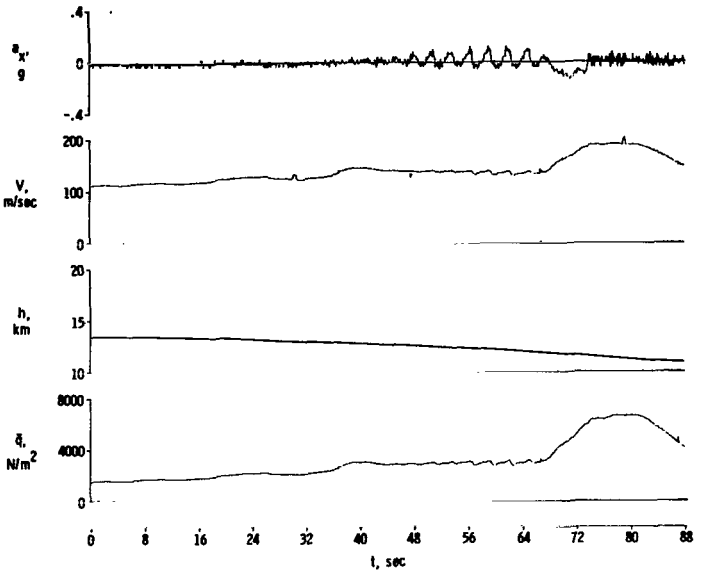

(d) Performance quantities.

Figure 19. Concluded.

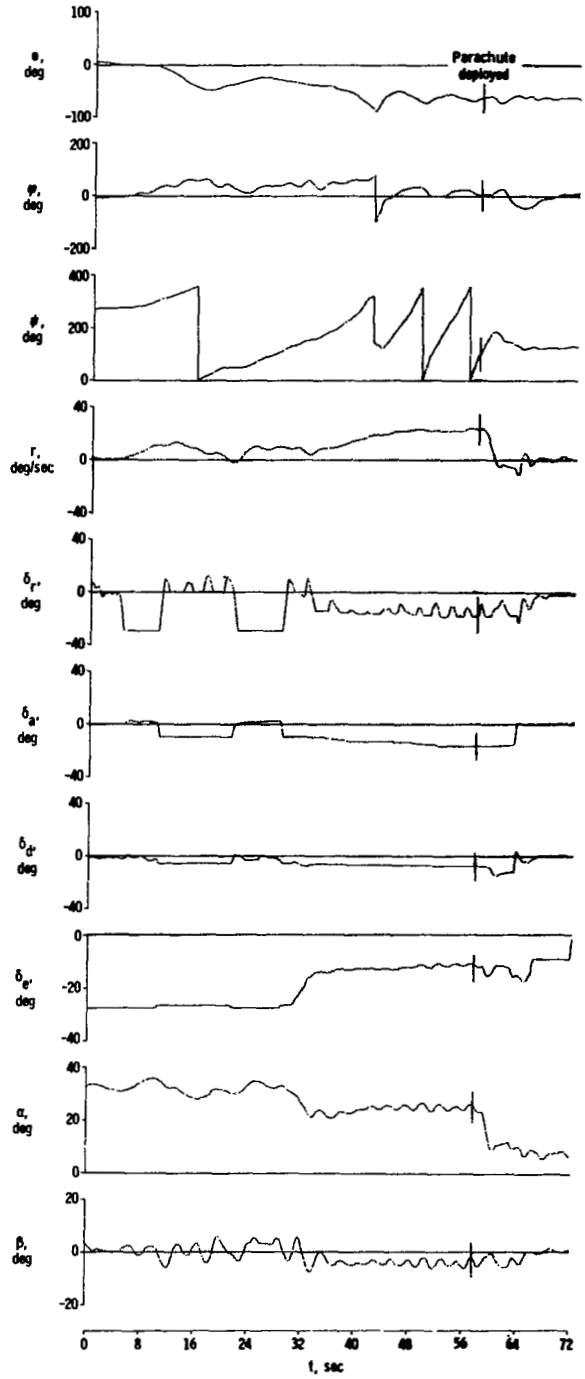

(a) Attitudes and related quantities.

Figure 20. Time histories of the second attempt to spin the large-scale model. Center of gravity at 26-percent mean aerodynamic chord; CAS.

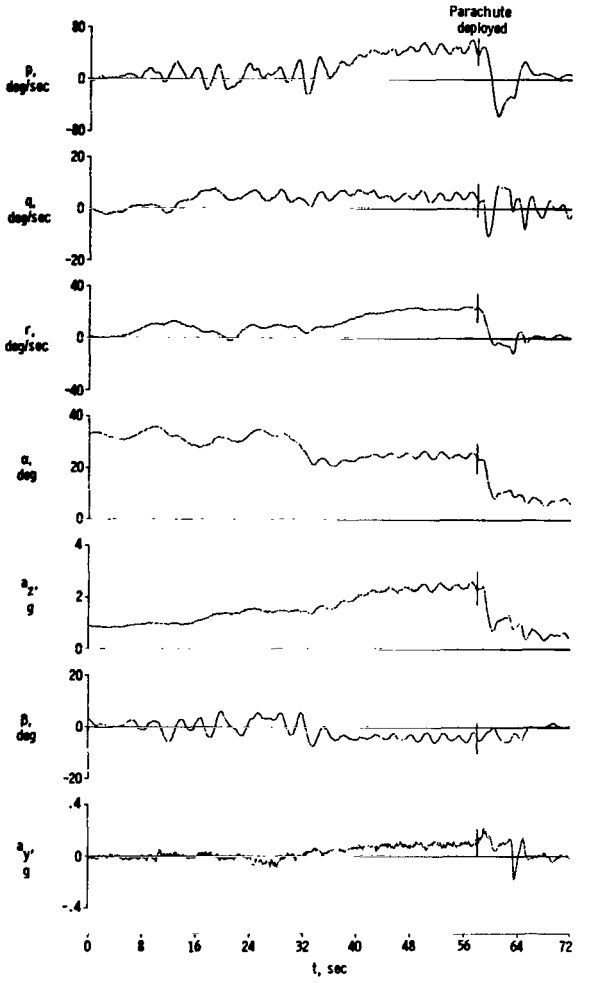

(b) Angular rates and related quantities.

Figure 20. Continued.

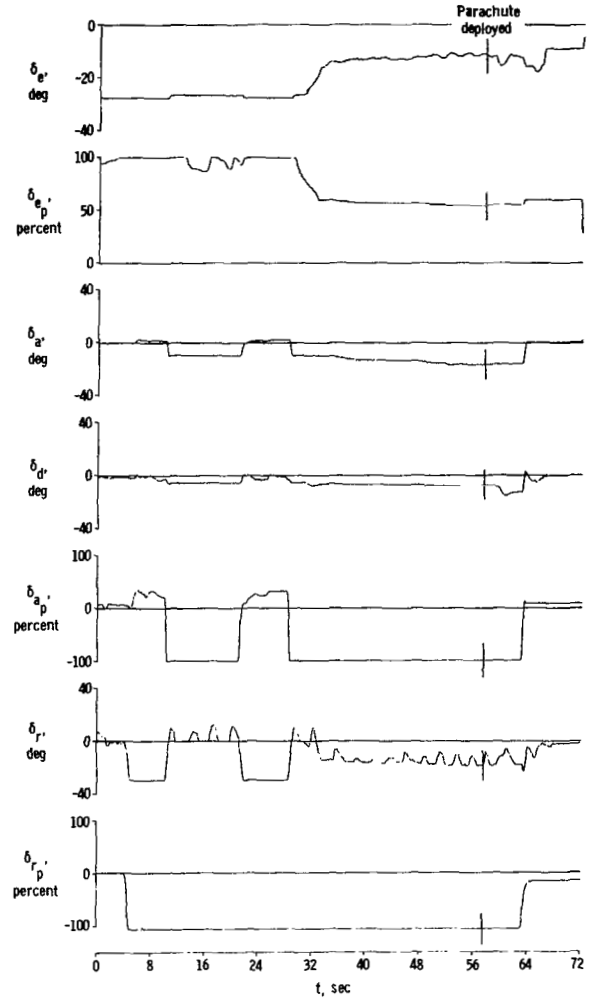

(c) Controls.

Figure 20. Continued.

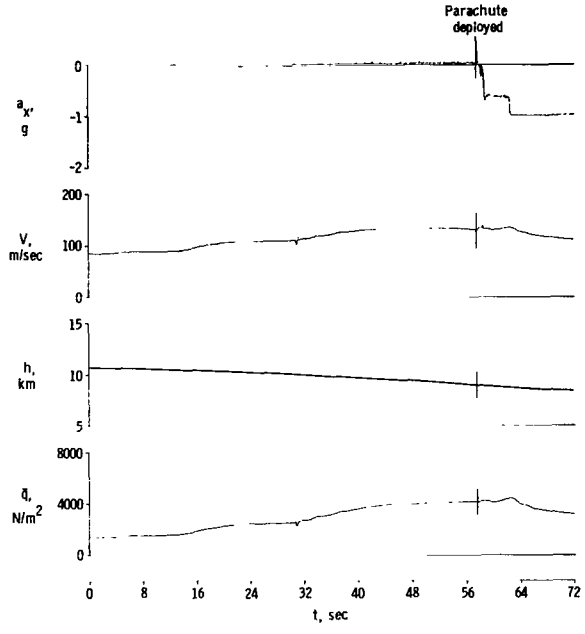

(d) Performance quantities.

Figure 20. Concluded.

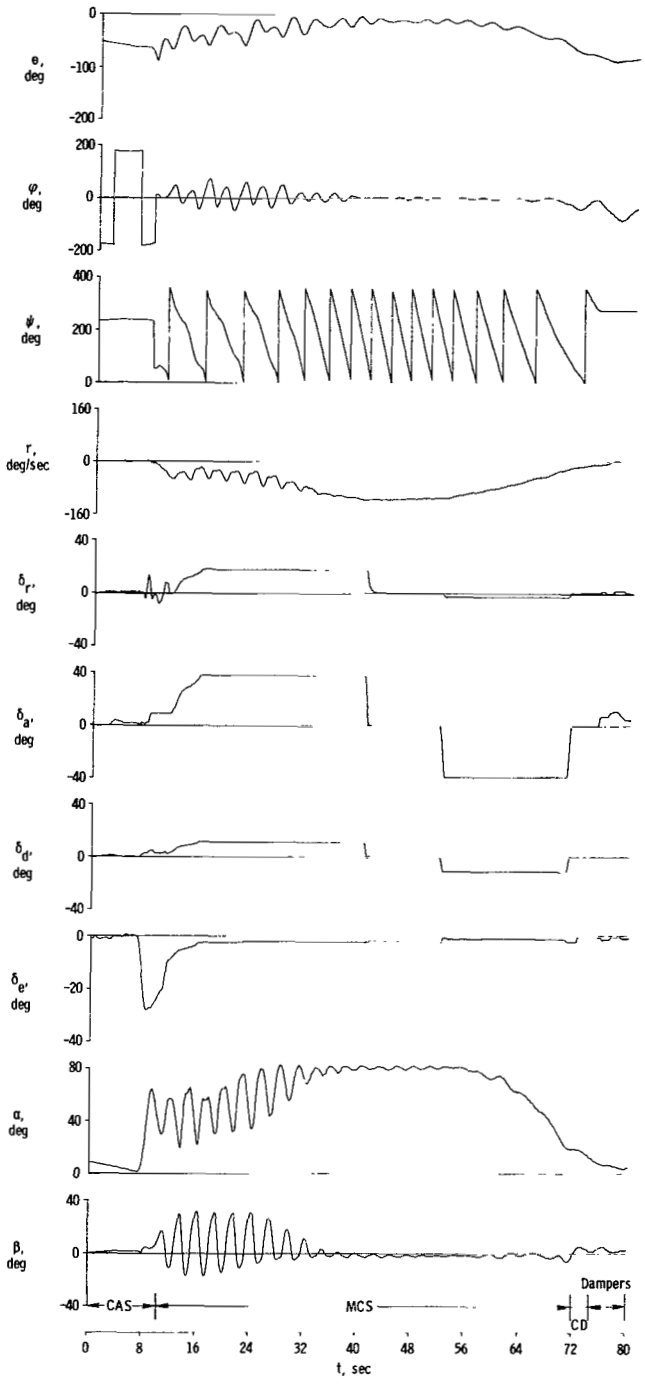

(a) Attitudes and related quantities.

Figure 21. Time histories of a high g erect spin at high altitude. Basic configuration; center of gravity at 30.3-percent mean aerodynamic chord.

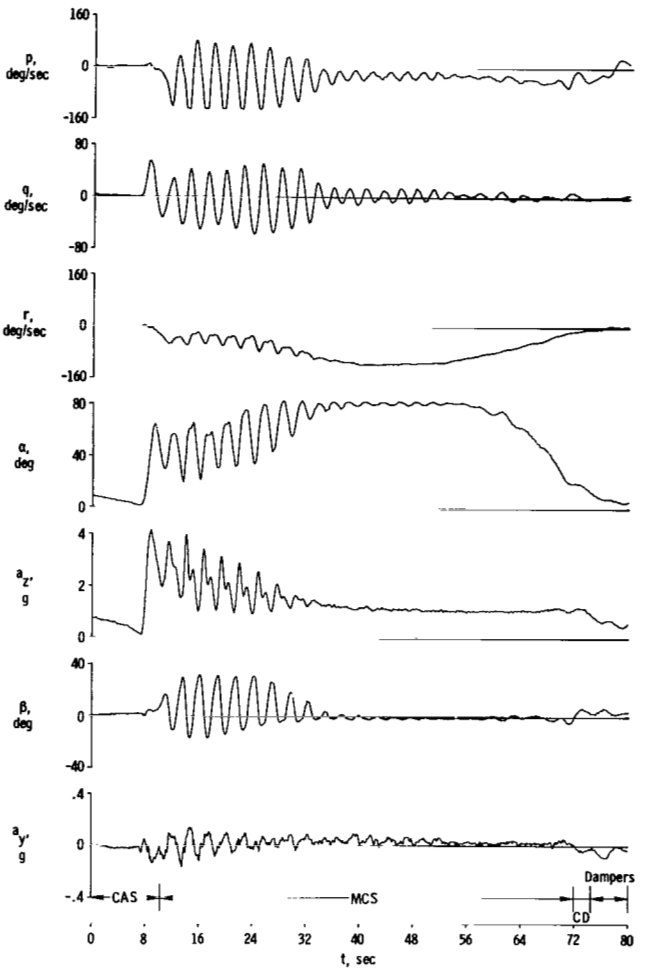

(b) Angular rates and related quantities.

Figure 21. Continued.

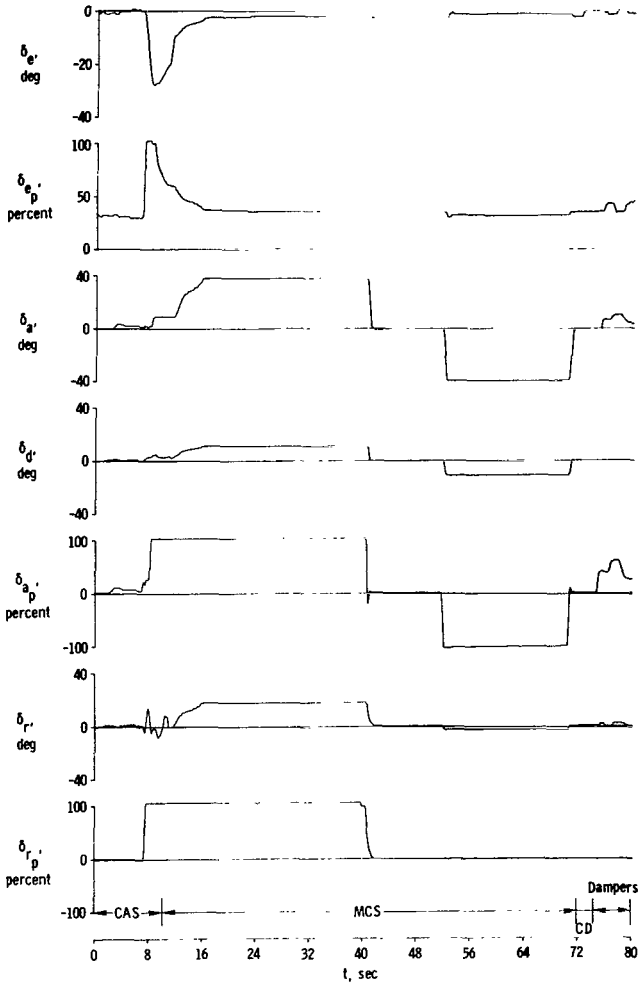

(c) Controls.

Figure 21. Continued.

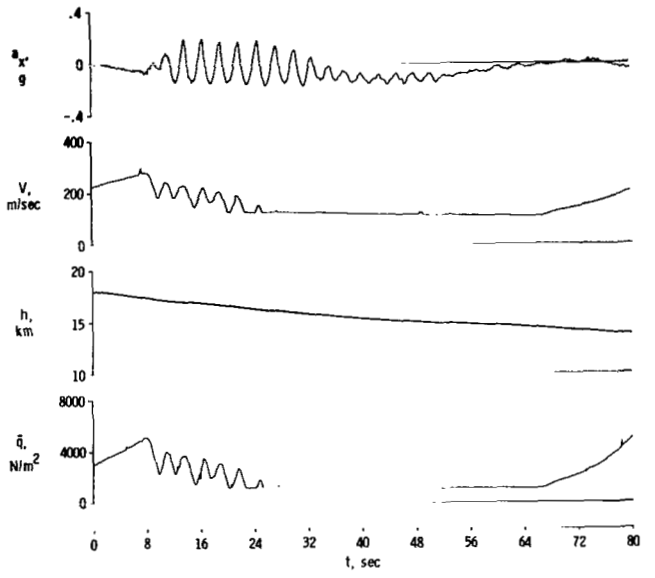

(d) Performance quantities.

Figure 21. Concluded.

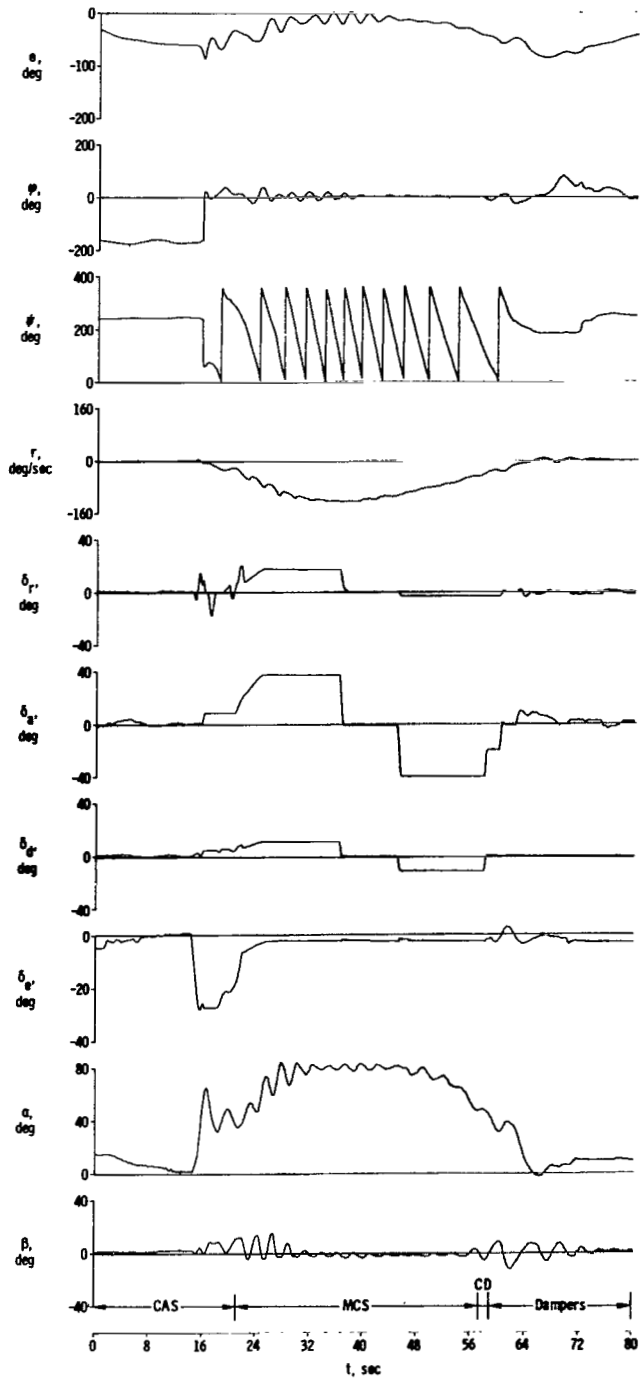

(a) Attitudes and related quantities.

Figure 22. Time histories of an erect spin repeated at high altitude. Basic configuration; center of gravity at 30.3-percent mean aerodynamic chord.

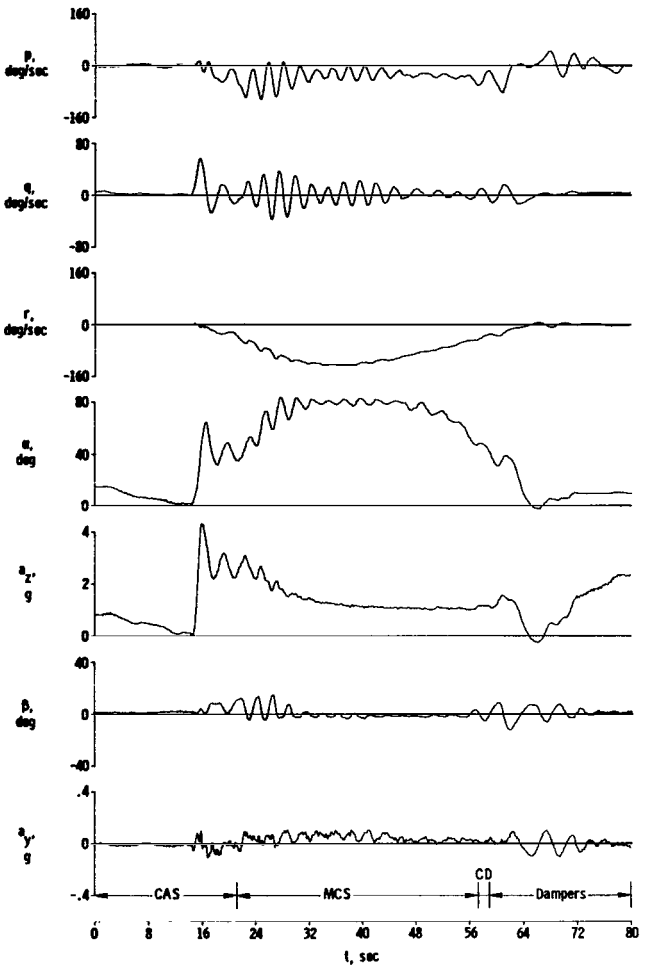

(b) Angular rates and related quantities.

Figure 22. Continued.

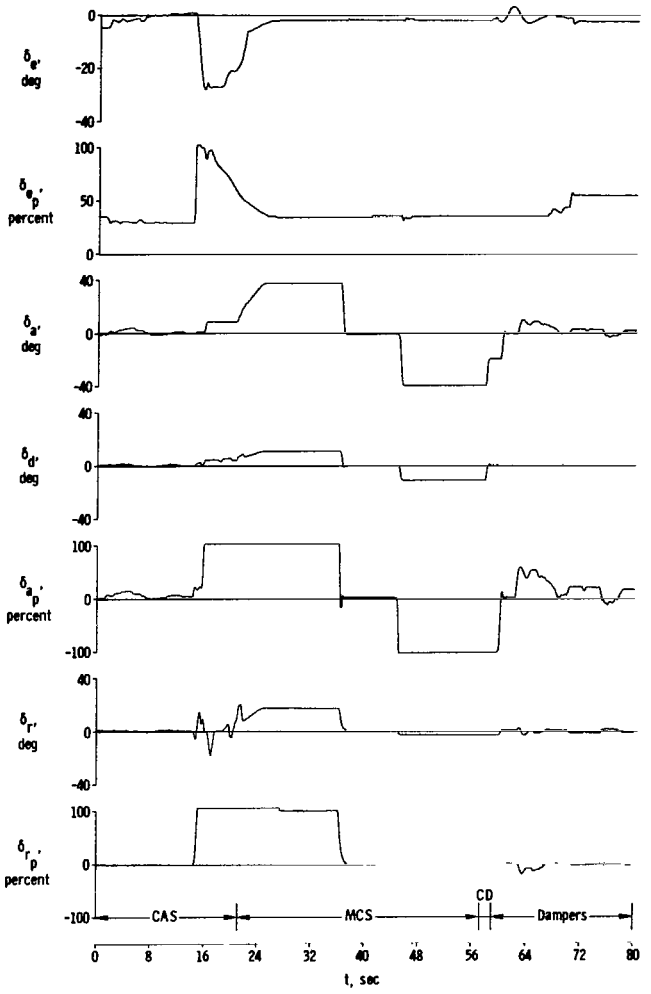

(c) Controls.

Figure 22. Continued.

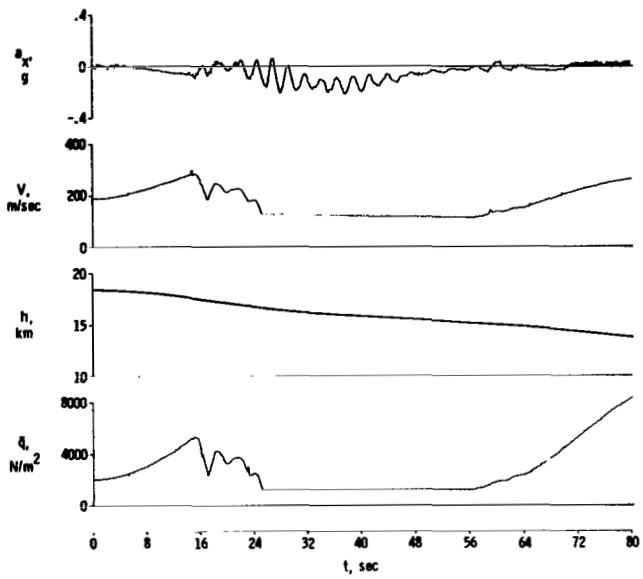

(d) Performance quantities.

Figure 22. Concluded.

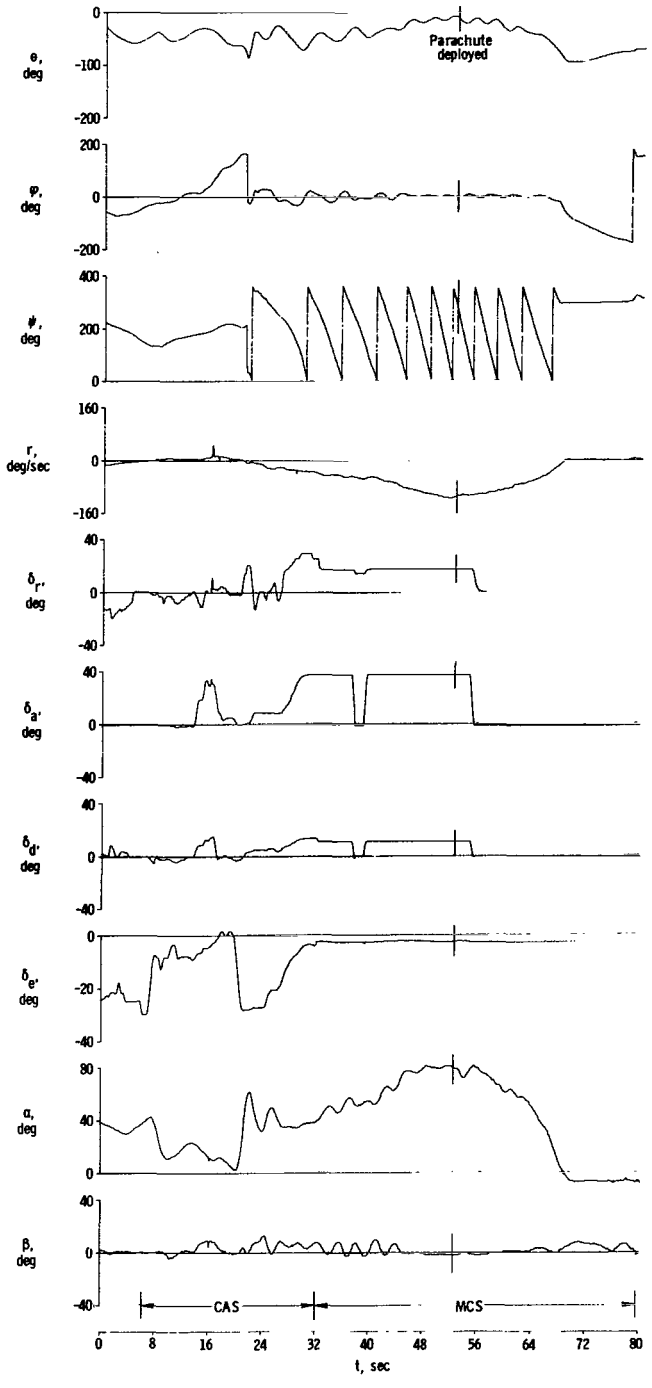

(a) Attitudes and related quantities.

Figure 23. Time histories of an erect spin at low altitude. High g entry technique; basic configuration; center of gravity at 30.3-percent mean aerodynamic chord.

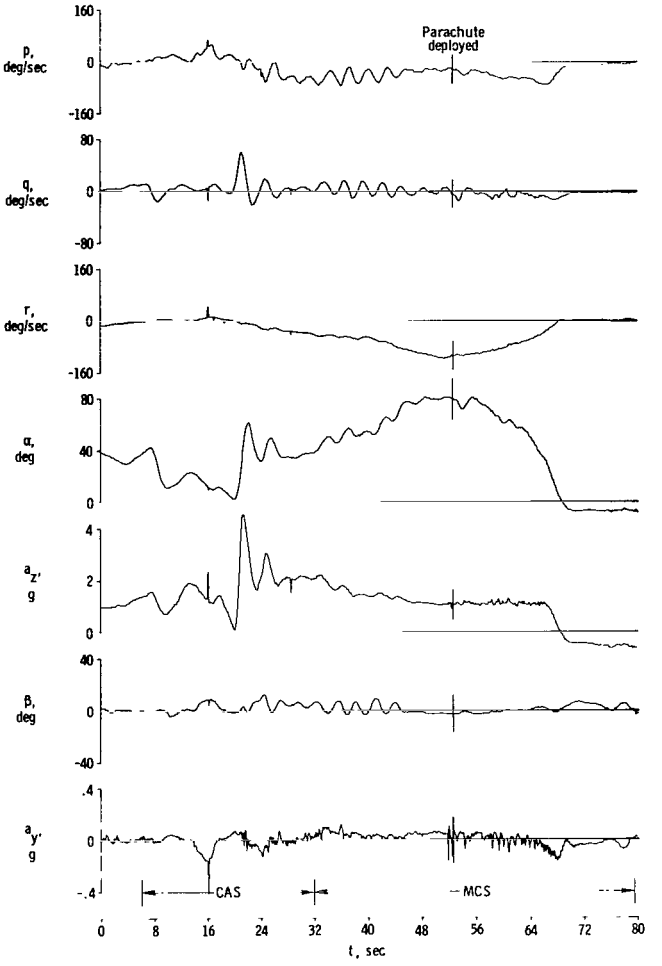

(b) Angular rates and related quantities.

Figure 23. Continued.

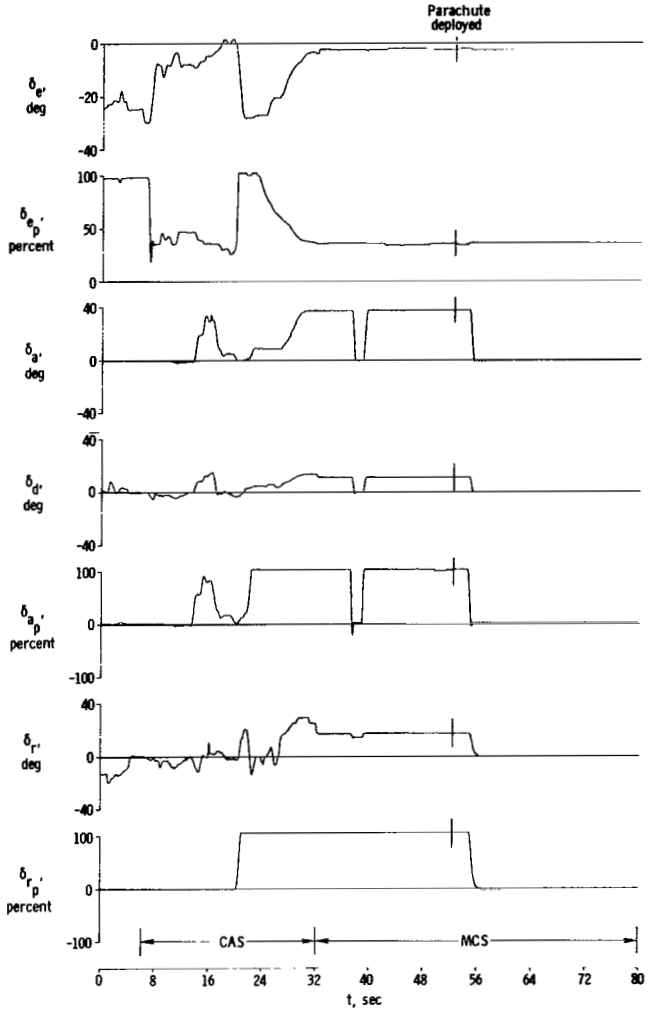

(c) Controls.

Figure 23. Continued.

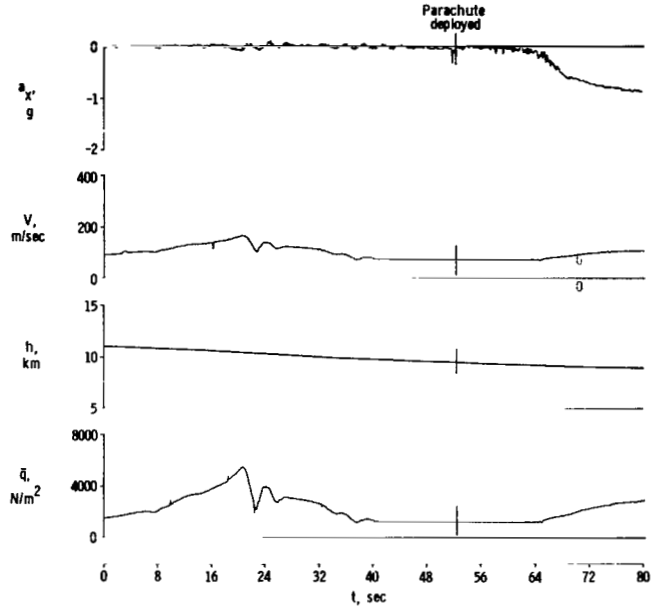

(d) Performance quantities.

Figure 23. Concluded.

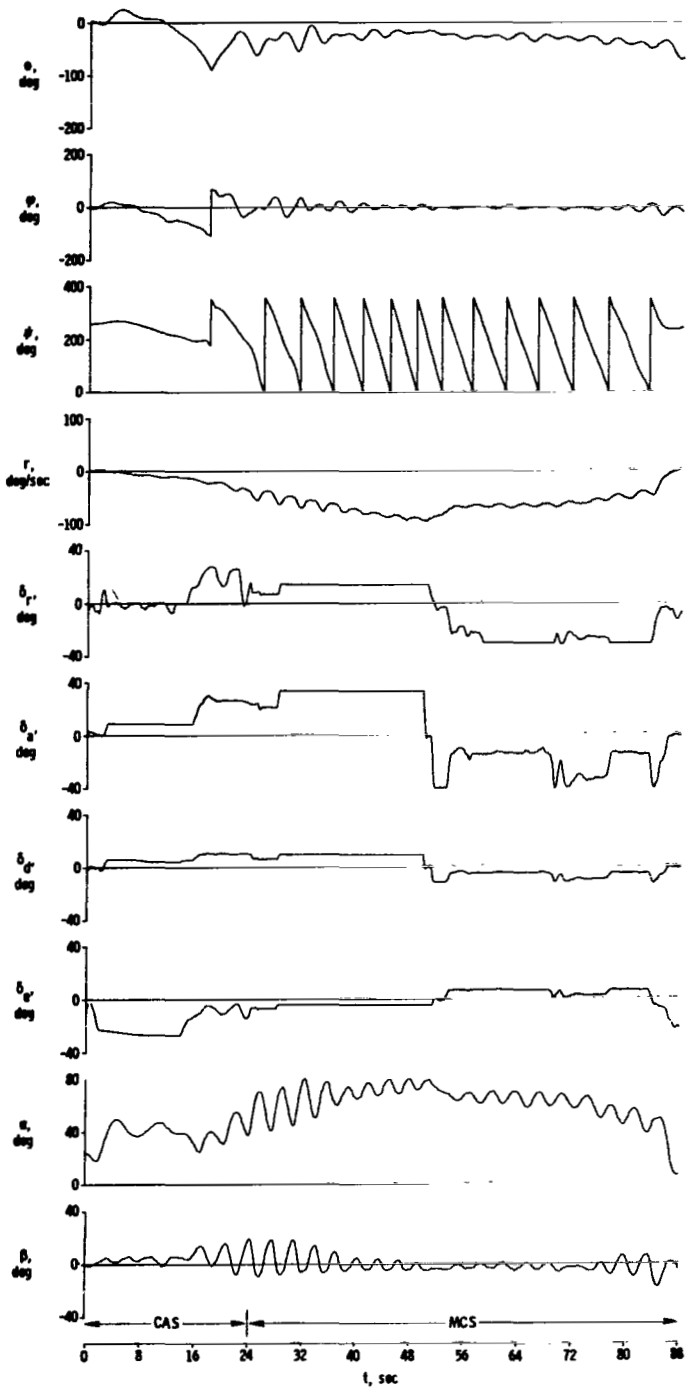

(a) Attitudes and related quantities.

Figure 24. Time histories of an erect spin. 1g entry; production configuration; center of gravity at 30.3-percent mean aerodynamic chord.

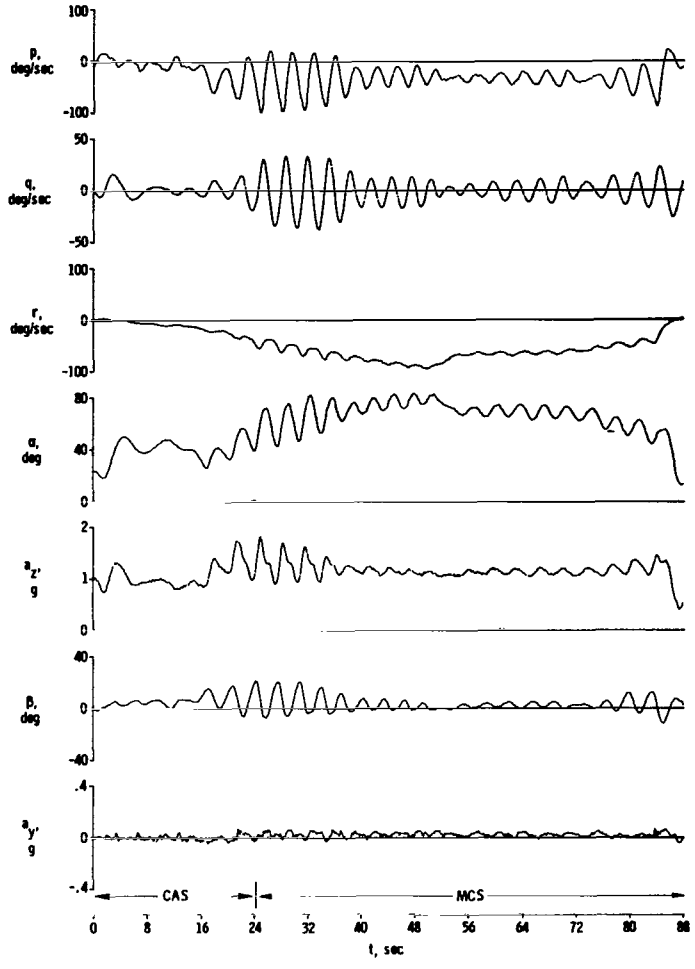

(b) Angular rates and related quantities.

Figure 24. Continued.

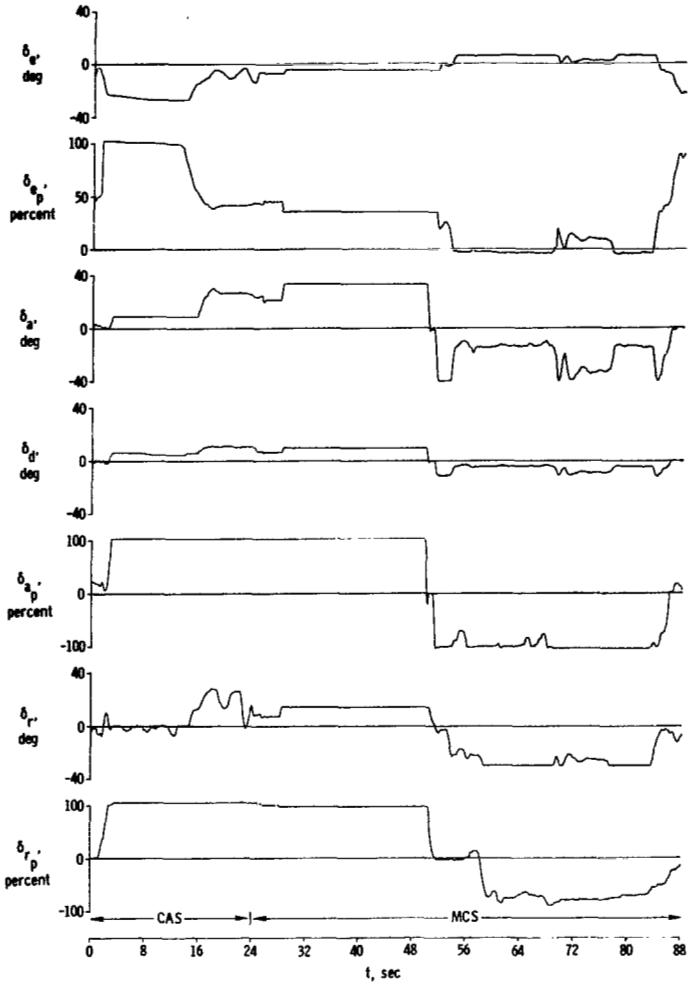

(c) Controls.

Figure 24. Continued.

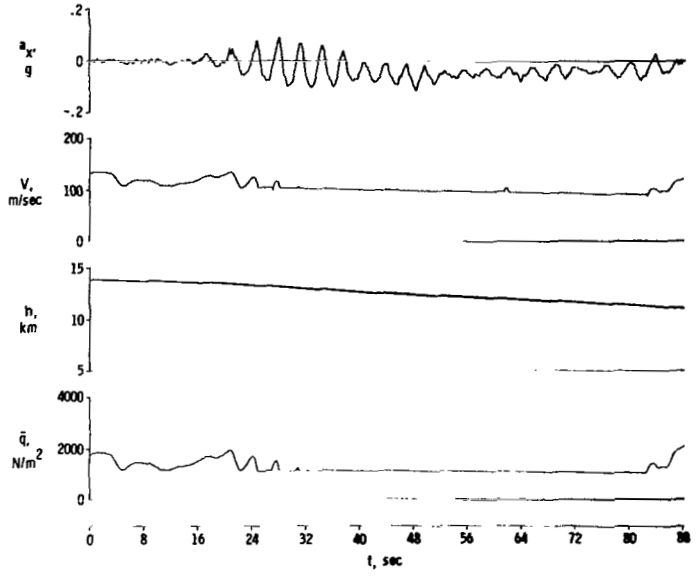

(d) Performance quantities.

Figure 24. Concluded.

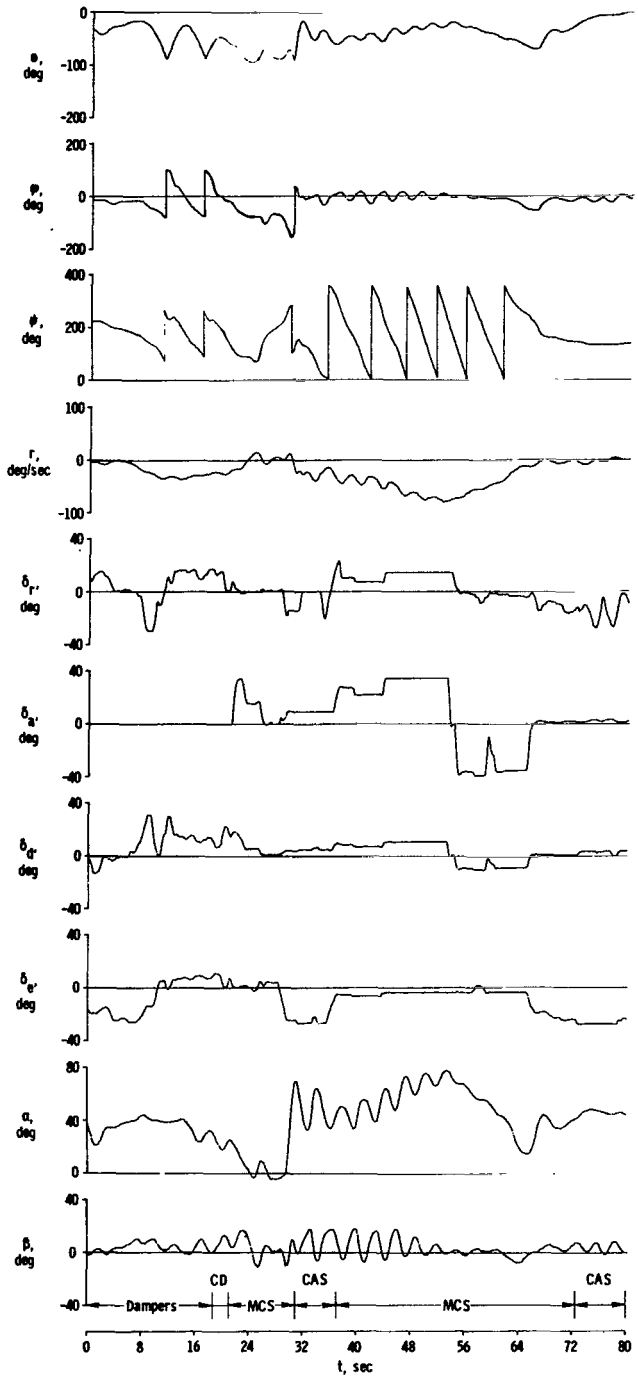

(a) Attitudes and related quantities.

Figure 25. Time histories of an erect spin. High g entry; production configuration; center of gravity at 30.3-percent mean aerodynamic chord.

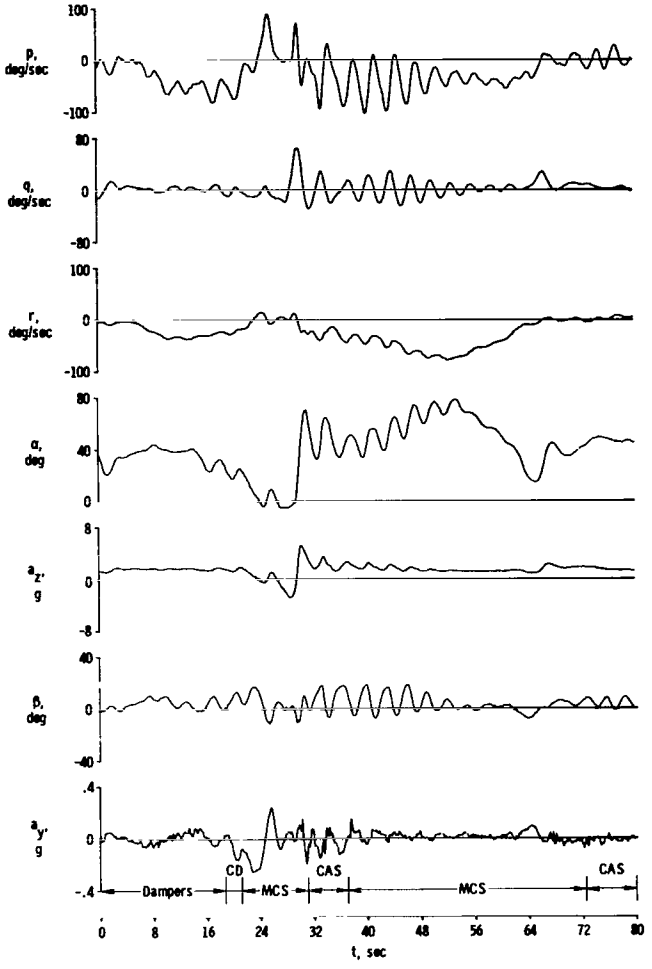

(b) Angular rates and related quantities.

Figure 25. Continued.

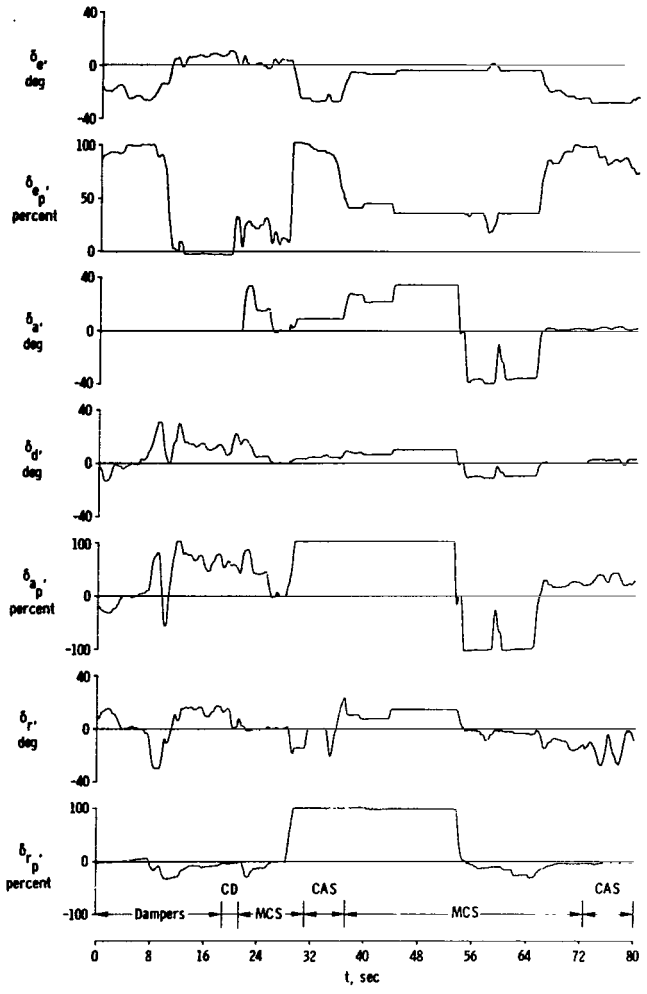

(c) Controls.

Figure 25. Continued.

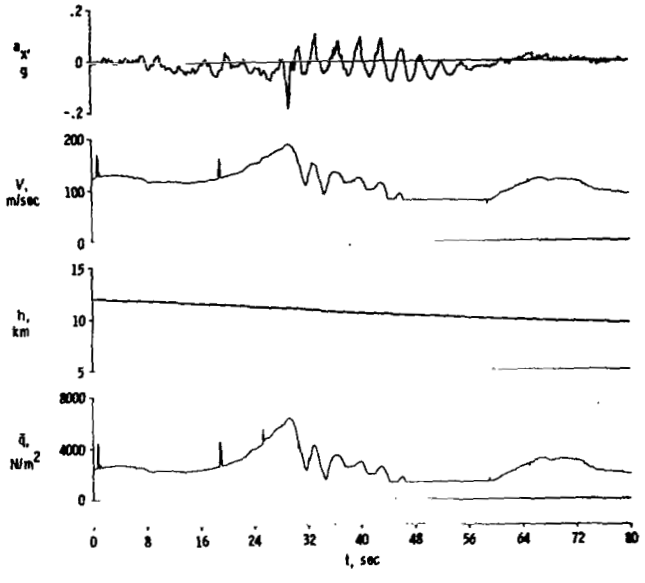

(d) Performance quantities.

Figure 25. Concluded.

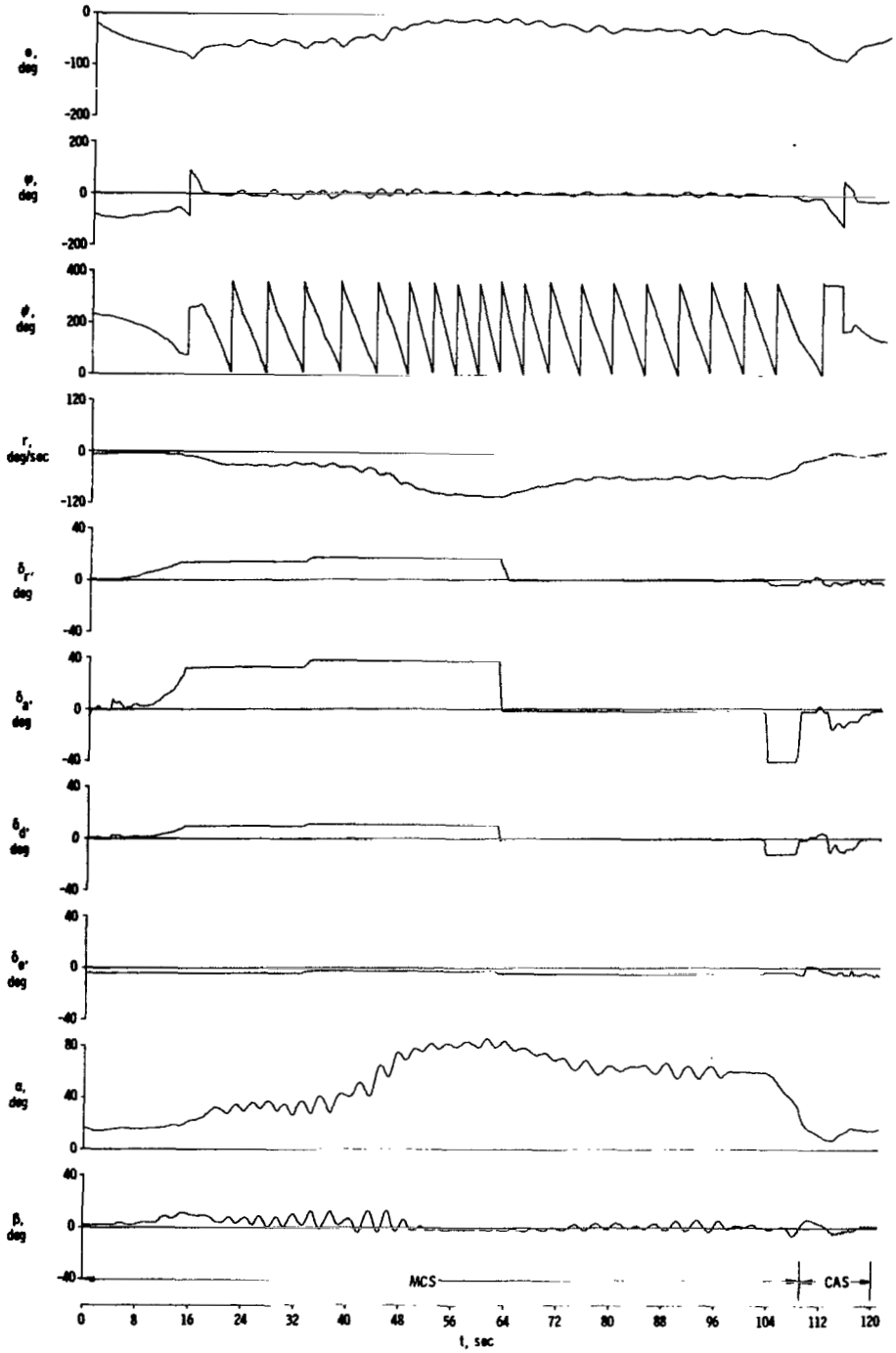

(a) Attitudes and related quantities.

Figure 26. Time histories of an erect spin with the MCS. "Knife edge" entry technique; production configuration; center of gravity at 30.3-percent mean aerodynamic chord.

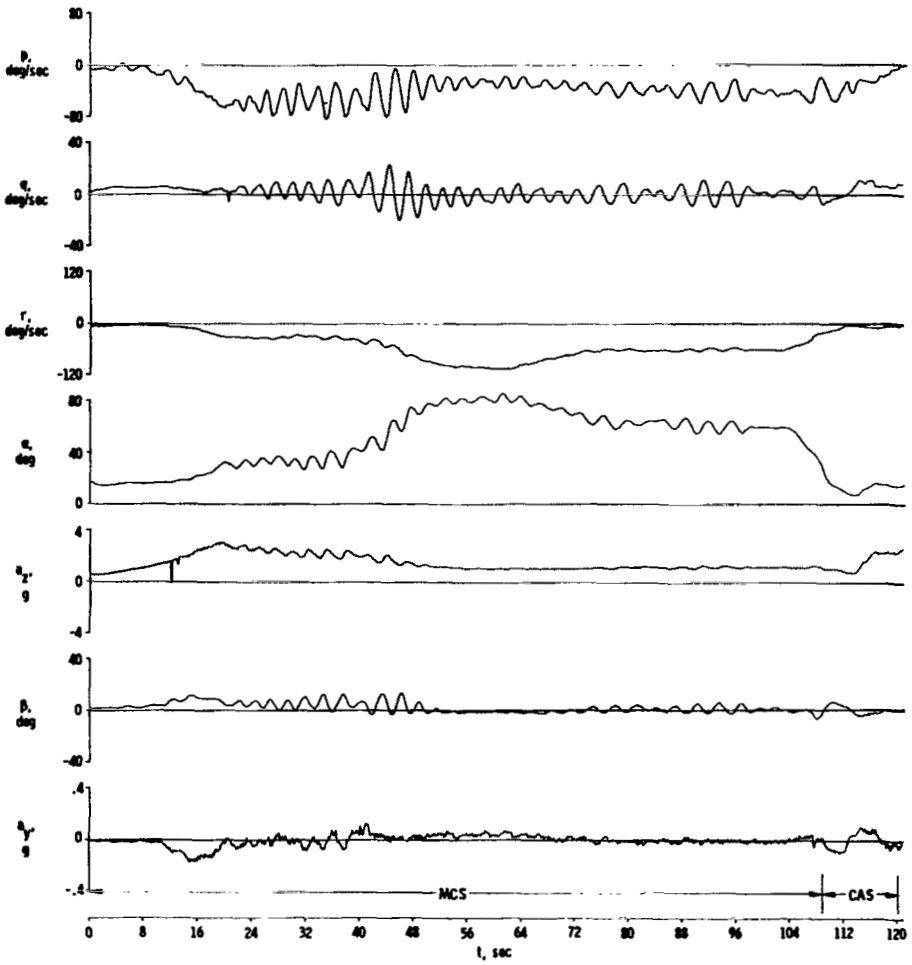

(b) Angular rates and related quantities.

Figure 26. Continued.

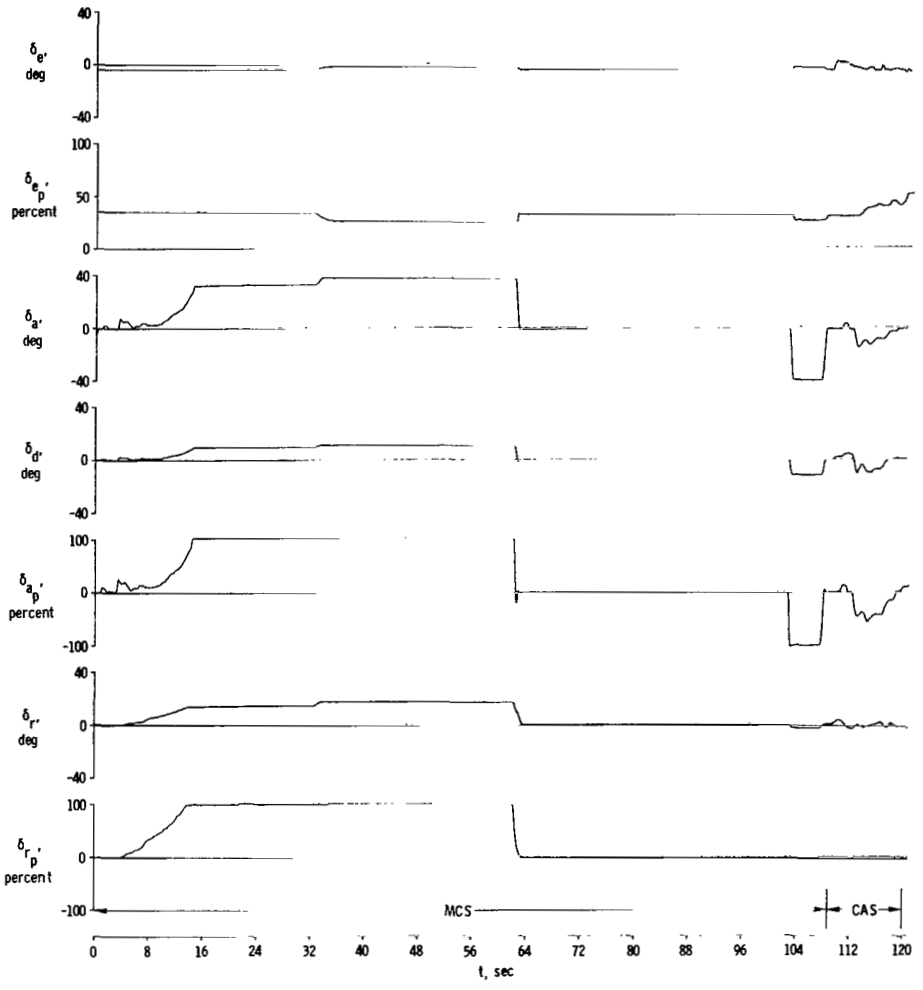

(c) Controls.

Figure 26. Continued.

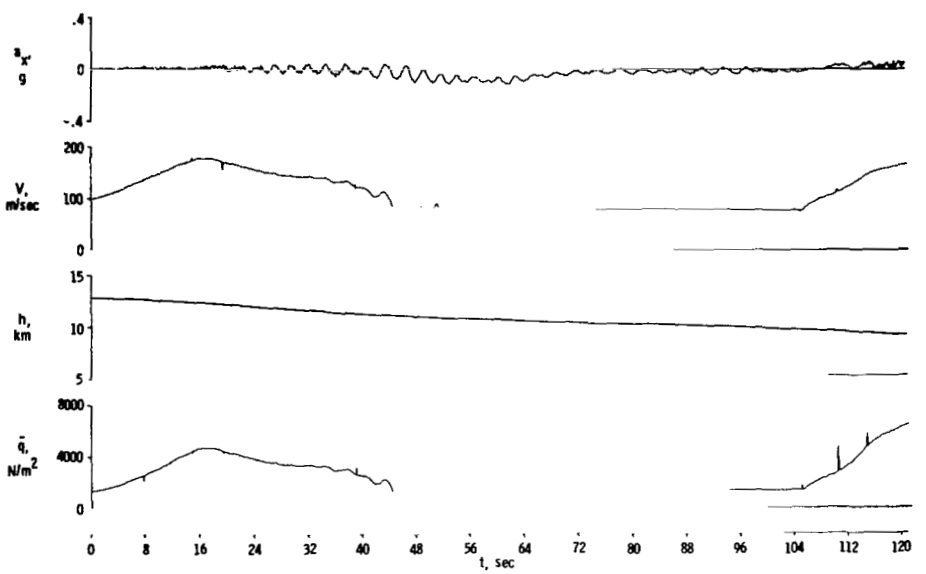

(d) Performance quantities.

Figure 26. Concluded.

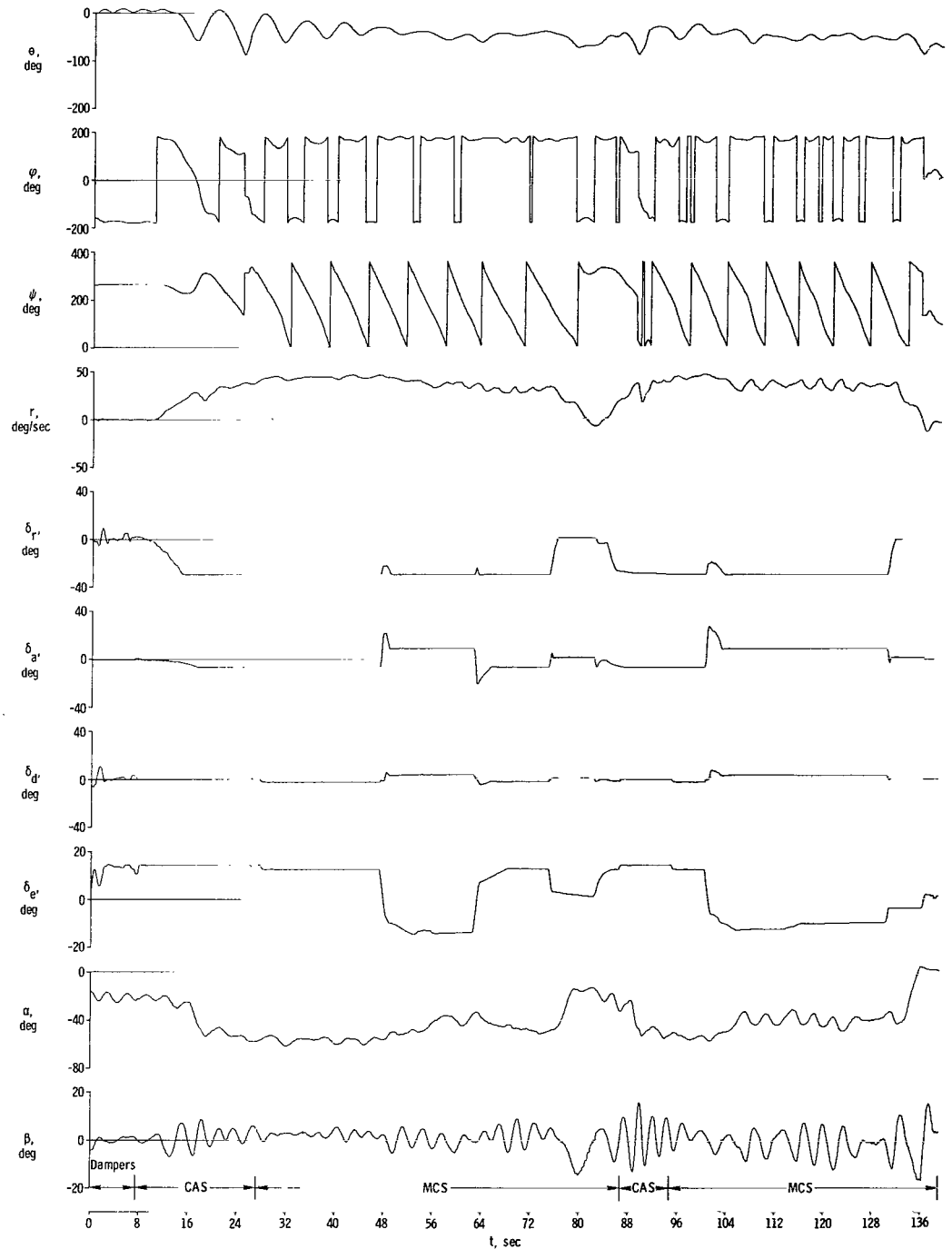

(a) Attitudes and related quantities.

Figure 27. Time histories of inverted spins at -1g. Production configuration; center of gravity at 30.3-percent mean aerodynamic chord.

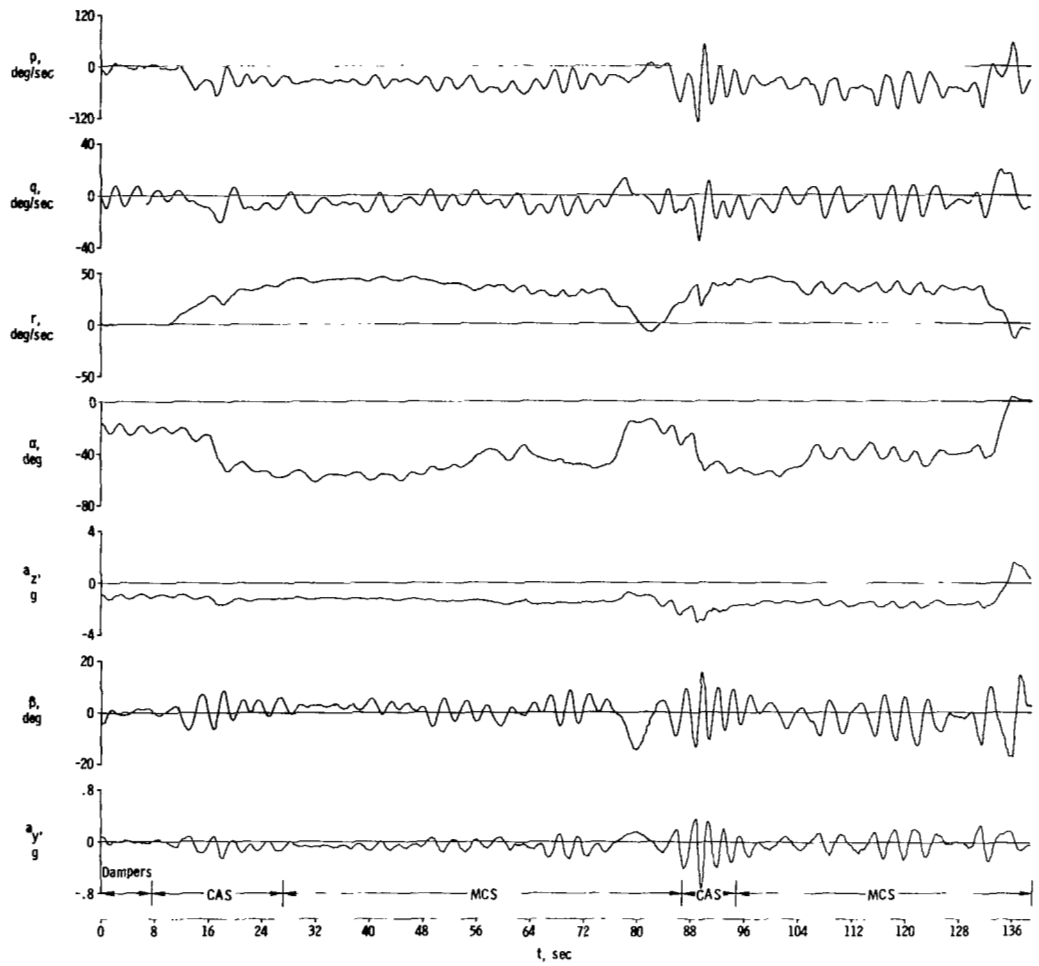

(b) Angular rates and related quantities.

Figure 27. Continued.

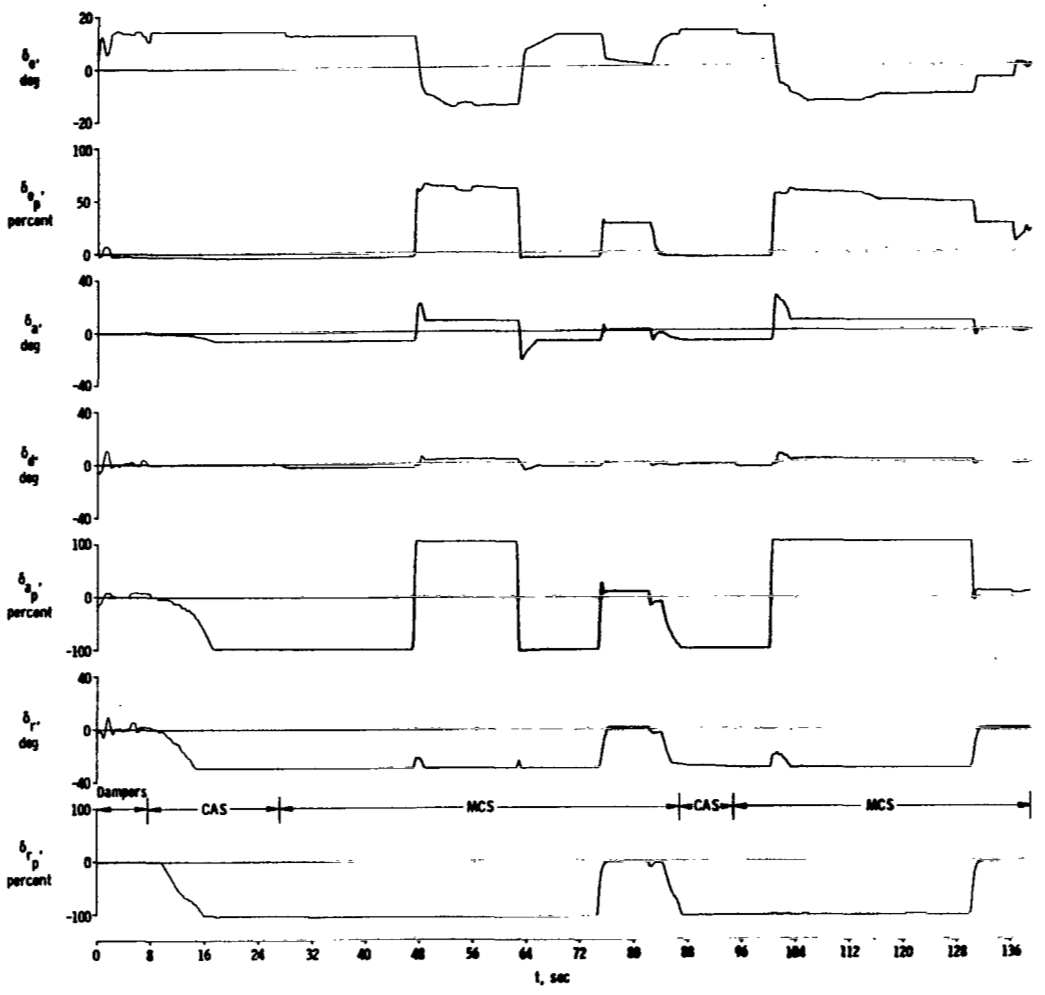

(c) Controls.

Figure 27. Continued.

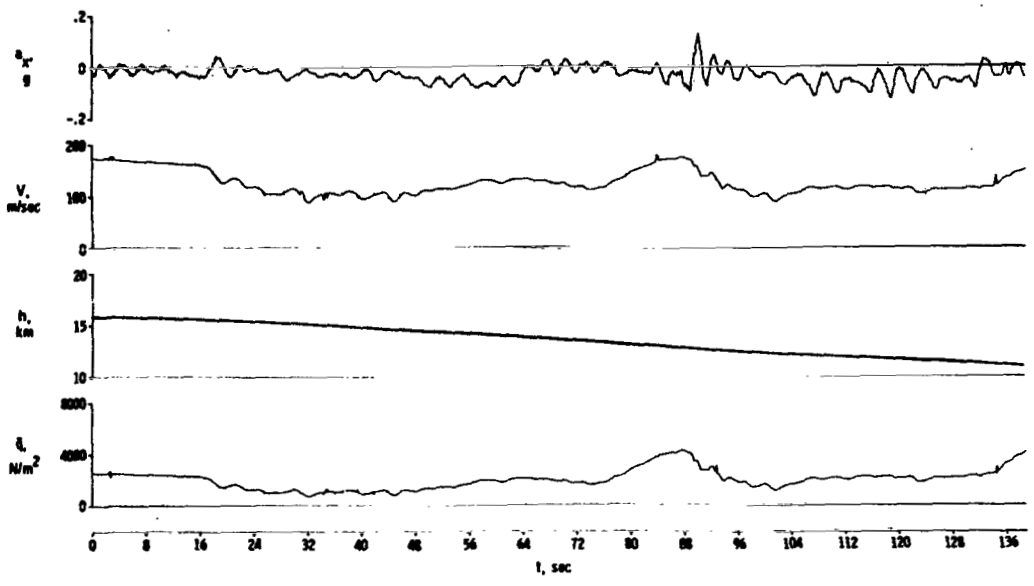

(d) Performance quantities.

Figure 27. Concluded.

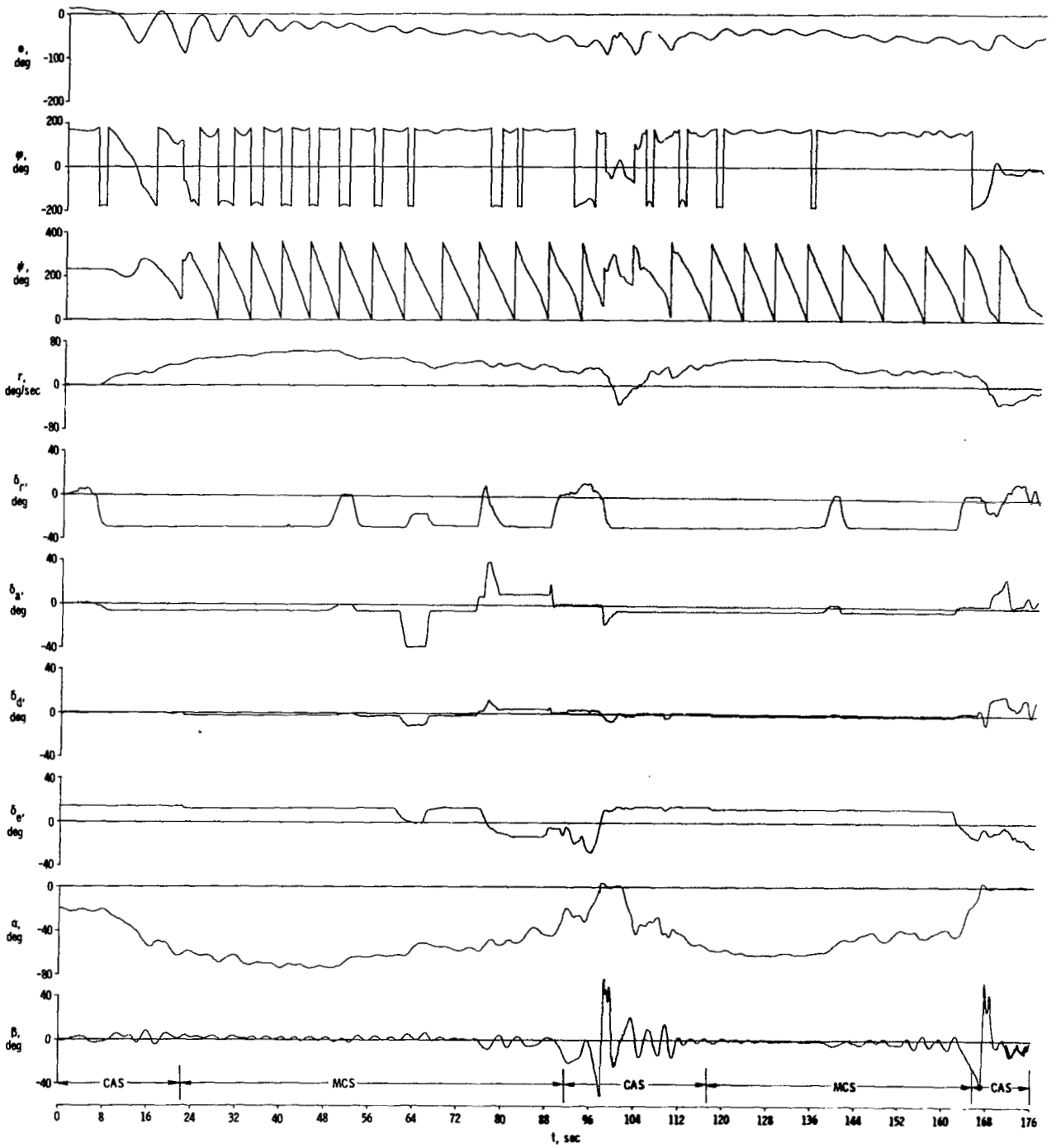

(a) Attitudes and related quantities.

Figure 28. Time histories of repeated inverted spins at -1g. Production configuration; center of gravity at 30.3-percent mean aerodynamic chord.

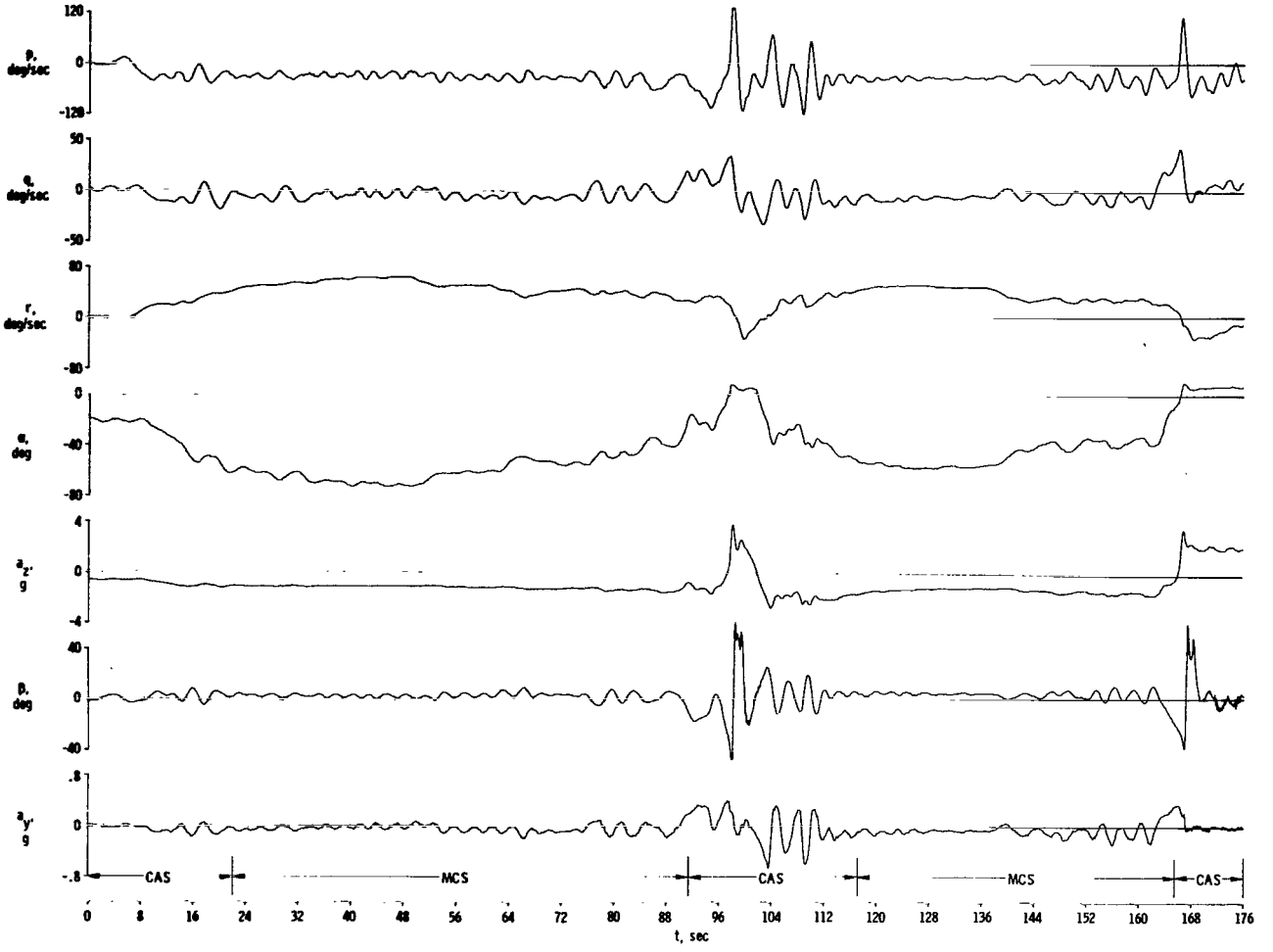

(b) Angular rates and related quantities.

Figure 28. Continued.

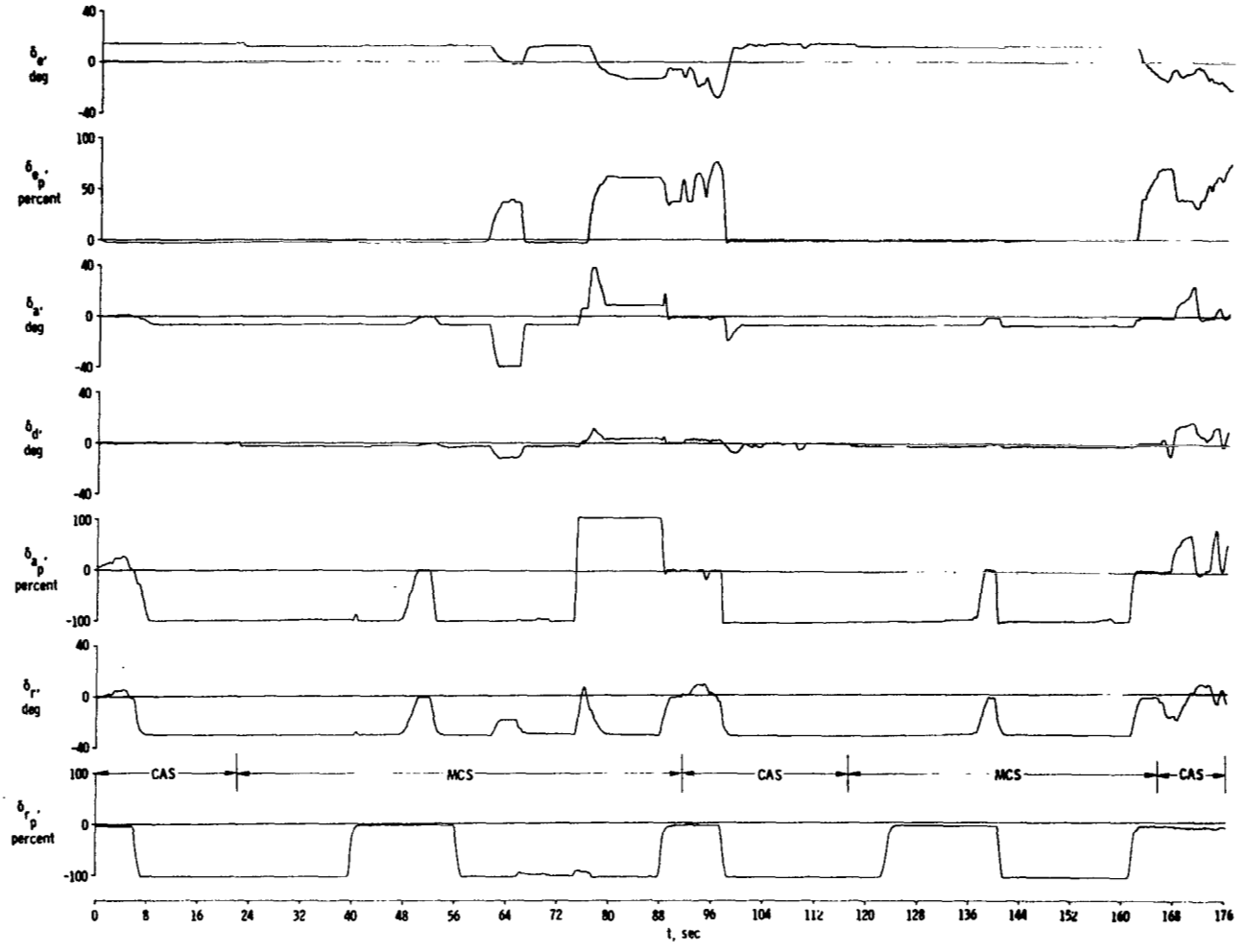

(c) Controls.

Figure 28. Continued.

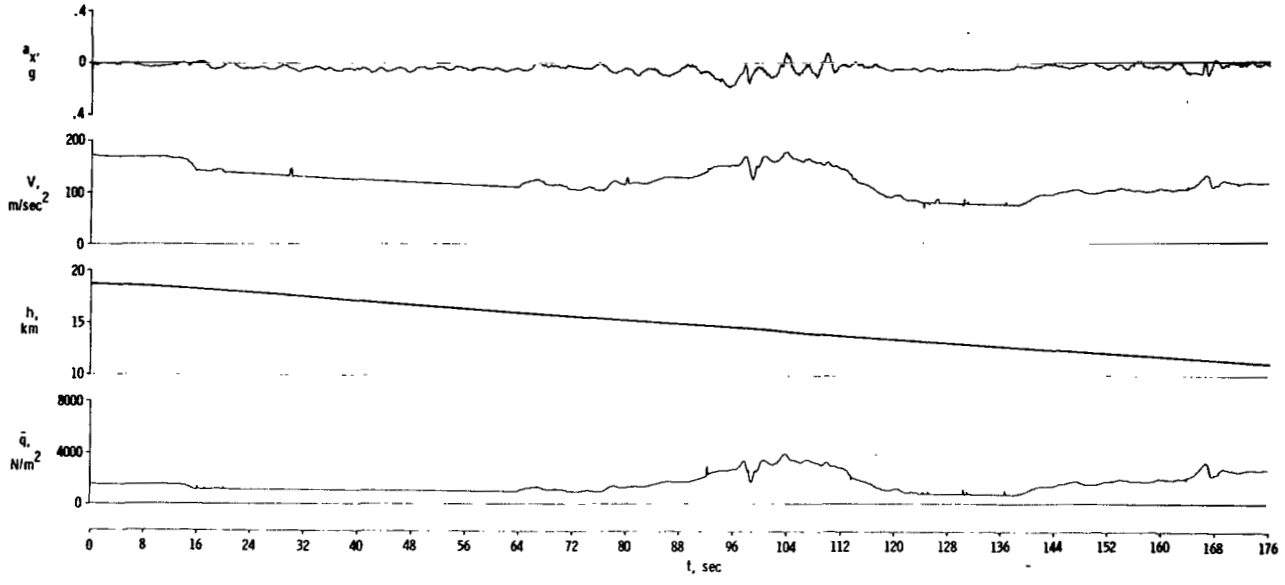

(d) Performance quantities.

Figure 28. Concluded.

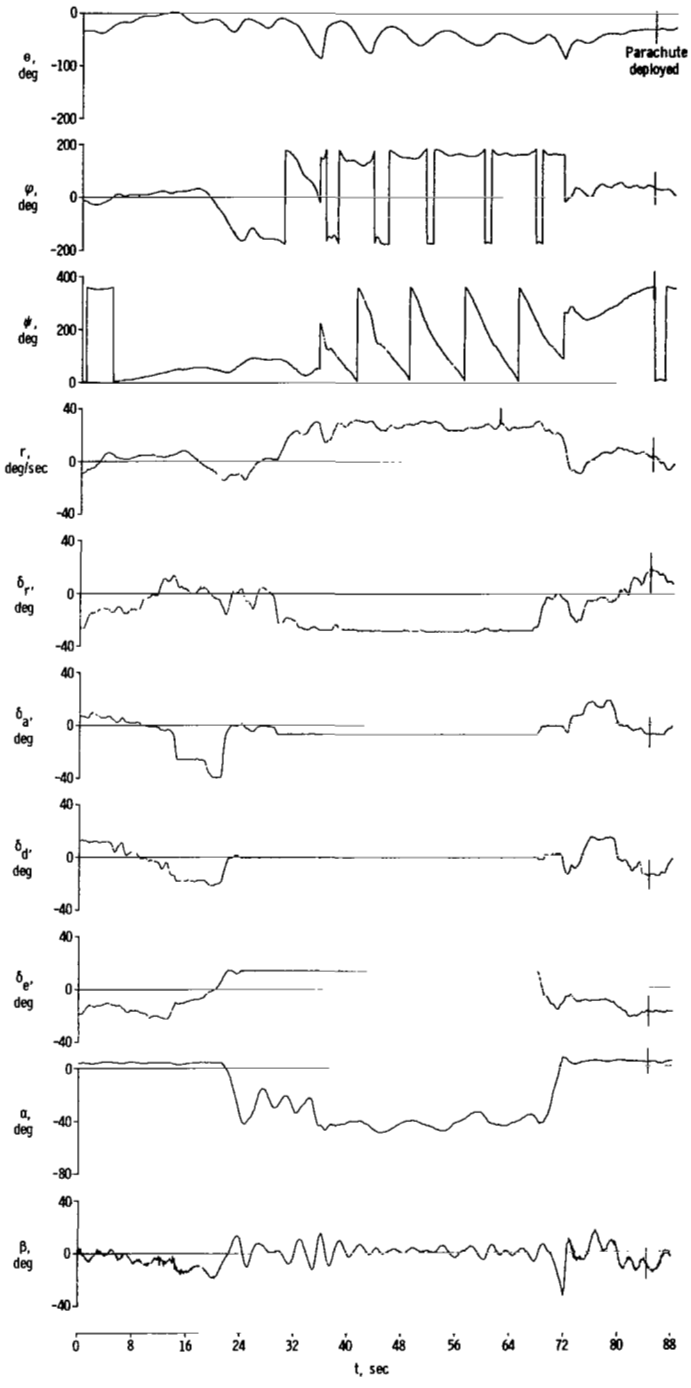

(a) Attitudes and related quantities.

Figure 29. Time histories of an inverted spin. Attempted "pullup" entry; production configuration; center of gravity at 30.3-percent mean aerodynamic chord; CAS.

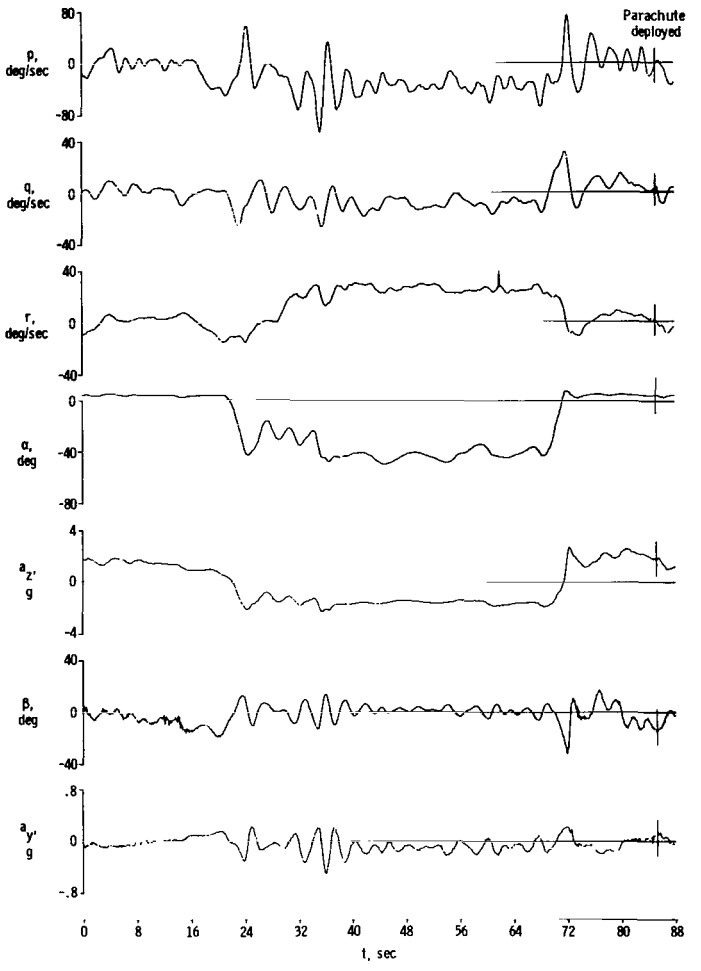

(b) Angular rates and related quantities.

Figure 29. Continued.

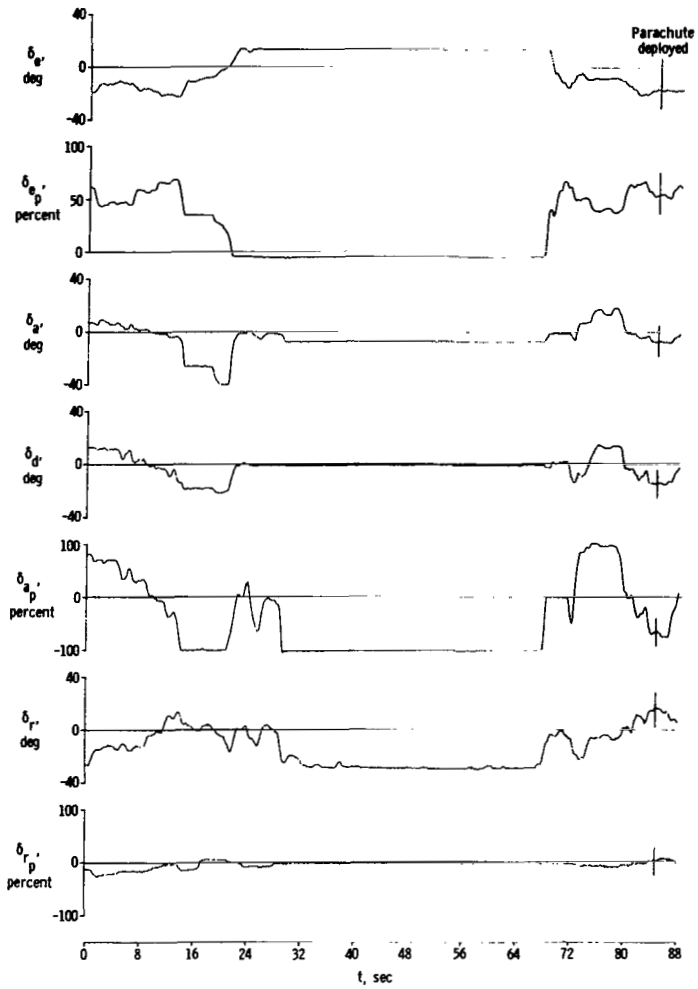

(c) Controls.

Figure 29. Continued.

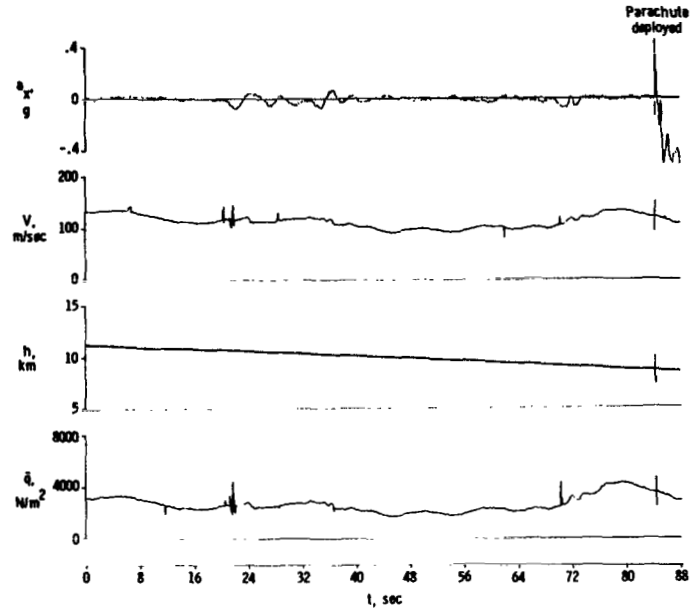

(d) Performance quantities.

Figure 29. Concluded.

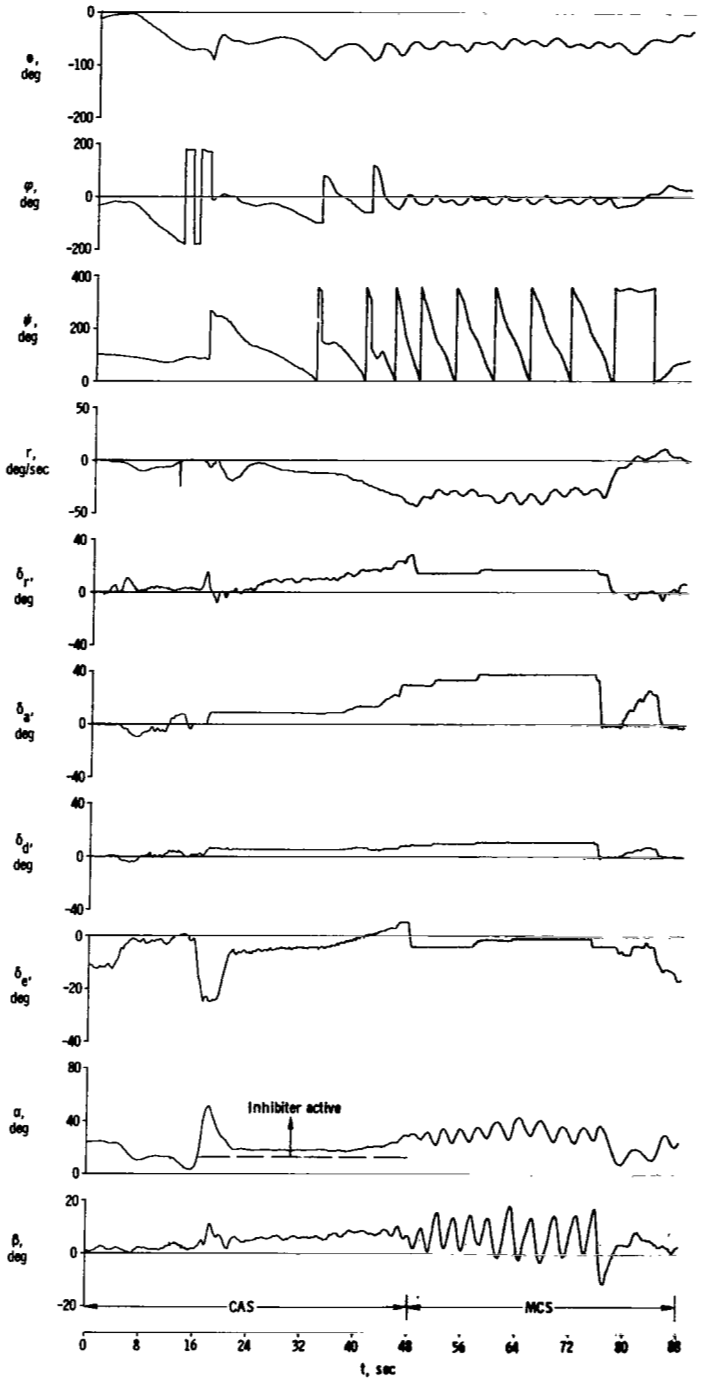

(a) Attitudes and related quantities.

Figure 30. Time histories of an attempt to force a spin with the high g entry technique to check the operation of the stall inhibiter. Center of gravity at 30.3-percent mean aerodynamic chord.

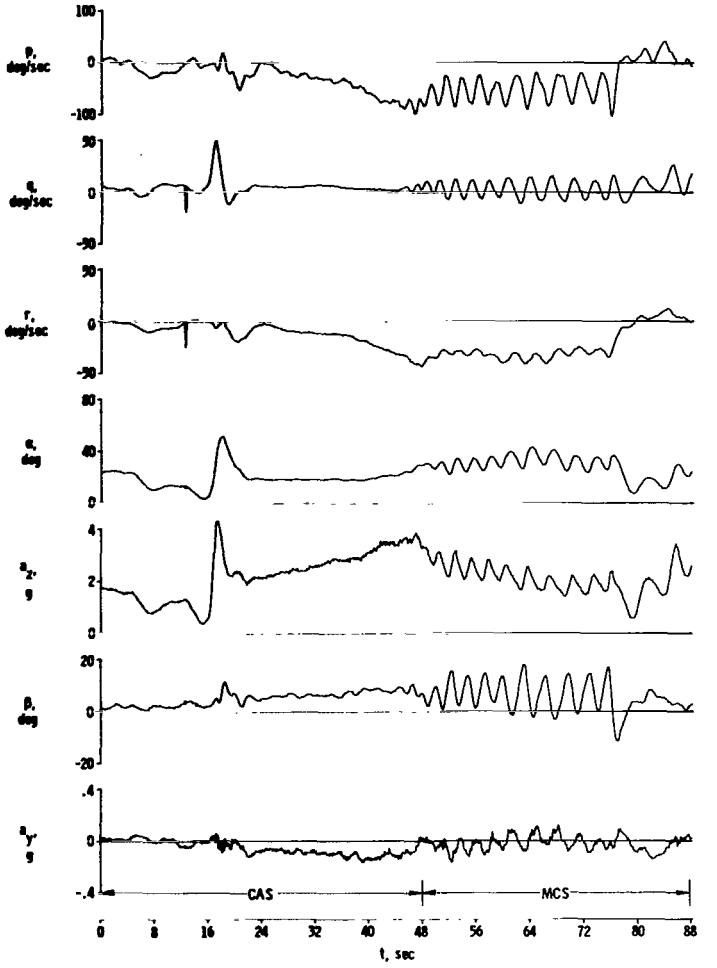

(b) Angular rates and related quantities.

Figure 30. Continued.

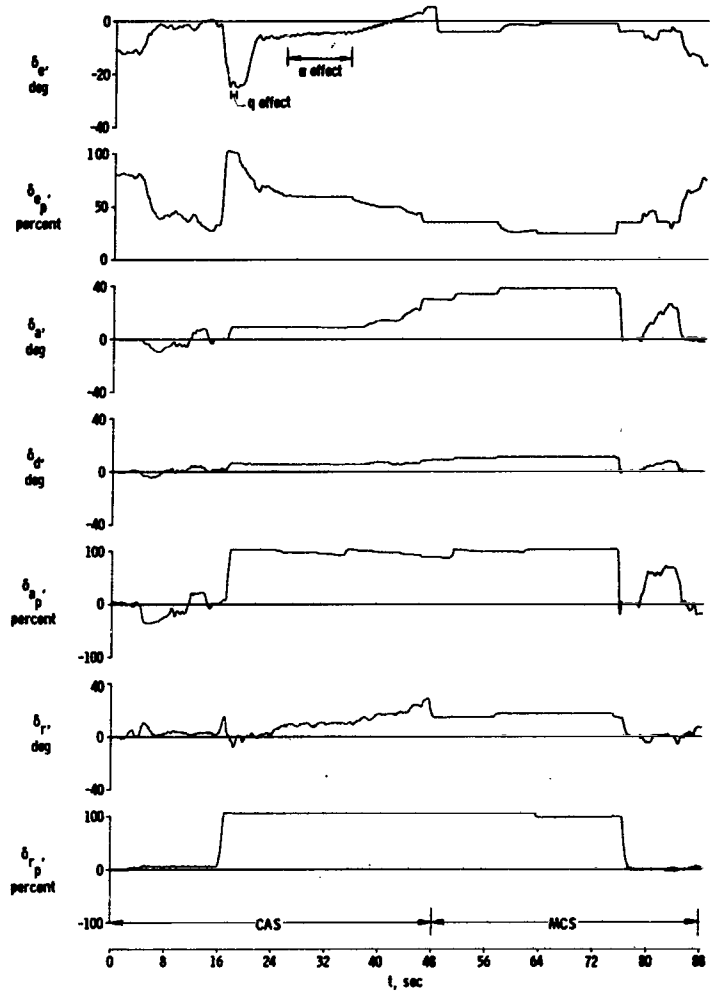

(c) Controls.

Figure 30. Continued.

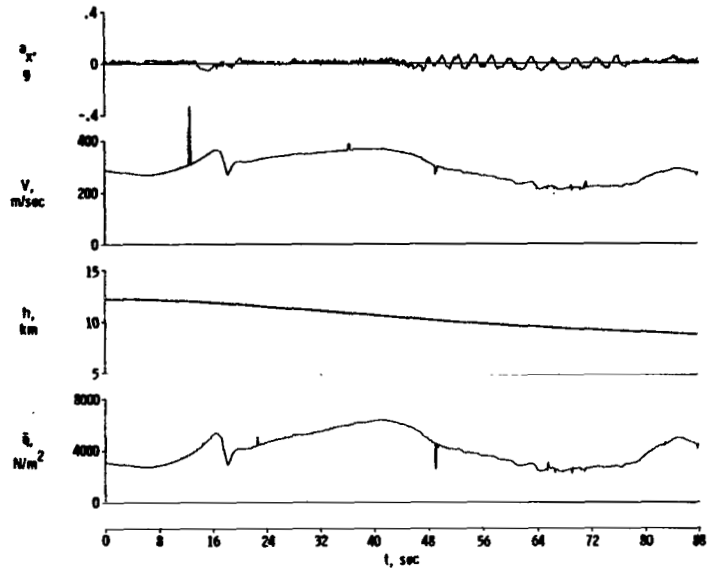

(d) Performance quantities.

Figure 30. Concluded.

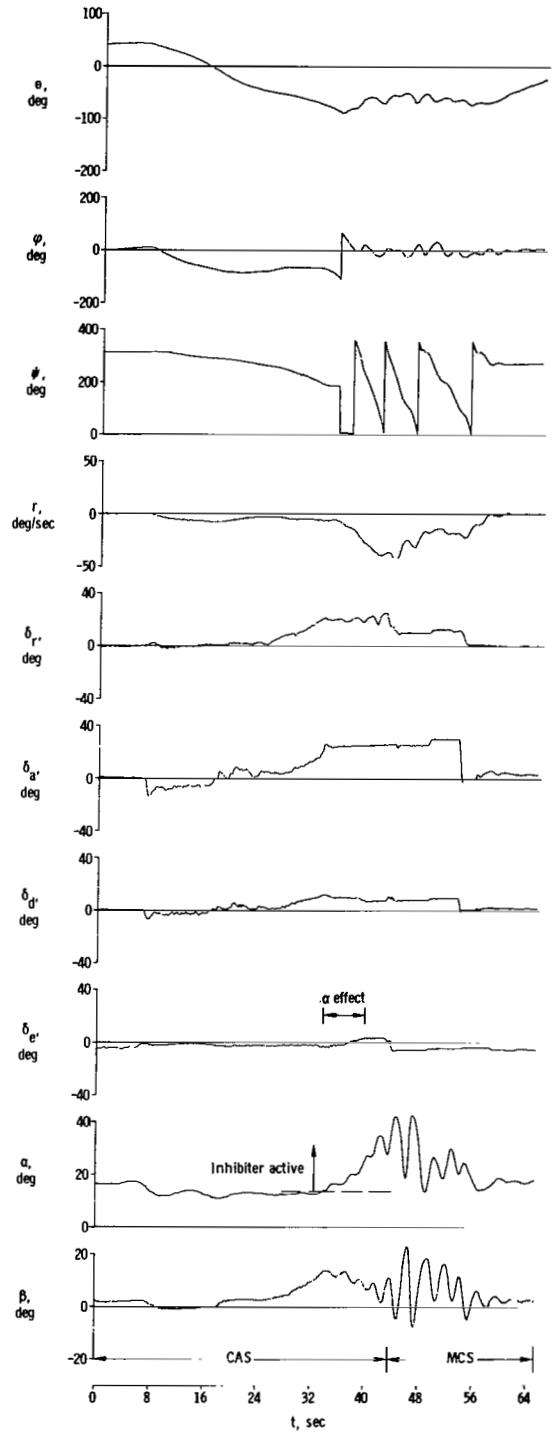

(a) Attitudes and related quantities.

Figure 31. Time histories of an attempt to force a spin using the "knife edge" entry technique to check the operation of the stall inhibiter. Center of gravity at 30.3-percent mean aerodynamic chord.

Error

An error occurred while processing this page. See the system log for more details.

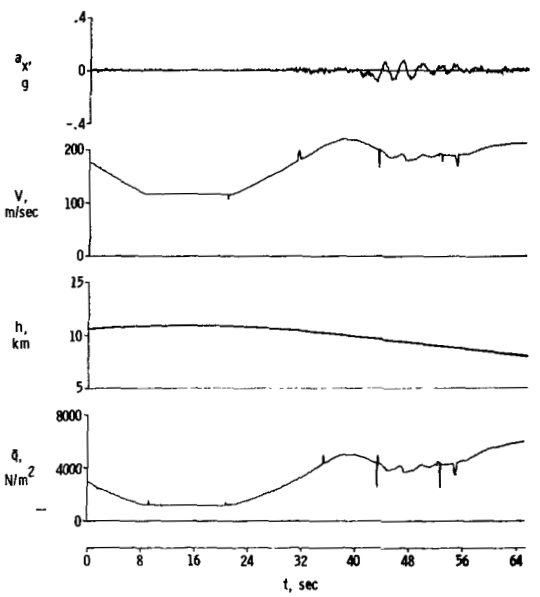

(d) Performance quantities.

Figure 31. Concluded.

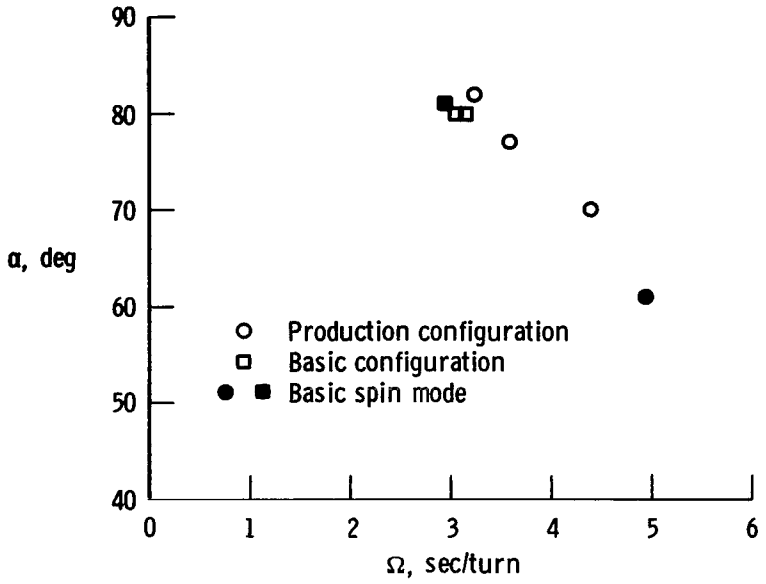

Figure 32. Airplane basic spin data from the large-scale airplane model tests. Center of gravity at 30.3-percent mean aerodynamic chord.

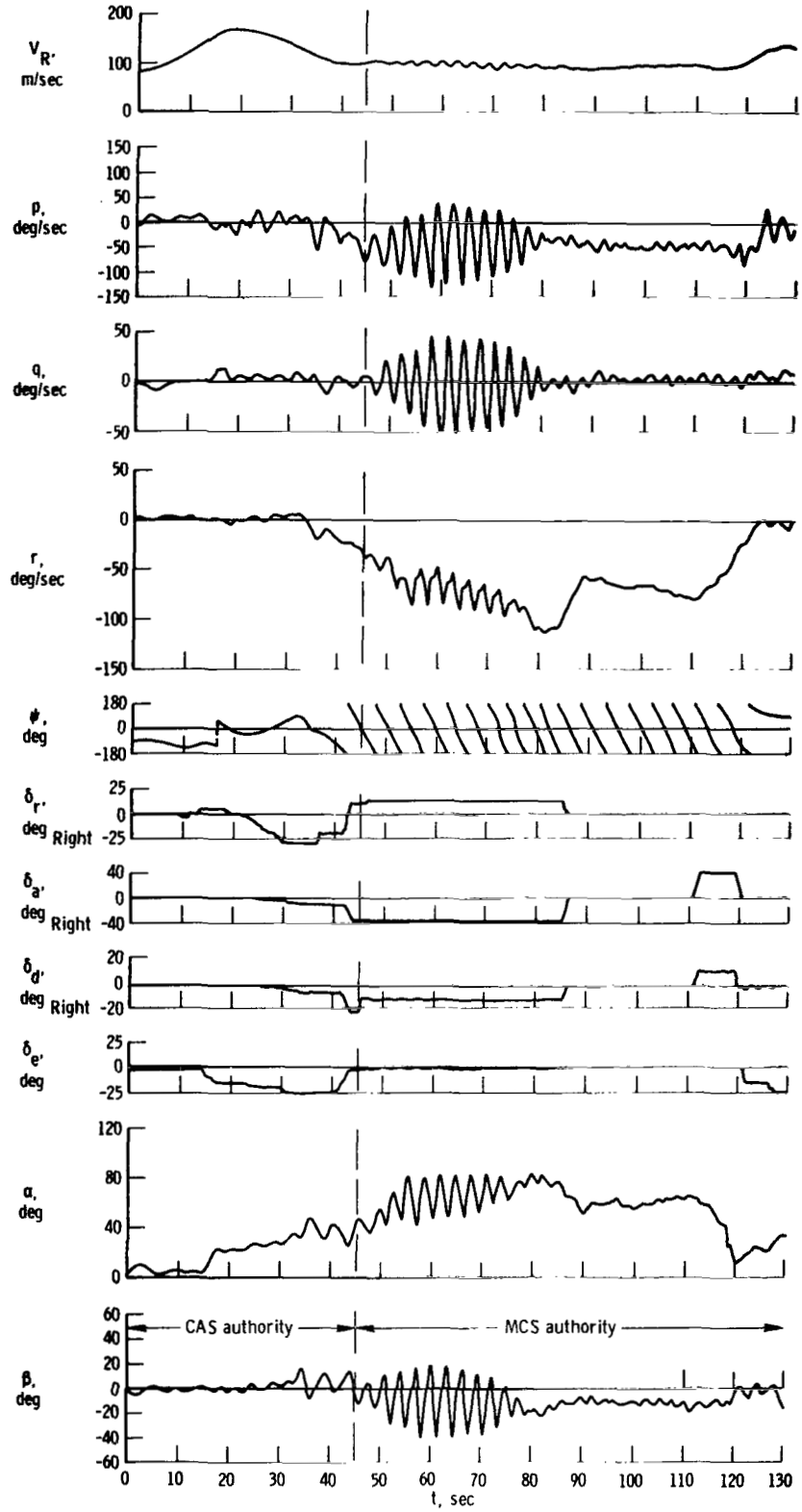

Figure 33. Time history of a spin of the Langley 13-percent-scale model. Center of gravity at 24-percent mean aerodynamic chord.

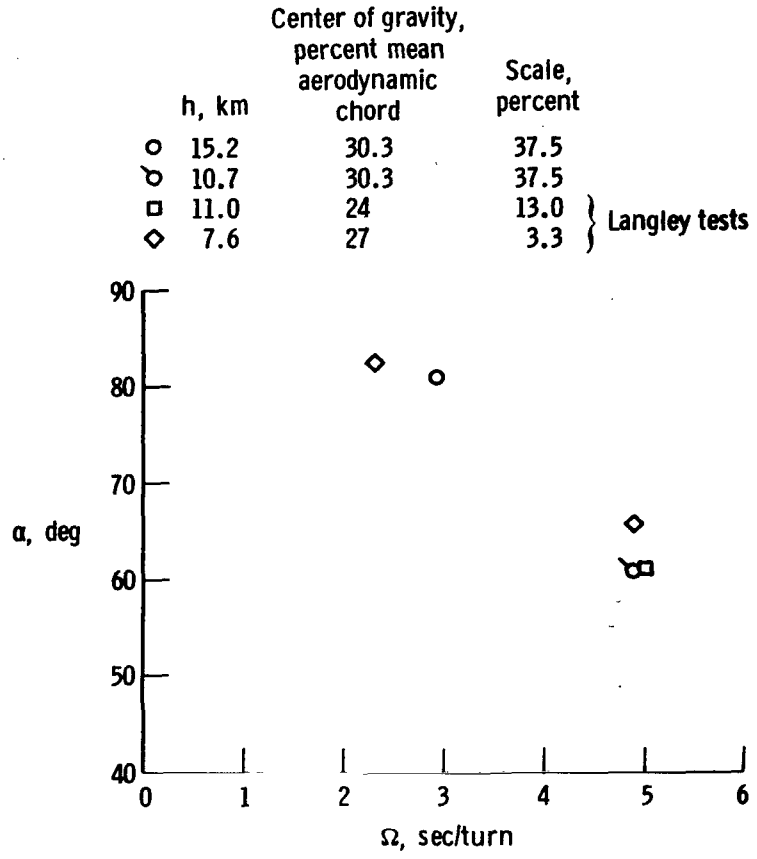

Figure 34. Comparison of scale model predictions of airplane spin characteristics.

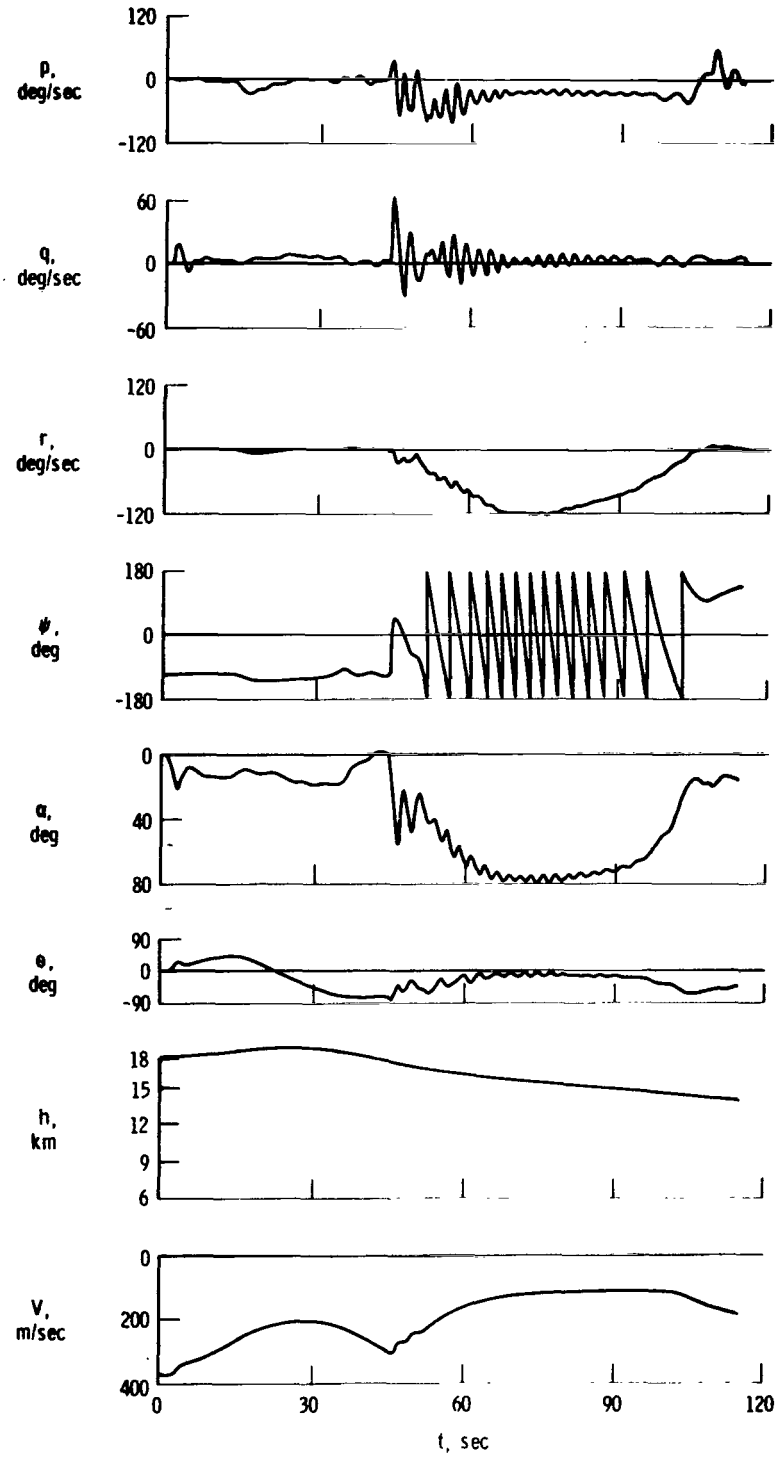

(a) Angular rates and related quantities.

Figure 35. Time histories of a piloted simulation of a spin for comparison with large-scale airplane model test results. Center of gravity at 30.3-percent mean aerodynamic chord.

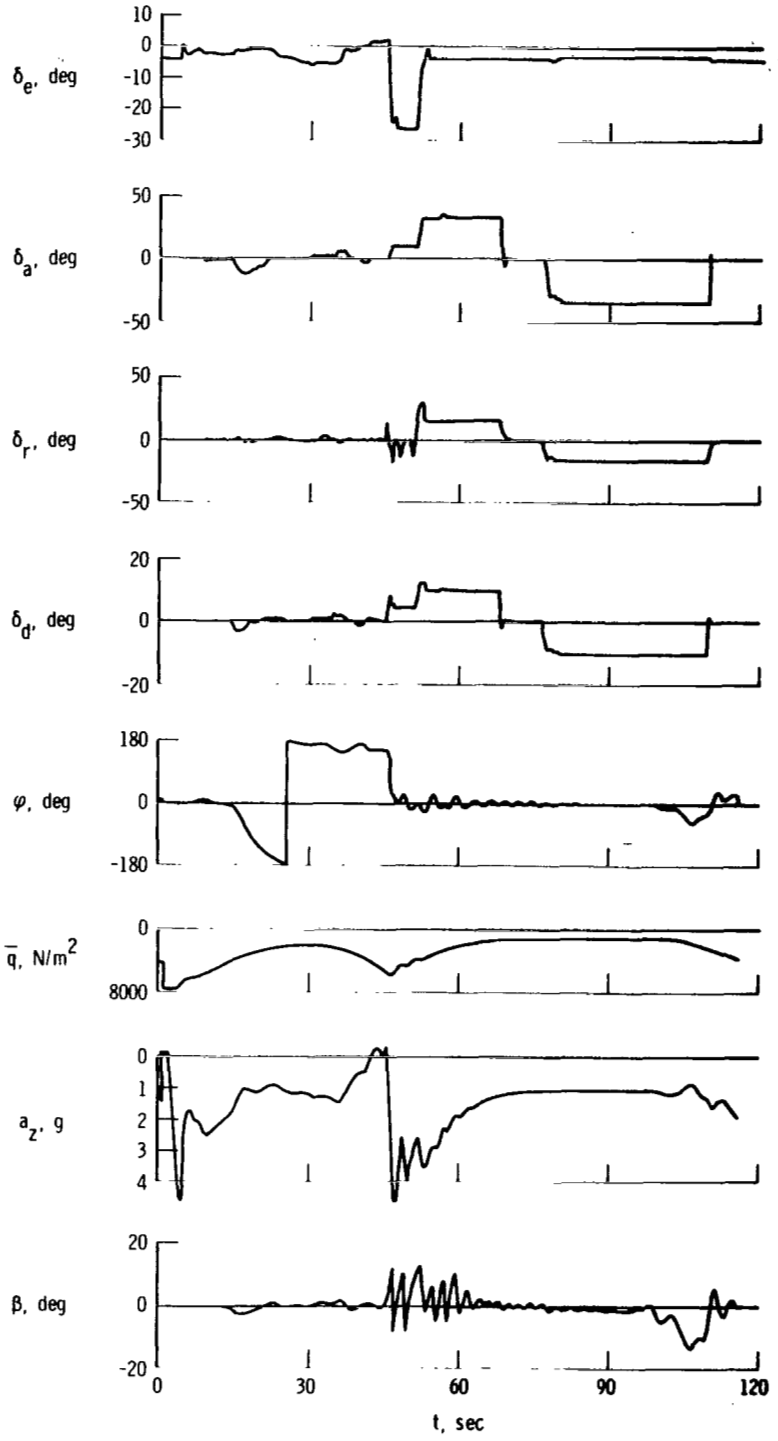

(b) Controls and related quantities.

Figure 35. Concluded.

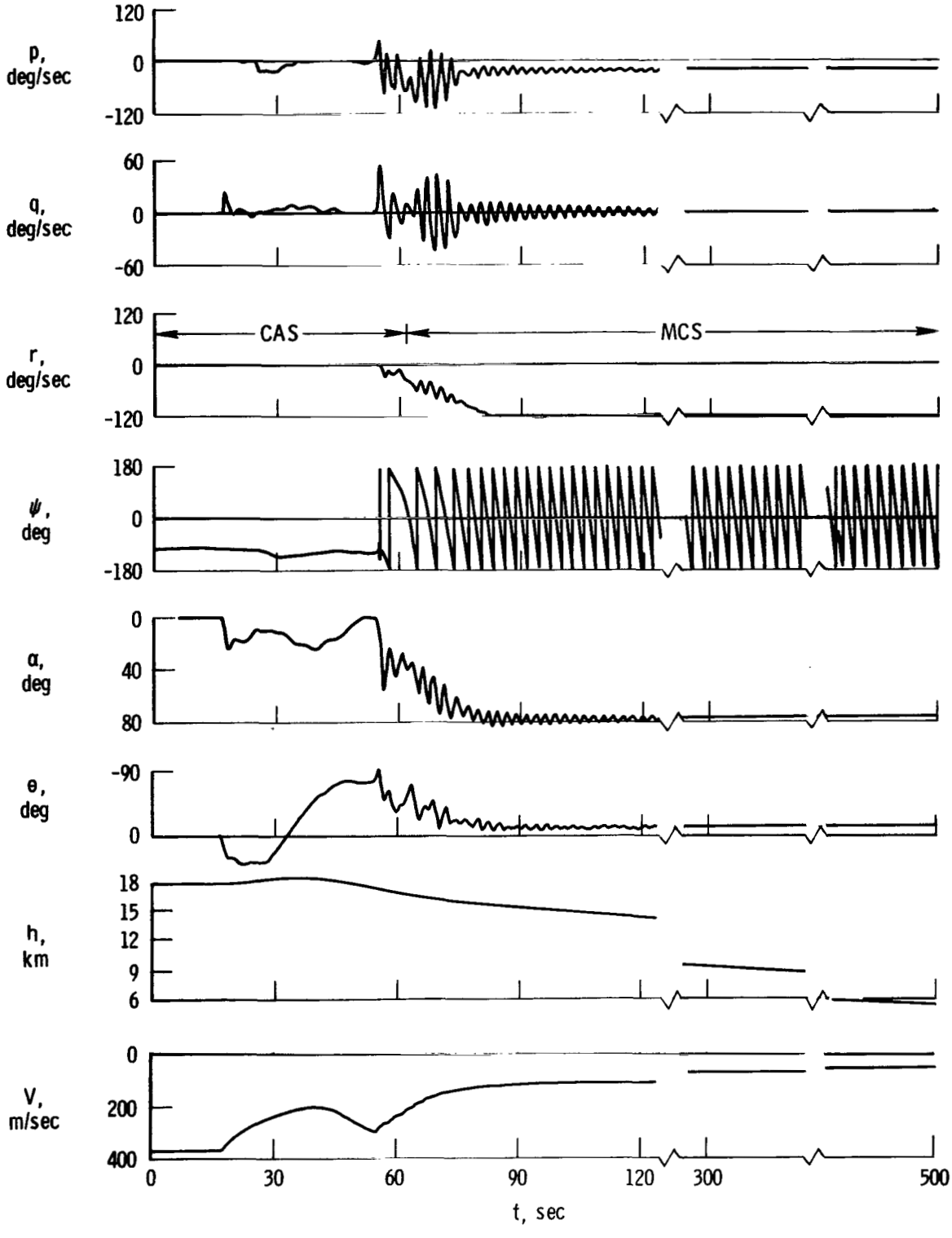

(a) Angular rates and related quantities.

Figure 36. Time histories showing the effect of altitude on the simulated airplane spin. Center of gravity at 30.3-percent mean aerodynamic chord.

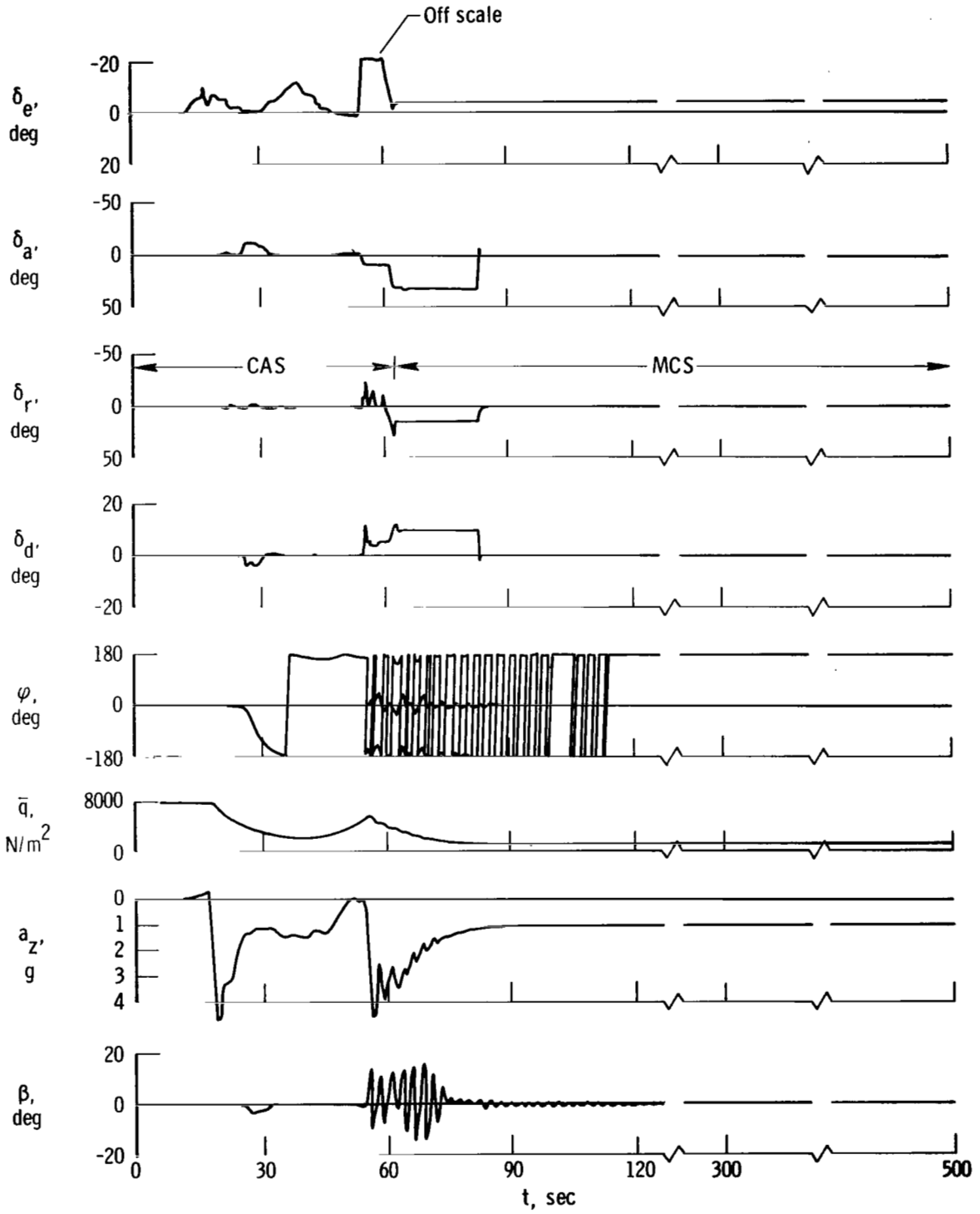

(b) Controls and related quantities.

Figure 36. Concluded.

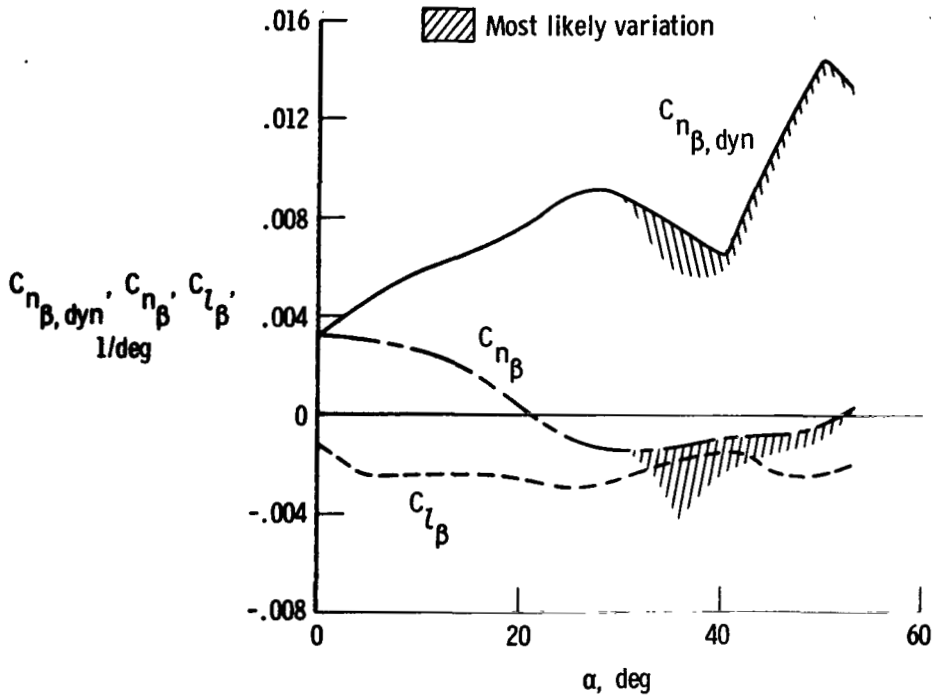

Figure 37. Stability derivative variation with angle of attack determined during the large-scale model flight program. Reynolds number approximately 4×10^6; low speed.

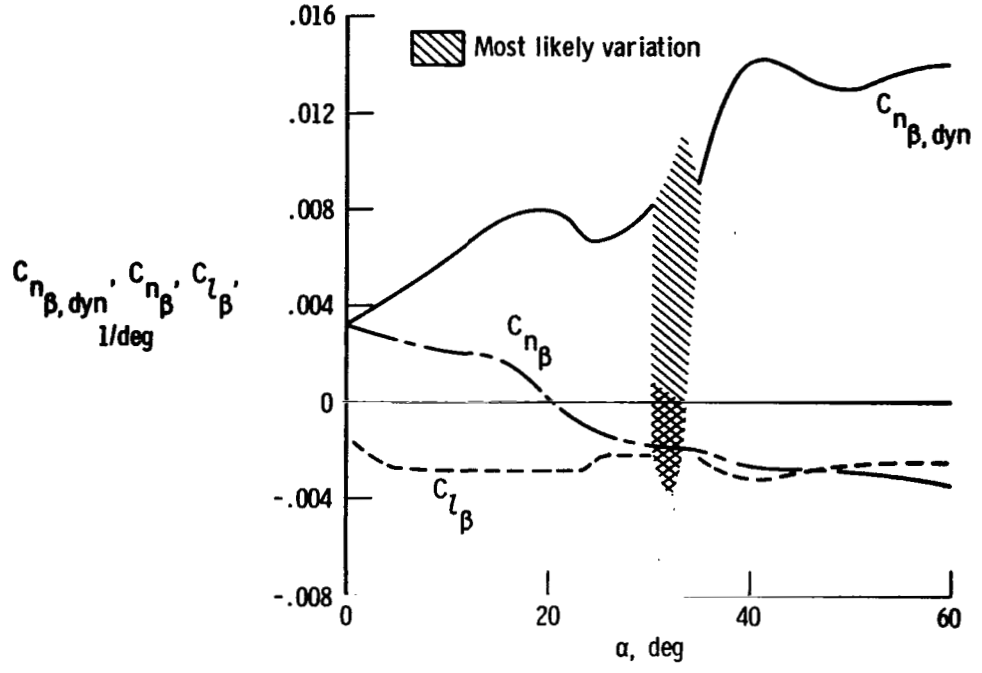

(a) 10-percent-scale model, Reynolds number = 0.8×10^6, Langley Full-Scale tunnel.

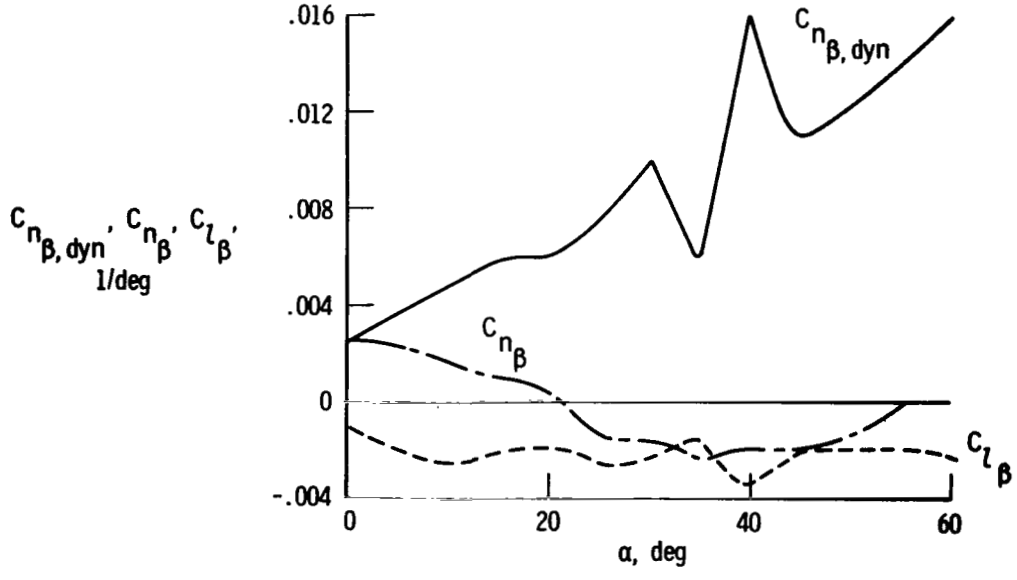

(b) 7.5-percent-scale model, Reynolds number = 4×10^6, Ames 12-Foot Tunnel.

Figure 38. Stability derivative variation with angle of attack from small-scale wind-tunnel models. Low subsonic speed.

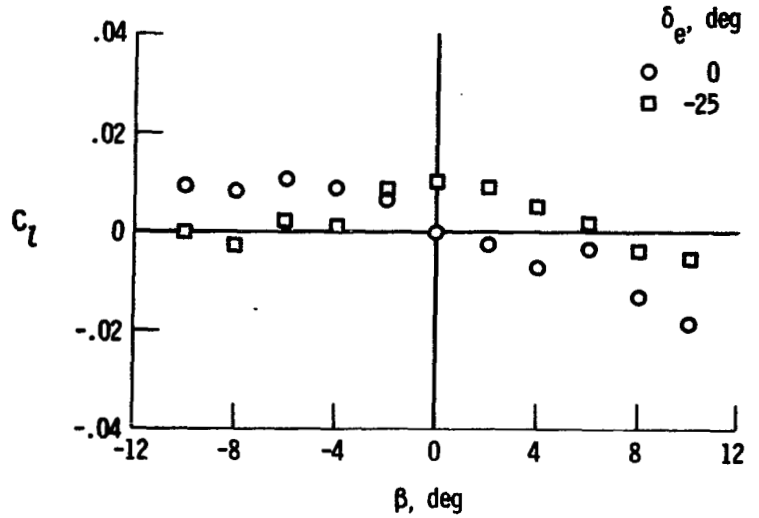

Figure 39. Effect of horizontal stabilator position on rolling-moment coefficient as a function of angle of sideslip. Reynolds number = 0.8×10^6; 10-percent-scale model; $\alpha = 32°$.

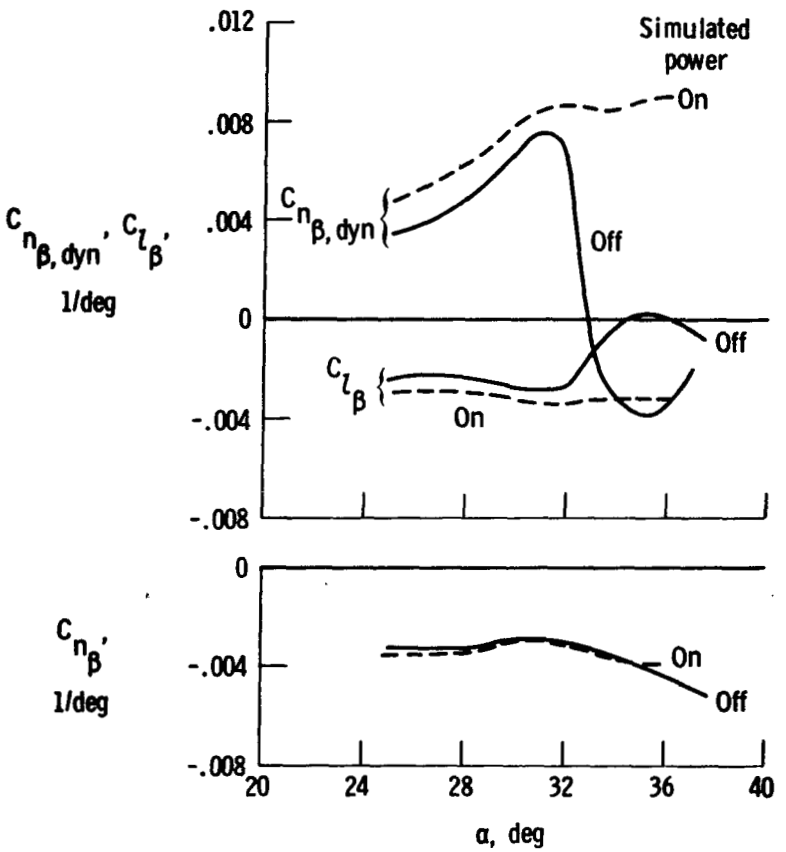

Figure 40. Lateral-directional derivatives from Ames 75-percent-scale model tests. Reynolds number = 10×10^6.

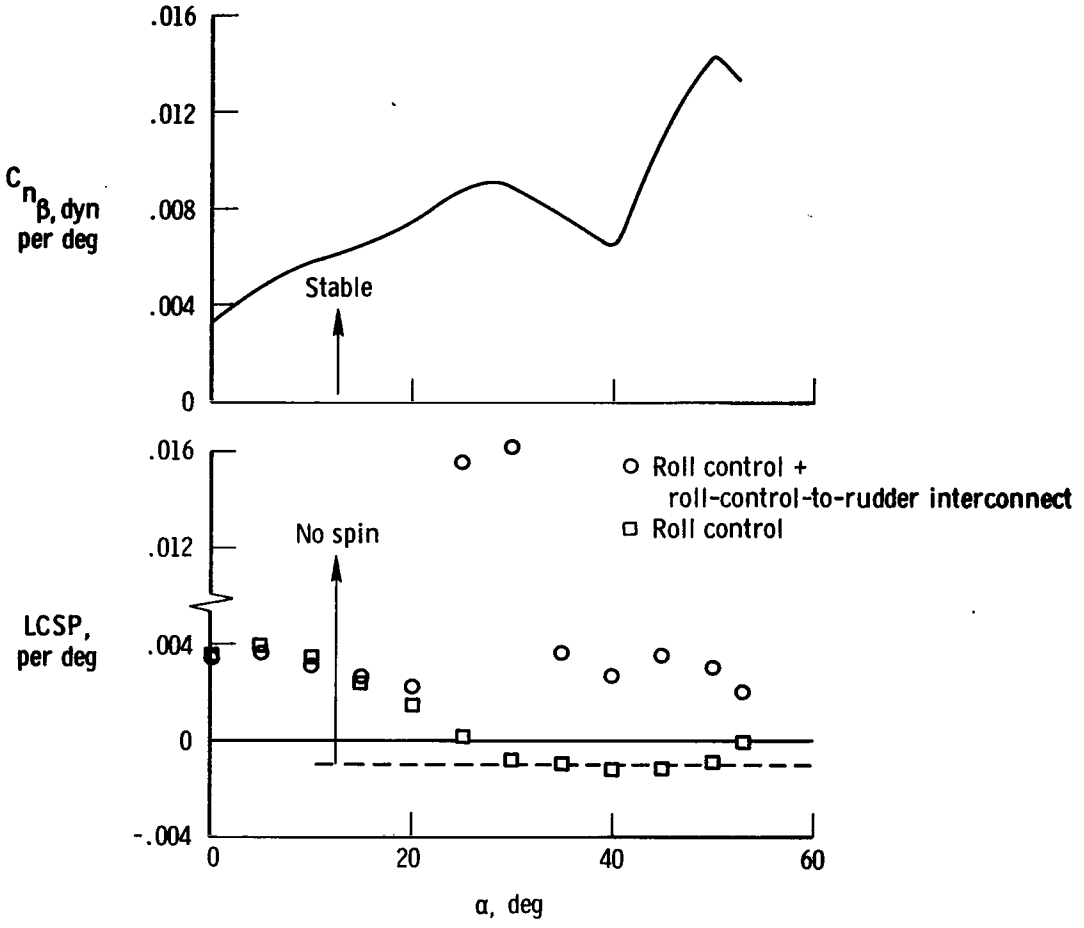

Figure 41. Comparison of the large-scale airplane model characteristics with the criterion of reference 9.

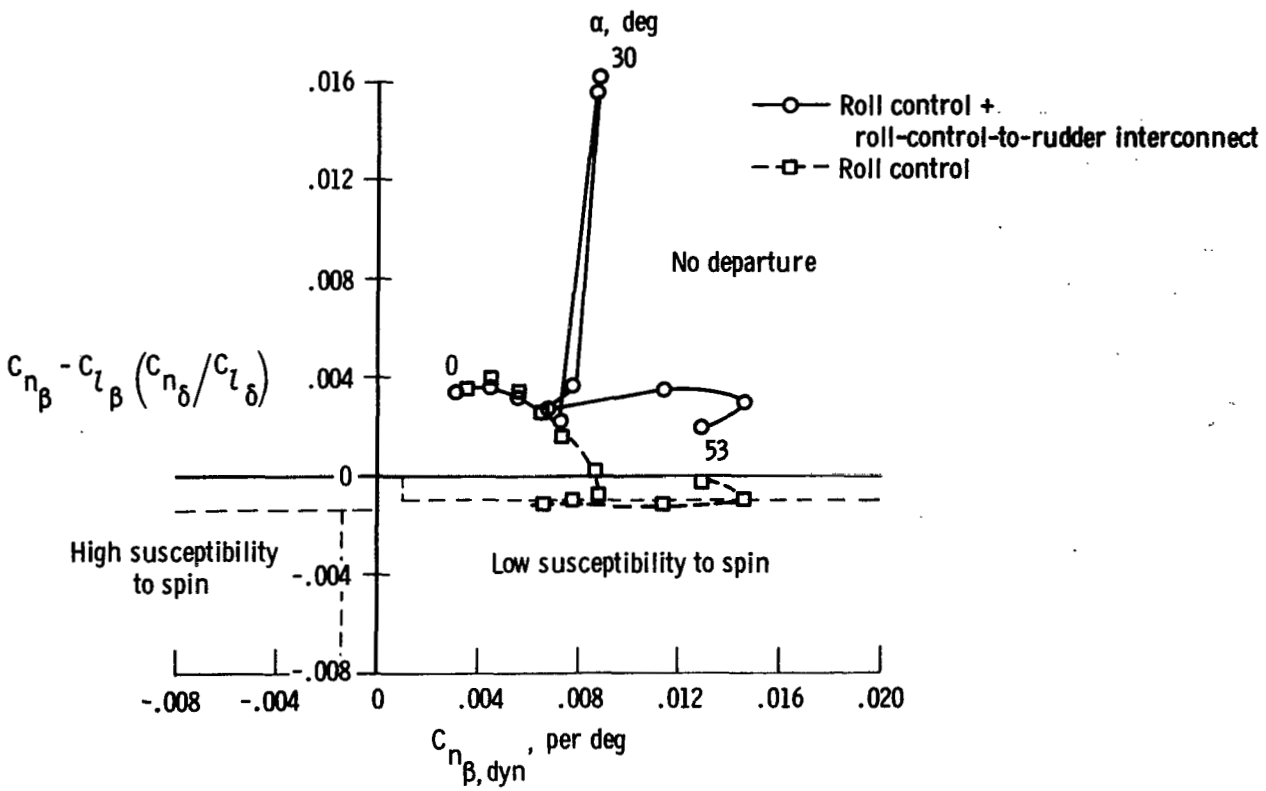

Figure 42. Comparison of the large-scale airplane model characteristics with the criterion of reference 10.

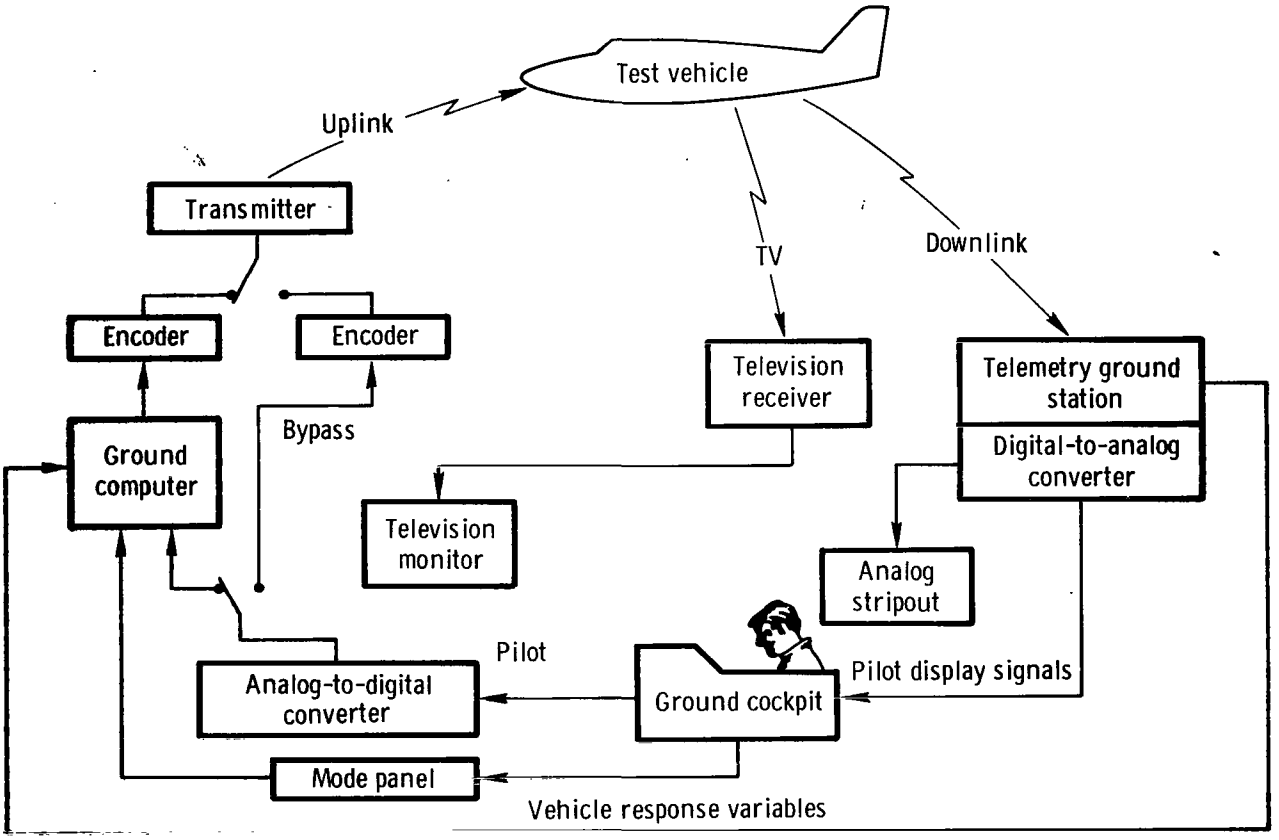

Figure 43. Remotely piloted model control loops.

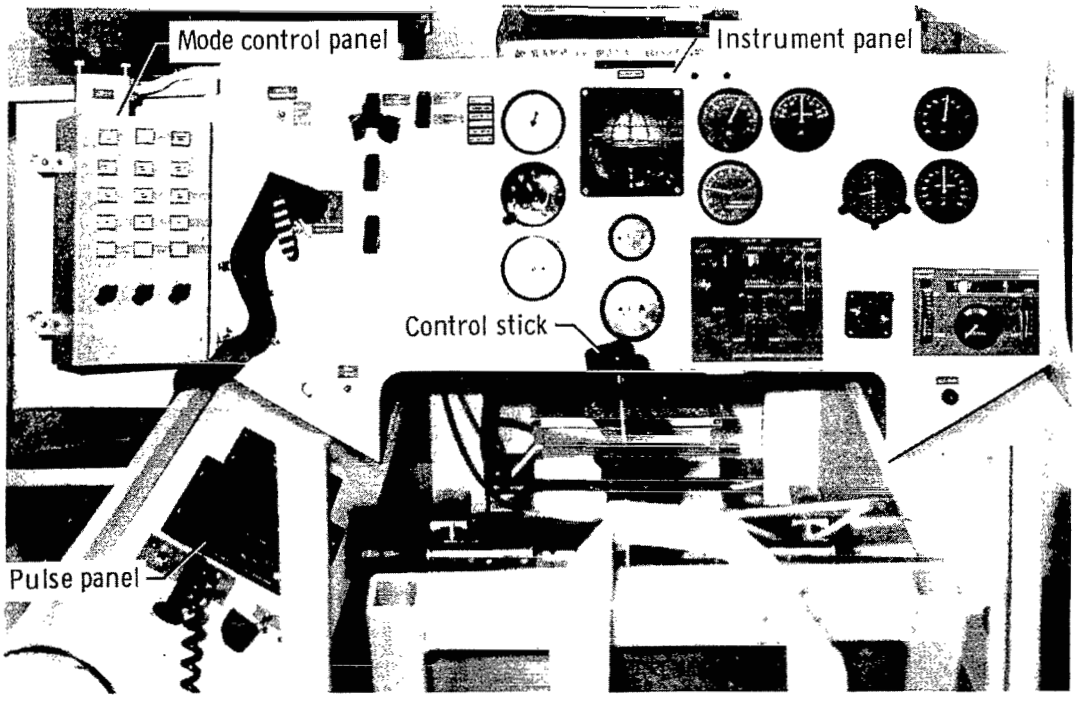

E-26991

Figure 44. Pilot's control station.

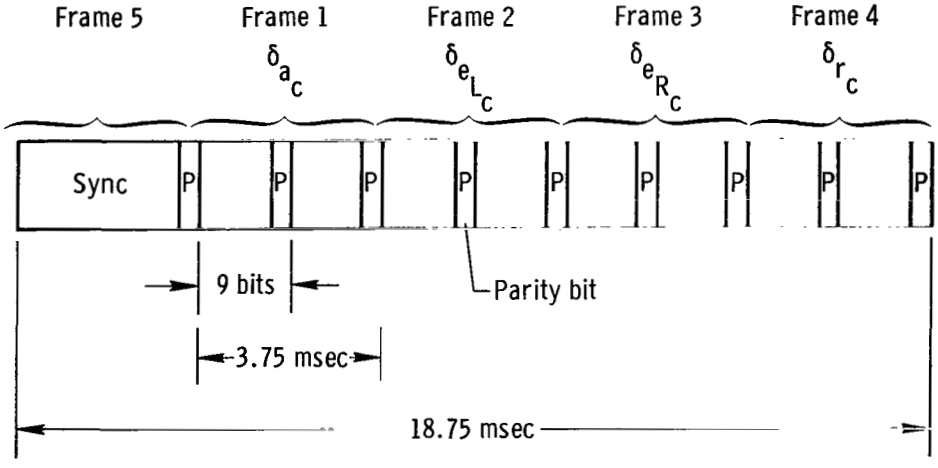

Figure 45. Telemetry uplink time schedule.

*U.S. GOVERNMENT PRINTING OFFICE: 1975 - 665689/62

"The aeronautical and space activities of the United States shall be conducted so as to contribute . . . to the expansion of human knowledge of phenomena in the atmosphere and space. The Administration shall provide for the widest practicable and appropriate dissemination of information concerning its activities and the results thereof."

—NATIONAL AERONAUTICS AND SPACE ACT OF 1958

NASA SCIENTIFIC AND TECHNICAL PUBLICATIONS

TECHNICAL REPORTS: Scientific and technical information considered important, complete, and a lasting contribution to existing knowledge.

TECHNICAL NOTES: Information less broad in scope but nevertheless of importance as a contribution to existing knowledge.

TECHNICAL MEMORANDUMS: Information receiving limited distribution because of preliminary data, security classification, or other reasons. Also includes conference proceedings with either limited or unlimited distribution.

CONTRACTOR REPORTS: Scientific and technical information generated under a NASA contract or grant and considered an important contribution to existing knowledge.

TECHNICAL TRANSLATIONS: Information published in a foreign language considered to merit NASA distribution in English.

SPECIAL PUBLICATIONS: Information derived from or of value to NASA activities. Publications include final reports of major projects, monographs, data compilations, handbooks, sourcebooks, and special bibliographies.

TECHNOLOGY UTILIZATION PUBLICATIONS: Information on technology used by NASA that may be of particular interest in commercial and other non-aerospace applications. Publications include Tech Briefs, Technology Utilization Reports and Technology Surveys.

Details on the availability of these publications may be obtained from:

SCIENTIFIC AND TECHNICAL INFORMATION OFFICE

NATIONAL AERONAUTICS AND SPACE ADMINISTRATION

Washington, D.C. 20546